

ENABLING PERSONALIZED MEDICINE THROUGH
PHARMACOKINETIC MODELING

By

MEGERLE LOUISE SCHERHOLZ

A dissertation submitted to the

School of Graduate Studies

Rutgers, The State University of New Jersey

In partial fulfillment of the requirements

For the degree of

Doctor of Philosophy

Graduate Program in Chemical and Biochemical Engineering

Written under the direction of

Ioannis P. Androulakis

And approved by

New Brunswick, New Jersey

January, 2019

ABSTRACT OF THE DISSERTATION

Enabling Personalized Medicine through Pharmacokinetic Modeling

By MEGERLE LOUISE SCHERHOLZ

Dissertation Director:
Ioannis P. Androulakis

Personalized medicine strives to deliver the ‘right drug’ at the ‘right dose’ at the ‘right time’ by considering the unique characteristics that define specialized populations of patients and contribute to inter-individual variability, a leading cause of therapeutic failure when not properly considered. Given the challenges of studying specialized patient subgroups in clinical trials as well as the high degree of control necessary to tease out differences across populations, physiologically based pharmacokinetic (PBPK) modeling emerged as a key tool to evaluate complex clinical phenotypes and to predict the potential distribution of patient responses. Unfortunately, the inherent variability of biological systems and knowledge gaps in physiological data often limit confidence in model predictions for special populations. Thus, a critical step in model development for special populations involves an in-depth analysis of estimated model input and evaluation of the underlying physiological mechanisms leading to variability in pharmacokinetics, both of which may be guided by global sensitivity analysis and advanced statistical techniques.

The benefits of global sensitivity as a means to refine parameter estimates and to understand how model behavior depended on the input parameter space were demonstrated using GastroPlus™ model, a well-known commercially available platform. Global

sensitivity analysis was performed in two stages using the Morris Method to screen for significant factors followed by quantitative assessment of variability using Sobol's sensitivity analysis. The 2-staged approach significantly reduced computational cost without sacrificing interpretation of model behavior, revealing nonlinearities and parameter interactions that would have been missed by local approaches. Furthermore, the utility of pharmacokinetic models to study the underlying and complex physiological mechanisms contributing to clinical differences across patient subgroups was revealed using Monte Carlo simulations by restricting model input to parameter combinations that described only biologically plausible model output. Through an integrated approach using a support vector machine, principal component analysis and global sensitivity analysis, specific combinations of parameters were shown to give rise to clinical phenotype, while individual parameters influenced the shape of the exposure profile. Augmenting analysis of the model input with global sensitivity analysis enabled an understanding of sexual dimorphism and inter-individual variability in pharmacokinetics.

Finally, a dynamic semi-mechanistic model that considered pharmacokinetics and pharmacodynamics was used to demonstrate how patients benefit from careful timing of drug delivery. In this study, a mathematical model was developed to explore chronopharmacological dosing of synthetic glucocorticoids and its influence on the endogenous glucocorticoid secretion. Considering the central regulatory function of endogenous glucocorticoids for metabolic, anti-inflammatory, immunosuppressive and cognitive signaling, maintenance of normal physiological functions regulated by glucocorticoids is essential to host survival, while chronic disruption leads to severe systemic complications. Therefore, a key objective in glucocorticoid research is the

development of novel dosing regimens that minimize the disruption of endogenous activity, while maintaining the pharmacological benefits of long-term therapy. Physiologically based modeling showed how chronic daily dosing resulted in modification of endogenous glucocorticoid activity with the extent of said changes dependent on the administration time and dose. However, simulations also revealed that endogenous glucocorticoid activity was preserved with proper timing of administration dependent on the dosage form. Furthermore, amending the model to account for inter-sex and inter-individual variability showed chronopharmacological dosing regimens can be further optimized by identifying the ‘right dose’ and ‘right time’ in the targeted patient populations by considering the underlying regulatory differences between males and females.

Acknowledgements

I thank my adviser Ioannis Androulakis for his guidance and support. I am grateful to Brenda Remy, Omar Sprockel, and Elena Zour for inspiring me to apply for the Bristol-Myers Squibb PhD fellowship and for their unwavering support while I completed my graduate studies full-time, as well as all my DPST colleagues who have been so encouraging. I would also like to thank Alison Acevedo, Clara Hartmanshenn, Kamau Pierre, Matthew Putnins, Mohit Kumar, Rohit Rao, and Seul-a Bae for their input and support during my time at Rutgers. I am especially grateful to Dan Wachter, Brittney Horner, Larissa Brady, my parents, my brother and all of my friends for their endless encouragement, both professionally and personally, these last few years.

Table of Contents

ABSTRACT OF THE DISSERTATION	ii
Acknowledgements	v
List of Tables	ix
List of Illustrations	x
CHAPTER 1: Background and Motivation	1
1.1 Introduction to personalized medicine	1
1.2 Overview of physiologically based pharmacokinetic models	2
1.3 Sourcing model input	5
1.4 Model parametrization for special populations	8
1.4.1 Sex	8
1.4.2 Circadian rhythms	11
1.5 Outline of dissertation	13
CHAPTER 2: A framework for 2-stage global sensitivity analysis of GastroPlus™ compartment models	16
2.1 Introduction	16
2.2 Global sensitivity methods	19
2.2.1 Morris method	19
2.2.2 Sobol sensitivity analysis	21
2.3 Approach	23
2.3.1 GastroPlus setup for selected drugs	23
2.3.2 Morris Method for GastroPlus	25
2.3.3 Sobol sensitivity analysis for GastroPlus	27
2.3.4 Development of the automated GastroPlus framework	28
2.4 Results	29
2.4.1 Stage 1: Screening for significant parameters	30
2.4.2 Identification of significant GastroPlus parameters by the Morris Method	31
2.4.3 Morris Method results in the context of ADME processes	35
2.4.4 Stage 2: Quantitative assessment of output variability	37
2.4.5 Sobol Method for acetaminophen	38
2.4.6 Sobol Method for risperidone	39
2.4.7 Sobol Method for atenolol	40

2.4.8	Sobol Method for furosemide	41
2.4.9	Parameter rankings by the Morris and Sobol methods were consistent.....	42
2.4.10	Quality of 2-stage global sensitivity analysis depends on screening with the Morris Method.....	43
2.5	Discussion.....	46
CHAPTER 3: Exploration of sexual dimorphism and inter-individual variability in multivariate parameter spaces for a pharmacokinetic compartment model.....		52
3.1	Introduction.....	52
3.2	Approach.....	54
3.2.1	Overview of model-based methodology	54
3.2.2	Overview of the selected model	55
3.2.3	Identification of initial parameter estimates for a generic population.....	57
3.2.4	Identification and analysis of male and female parameter subspaces	58
3.2.5	Support vector machine for binary classification.....	59
3.2.6	Principal component analysis.....	60
3.2.7	Sobol sensitivity analysis	60
3.3	Results.....	61
3.3.1	Identification of simulated male and female populations	61
3.3.2	Separation of model input into male and female parameter subspaces.....	64
3.3.3	Identification of parameter correlations in model input.....	66
3.3.4	Identification of model input driving inter-individual variability within each population.....	68
3.3.5	Relating sexual dimorphism and inter-individual variability.....	70
3.4	Discussion.....	71
CHAPTER 4: Modeling the influence of chronopharmacological administration using an integrated semi-mechanistic PKPD model.....		76
4.1	Introduction.....	76
4.2	Approach.....	80
4.2.1	Description of the HPA axis model.....	80
4.2.2	Description of pharmacokinetic models for synthetic GC administration ..	84
4.2.3	Dosing experiments.....	87
4.3	Results.....	88
4.3.1	Pharmacokinetic profiles for the synthetic glucocorticoid.....	88

4.3.2	Influence of once-daily chronopharmacological dosing of synthetic GCs on the cortisol circadian rhythm.....	89
4.4	Discussion.....	99
CHAPTER 5: Modeling sexual dimorphism and inter-individual variability in response to chronopharmacological administration of synthetic glucocorticoids		105
5.1	Introduction.....	105
5.2	Approach.....	107
5.2.1	Adaptation of the HPA Axis model to nocturnal species.....	107
5.2.2	Parametrization of the Model.....	108
5.3	Dosing Experiments.....	109
5.4	Results.....	109
5.4.1	Male and female rat subpopulations used in dosing experiments.....	109
5.4.2	Influence of once-daily chronopharmacological dosing on corticosterone rhythmicity in male and female rats	110
5.4.3	Influence of dosing strength on the corticosterone activity in male and female rats	114
5.5	Discussion.....	115
CHAPTER 6: Conclusions.....		119
Acknowledgement of Publications		122
References.....		123
Appendix.....		144
6.1	Supplementary Figures	144
6.2	Supplementary Tables.....	159

List of Tables

Table 1: Significant parameters determined by the Morris Method for the GastroPlus models	35
Table 2: Parameter ranking determined by the Morris and Sobol sensitivity methods for C_{\max}	43
Table 3: Target male and female pharmacokinetic model output for selection of parameter sets from stochastic sampling	59
Table 4: Summary of Parameter Rankings for Support Vector Machine, Principal Component loadings, and Sobol sensitivity analysis	71

List of Illustrations

Figure 1: Automated GastroPlus framework for global sensitivity analysis. GastroPlus parameter sets were generated in MATLAB and then AutoIt was used to update the parameters in the GastroPlus interface according to the sample space, to run simulations for each parameter set, and to transfer GastroPlus predictions back to MATLAB for calculation of sensitivity measures.	29
Figure 2: Morris Method results for acetaminophen C_{max} using $r = 1$ to 40 and sampling bounds of $\pm 20\%$. The error bars represent the standard deviation in μ^* from 3 independent analyses at each sample size.	31
Figure 3: Representative Morris Method results for acetaminophen and risperidone C_{max} . The values of μ^* were determined using $r = 20$ and sampling bounds of $\pm 20\%$. The cutoff for significance (indicated by dotted red line), corresponded to 10% of the maximum μ^* for C_{max} associated with each drug.	32
Figure 4: Representative Morris Method results for atenolol and furosemide C_{max} . The values of μ^* were determined using $r = 20$ and sampling bounds of $\pm 20\%$. The cutoff for significance (indicated by dotted red line), corresponded to 10% of the maximum μ^* for C_{max} associated with each drug.	33
Figure 5: Influences of ADME processes according to the Morris Method. The percent contributions in (a) were determined by the sum of μ^* associated with parameters in each group relative to the sum of all μ^* for all groups. These contributions were then used to identify the key process influencing each model output in (b). Parameters contained in each group are provided in Supplementary Table 3.....	37
Figure 6: Sobol Method for acetaminophen C_{max} . The sensitivity measures were determined using $N=4,000$ for parameters identified by the Morris Method based on μ^* . The first-order and total effects are given in (a). The second-order interactions are given in (b).....	39
Figure 7: Sobol Method for risperidone C_{max} . The sensitivity measures were determined using $N=3,000$ for parameters identified by the Morris Method based on μ^* . The first-order and total effects are given in (a). The second-order interactions are given in (b).	40
Figure 8: Sobol Method for atenolol C_{max} . The sensitivity measures were determined using $N=4,000$ for parameters identified by the Morris Method based on μ^* . The first-order and total effects are given in (a). The second-order interactions are given in (b).	41
Figure 9: Sobol Method for furosemide C_{max} . The sensitivity measures were determined using $N=5,000$ for parameters identified by the Morris Method based on μ^* . The first-order and total effects are given in (a). The second-order interactions are given in (b).	42
Figure 10: Relationships between model input and output for acetaminophen C_{max} . The values of μ^* and σ determined using $r = 20$ and the average ratio σ/μ^* from triplicate analysis are plotted in (a) and (b), respectively, for sampling bounds of $\pm 20\%$ and $\pm 50\%$. Error bars in (a) represent the standard deviation associated with μ^* and σ for triplicate	

analyses. The distribution of elementary effects for each replicate analysis are given in (c) for body weight. 45

Figure 11: GastroPlus predictions for acetaminophen at the sampling bounds. The plasma concentration profiles predicted by GastroPlus when body weight and the gastric pH were set to the upper and lower limits are given in (a) and (b) for sampling bounds of $\pm 20\%$ and $\pm 50\%$, respectively. 46

Figure 12: Schematic outlining the model-based approach for isolation of male and female model parameter subspaces using stochastic sampling and global sensitivity analysis. Random samples are drawn from each parameter distribution with mean (μ) and standard deviation (σ) for the mixed sex population. Parameter sets associated with model output within the acceptable male or female ranges are specified as male or female accordingly. The isolated male and female parameter subspaces are then used for the global sensitivity analysis to identify parameters with the greater influence on model output. Parameter sets associated with model output outside the acceptable ranges are considered biologically implausible and discarded. 55

Figure 13: Probability density distributions of model input parameters for the simulated male and female populations. The probability density distributions are given for the simulated male and female populations isolated from sampling (blue and red lines, respectively) and the original mixed sex population used as the starting point for sampling (black line). The p-values are reported for the comparison of population distributions according to the Kolmogorov-Smirnov (KS) test and the comparison of population medians according to the Wilcoxon Rank Sum (WRS) test. Sex differences that were not statistically significant were indicated by NS (not significant). 62

Figure 14: Probability density distributions of model output for the simulated male and female populations. The probability density distributions are given for the simulated male and female populations isolated from sampling (blue and red solid lines, respectively) and the original clinical populations (blue and red dotted lines). The p-values are reported for the comparison of the population medians according to the Wilcoxon Rank Sum (WRS) test. Sex differences that were not statistically significant were indicated by NS (not significant). 63

Figure 15: Plasma concentration profiles for the simulated and clinical populations. The mean plasma concentration profiles for the male and female populations are given in subplots (A) and (B), respectively. The light shaded area represents the experimentally observed standard deviation whereas the darker shaded area represents the standard deviation associated with model predictions corresponding to the isolated male and female parameter sets. 64

Figure 16: Separating hyperplane coefficients using model input as support vector machine (SVM) predictors. A binary classifier was developed using a randomly selected subset of 1,000 male and 1,000 female parameter sets for 1,000 bootstrapped samples to identify which parameters separated model output into the two phenotypes. The distributions of hyperplane coefficients for the bootstrapped samples are given in subplots (A) through (I) with the mean values of hyperplane coefficients reported in subplot (J). 65

Figure 17: Approximation of the separating hyperplane between male and female model input using two predictors. The hyperplane using the most significant predictors (highest β_i values) and the least significant predictors (lowest β_i values) are given in subplots (A) and (B), respectively. The black line in (A) corresponds to the mean hyperplane for the 1,000 bootstrapped samples. The shaded area represents the potential location of the boundary between males and females when the separating hyperplane parameters were within 1 standard deviation of the mean values. The scatter plot shows the z-scores for the given parameters associated with male subjects (blue) and female subjects (red) from one representative bootstrapped sample. 66

Figure 18: Separating hyperplane between male and female populations using principal components. The 3D scores plot in (A) shows the separating hyperplane using the first three principal components. The percentage of variability explained by each principal component is indicated in the axis labels. The black surface corresponds to the mean boundary of the 1,000 bootstrapped samples. The pink surface corresponds to the boundary when the separating hyperplane are $+1\sigma$ of the mean values. The green surface corresponds to the boundary when the separating hyperplane are -1σ of the mean values. The scatter plot shows the principal component scores for the male subjects (blue) and female subjects (red) from one representative sample. The mean separating hyperplane parameters for the support vector machine (SVM) are given in (B) where the error bars represent the standard deviation of the 1,000 bootstrapped samples. The mean loadings for the first principal component are given in subplot (C) with error bars that represent the standard deviation for the 1,000 samples. 68

Figure 19: Sobol sensitivity analysis for male and female parameter subspaces. The first order sensitivity measures for male and female parameter subspaces are given in subplots (A) and (B), respectively using C_{max} , t_{max} , and AUC_{0-t} as the model output. A higher value corresponds to a parameter which explains a greater proportion of the variability in model output. 70

Figure 20: Model Schematic: A schematic of the model depicting the primary interactions in the hypothalamus-pituitary-adrenal (HPA) axis. The synthetic glucocorticoids (GC) competitively bind to the glucocorticoid receptor and contribute to the negative feedback arm of the HPA axis. Synthetic GCs are administered by either a bolus injection directly into systemic circulation or by oral administration. Appearance in systemic circulation following oral administration is indicated by the orange line..... 81

Figure 21: Pharmacokinetic profiles for a bolus injection, a fast-acting oral dose, and a slow-acting oral dose of synthetic GCs. Representative profiles are shown for a nominal dose of 1x. Plasma concentration is given in arbitrary units (a.u.). 89

Figure 22: Modified cortisol profiles after dosing of synthetic glucocorticoids (GC) by bolus injection at the nominal amount (1x). The modified cortisol rhythm is indicated by the blue line. The black line corresponds to the nominal cortisol profile based on endogenous HPA axis activity. The pharmacokinetic profiles for the bolus injection are indicated by the dotted green line. The grey shaded areas represent the time at which the system is not exposed to light. Cortisol concentration is given in arbitrary units (a.u.)... 90

Figure 23: Amplitude and phase of the modified cortisol rhythm after once-daily chronopharmacological dosing of synthetic glucocorticoids. The relative amplitude and

difference in the acrophase of the modified cortisol rhythm after a repeated once-a-day administration of a bolus injection, fast-acting oral dose, or slow-acting oral dose are shown in A and B, respectively. The nominal cortisol rhythm (indicated by the black line) is given for reference to show how dosing times align with the baseline circadian rhythm. The shaded areas represent the simulated night, that is the time at which the system is not exposed to light. The change in amplitude is calculated by Relative Amplitude (%) = $[(\text{Amp}_{\text{treatment}} - \text{Amp}_{\text{baseline}})/\text{Amp}_{\text{baseline}}] \times 100\%$. A negative value for phase difference indicates an advance in the acrophase (i.e. peaks earlier in the simulated day relative to the nominal cortisol rhythm) while a positive value indicates a delay in the acrophase (i.e. peaks later in the simulated day). Cortisol concentration is given in arbitrary units (a.u.).

..... 91

Figure 24: Relationship between the relative amplitude and phase difference of the modified cortisol rhythm after long-term once-daily chronopharmacological dosing of synthetic glucocorticoids. Amplitude and phase for the modified cortisol rhythms after chronic administration of a daily bolus injection and the slow-acting oral dose are shown in A and B, respectively. Marker labels correspond to the time of administration. Marker color indicates the administration time relative to the nominal cortisol rhythm where blue circles correspond to dosing times from 8:00 PM to 6:00 AM (ascending phase of baseline rhythm), red squares correspond to dosing times from 7:00 AM to 8:00 AM (near peak of baseline rhythm), green diamonds correspond to dosing times from 9:00 AM to 5:00 PM (descending phase of baseline rhythm), and yellow triangles correspond to dosing times from 6:00 PM to 7:00 PM (near nadir of baseline rhythm).

..... 93

Figure 25: Amplitude of the modified cortisol rhythm after single and repeated once-daily chronopharmacological dosing of synthetic glucocorticoids by bolus injection at the nominal dose. The relative amplitude associated with the modified cortisol rhythm after a single injection and after long-term once-daily IV dosing are shown. The relative change in amplitude is calculated by Relative Amplitude (%) = $[(\text{Amp}_{\text{treatment}} - \text{Amp}_{\text{baseline}})/\text{Amp}_{\text{baseline}}] \times 100\%$. Cortisol concentration is given in arbitrary units (a.u.).

.....94

Figure 26: Influence of chronic once-daily chronopharmacological dosing on the total cortisol exposure. The relationship between the 24-hour AUC and amplitude change after long-term dosing of a daily bolus injection at the nominal dose (1x) is shown in A. The modified cortisol profiles after dosing and for the baseline conditions are given in B for selected dosing times. The grey shaded areas represent the simulated night, that is the time at which the system is not exposed to light. Cortisol concentration is given in arbitrary units (a.u.).

..... 95

Figure 27: Influence of dosing strength on the relative amplitude after chronic once-daily chronopharmacological dosing of a bolus injection. The relative amplitude for the modified cortisol rhythms are given for the once-daily chronopharmacological dosing regimens that resulted in the greatest inductive and suppressive effects at each strength of the IV dose. The administration times corresponding to these changes in amplitude are indicated in the figure.

..... 97

Figure 28: Male and female parameter subspaces for sex-specific parameters used in dosing experiments. The subset of 100 male rats and 100 female rats were selected from the original populations established by Rao et al. [200].

..... 110

Figure 29: Differences in basal HPA activity between male and female rat populations. The corticosterone profiles for the subpopulations of the male and female rats used in the dosing experiments are given in (A) and (B), respectively. The grey shaded areas represent the time at which the system is not exposed to light. Corticosterone concentration is given in arbitrary units (a.u.)..... 111

Figure 30: Modified corticosterone profiles after dosing of synthetic glucocorticoids (GC) by bolus injection at the nominal amount (1x). The corticosterone rhythms with and without dosing are given in (A) for male rats and (B) for female rats. The solid line corresponds to the nominal corticosterone profile based on endogenous HPA axis activity. The modified corticosterone rhythm is indicated by the dotted line. The pharmacokinetic profiles for the bolus injection are indicated by the black line. The grey shaded areas represent the time at which the system is not exposed to light. Corticosterone concentration is given in arbitrary units (a.u.)..... 111

Figure 31: Population mean amplitude and phase of the modified corticosterone rhythm after once-daily chronopharmacological dosing of synthetic glucocorticoids in male rats and female rats. The relative amplitude and difference in the acrophase of the modified corticosterone rhythms after a repeated once-a-day administration of a bolus injection, fast-releasing oral dose, or slow-releasing oral dose are shown in (A) and (C) for male rats and in (B) and (D) for female rats, respectively. The colored shaded areas represent ± 1 standard deviation of the population mean for amplitude and phase changes. The gray shaded areas represent the simulated night. A negative value for phase difference indicates an advance in the acrophase (i.e. peaks earlier in the simulated day) while a positive value indicates a delay in the acrophase (i.e. peaks later in the simulated day)..... 112

Figure 32: Amplitude and phase of the modified corticosterone rhythm after once-daily injection at 4:00 AM and 4:00 PM in male and female rats. The relative amplitude and phase difference for the modified corticosterone rhythms are given for each individual defined by three sex-dependent parameters..... 114

Figure 33: Influence of dosing strength on the amplitude of the modified corticosterone rhythm following chronic once-daily dosing of a bolus injection in male and female rats. The amplitude is given for the dosing times which resulted in the greatest inductive and suppressive effects at each strength in male rats (A) and female rats (B). The error bars represent ± 1 standard deviation of the population mean for amplitude and phase changes. 115

CHAPTER 1: Background and Motivation

1.1 Introduction to personalized medicine

Inter-person variability can lead to therapeutic failure and adverse effects in individuals or specialized subpopulations of patients during clinical practice [1]. Historically, clinicians were tasked with identifying factors driving differences in patient response by conducting ad hoc post-trial analyses [2]. Currently, researchers are looking to capture this patient variability upfront through personalized medicine, striving to deliver the ‘right drug’ at the ‘right dose’ by individualizing treatment [3] for the ‘right disease’ and at the ‘right time’ [4]. While ‘right drug’ emphasizes the need for therapies specifically designed for subpopulations of patients, ‘right dose’ highlights the need to maintain the drug plasma concentration within the therapeutic window to optimize patient benefit and minimize patient risk [3]. At the individual level, these differences are attributed to a person’s clinical phenotype, collectively defined by the individual’s metabolome, proteome, transcriptome, and genome [3]. While much of the discussion focuses on genetic or genomic based therapies, a broader interpretation for personalized medicine is “the use of combined knowledge (genetic or otherwise) about a person to predict disease susceptibility, disease prognosis, or treatment response and thereby improve that person’s health [5]”.

Personalized medicine remains a very current challenge, despite a strong interest from researchers and physicians for decades. As knowledge in the field advances, the need for physiologically suited therapies is more apparent. Important physiological and pharmacokinetic differences exist between patients according to sex, age, ethnicity, disease state, and pregnancy. Personalized medicine has the potential to improve disease

prevention and treatment by tailoring therapies to the unique physiological and environmental factors that describe a subpopulation or an individual patient [6,7]. Therefore, identifying factors with the potential to impart the greatest effect on bioavailability and ultimately drug response is a critical step to explaining clinical observations, and understanding the usefulness of a particular treatment for maximized efficacy and minimized adverse effects across special populations or patient subgroups [8].

Inter-patient and inter-subpopulation variability can be difficult to represent in clinical studies without very large numbers of patients and can be further complicated by technical and ethical obstacles for certain subpopulations such as pediatrics or pregnant women. For these reasons, clinical studies often omit or include limited numbers of patients whose physiological backgrounds may lead to higher variations in data. These complexities hinder the progress of personalized medicine which prompts for an alternative approach to lessen the financial and ethical burden of experimental trials. A solution lies in modeling and statistical-based methodologies, which support the *in silico* exploration of pharmacokinetics and pharmacodynamics through virtual population studies. These models leverage the interplay between drug specific characteristics and human physiology, portrayed by the model input parameters, to emulate specific physiological or pathological conditions and can aid in the development of treatment options for the physiology of interest.

1.2 Overview of physiologically based pharmacokinetic models

Physiologically based pharmacokinetic (PBPK) modeling was first presented in 1937 in Teorell's "Kinetics of Distribution of Substances Administered to the Body" [9].

However, the mathematical complexity of the model exceeded the knowledge and computational power at that time. Today, improvements in computing technology combined with the pressing need to study the pharmacokinetics of compounds quickly and efficiently enabled PBPK modeling to emerge as a powerful simulation tool. Beginning in the 1990s, the United States Food and Drug Administration (US FDA) encouraged the use of modeling and simulation to establish the best dosing strategy and characterize patient risk in a variety of complex clinical scenarios, minimizing the need for animal studies to predict human exposure [10] and enabling streamlined drug development and regulatory review [11,12]. Through model-based regulatory research and clinical trial simulations, traditional drug development and regulatory review is shifting from inefficient and empirical to quantitative and mechanistic, enabling a deeper understanding of the behavior of drugs within the body while offering an explanation for sources of variability in exposure and drug response [13]. From a broader context, PBPK models play an extensive role in the design of clinical pharmacology studies, identification of additional studies to address gaps or residual risks, as well as an understanding of risk-benefit relationships for new entities [6]. Physiologically based pharmacokinetic and pharmacodynamic models enable enhanced specificity of diagnostic and therapeutic technologies, differentiation of responders from non-responders, reduced inter-patient variability, and fewer adverse events [4].

PBPK models mathematically describe human physiology through a series of organ and tissue compartments connected by a circuit of flowing blood, subdivided as arterial and venous blood pools. The properties of each compartment are described by a system of differential equations to explain time-dependent drug exposure. The level of scrutiny to

which ADME (absorption-distribution-metabolism-elimination) processes are described across bodily tissues depends on the desired, required or achievable level of detail, and by extension the complexity of the model structure. In the simplest form, pharmacokinetic models are empirical with the model structure determined from existing clinical data. In this manner, model development requires little knowledge of the system itself, only known input, such as the drug administered and patient body weight, as well as a measured output (drug concentration in blood, saliva, urine, etc.). The number of exponential terms (or compartments) needed to describe the resulting drug concentration profile is identified and the modeling framework is established as a basic compartment model [14,15]. The resulting model requires only a limited number of parameters to describe the bidirectional transport of drug between these compartments. Thus, the physicochemical properties of the drug, *in vivo* behavior, associated biological processes, and all other considerations affecting drug transport are ultimately lumped into these few parameters. Empirical model development follows a methodology referred to as top-down, where the model is strictly limited to the clinical data from which it was built with minimal predictive power in other clinical scenarios [16].

As an extension of fitted compartment models, the model structure may incorporate some basic knowledge of drug behavior and human physiology to better describe the ADME processes. These physiologically based models draw data from *in vitro* experiments as well as *in vivo* preclinical and clinical data as opposed to traditional data-fitting and to bottom-up approaches which advocate modeling entirely on a virtual basis. Kostewicz et al. classified PBPK modeling as a “middle out” approach, where the model is built and refined during the drug development process in an iterative manner as more *in vitro* and/or

in vivo data become available [17]. PBPK models no longer consider only model input (i.e. body weight, dose) and output (i.e. plasma concentration profiles) to establish model structure, but attempt to describe drug transport and behavior in a physiologically meaningful way. Physiologically based models have a wide range of mechanistic detail, ranging from minimal PBPK in which major physiological features of the body are grouped together based on defining characteristics (blood flow, tissue/blood partitioning, volume, etc.) to whole body PBPK models which have the ability to describe drug partitioning in specific tissues or organs [18,19]. Equally complex models are those that account for saturable processes such as active transport and enzyme kinetics [20,21], while the simplest form of a PBPK model exists as a single-organ, described by the well-stirred tank model [22]. This richness in information is precisely what gives PBPK models tremendous potential for robust simulations and suitability for development of personalized treatments, from the discovery phase through regulatory review.

Furthermore, PBPK models can combine deterministic and non-deterministic components to enable simulation of both individual pharmacokinetics and population variability. The deterministic component represents the biological and chemical systems of the body whereas the non-deterministic portion describes mathematically the uncertainty and variability for a given population [23]. The extent of model calibration depends on the objective of the model and rigor needed to capture individual and population dynamics.

1.3 Sourcing model input

Although PBPK modeling has come a long way due to the advancements in technology and computing power, the emergence of user-friendly software, and

improvements in *in vitro* methodologies, there is still a lengthy road before acceptance by pharmacologists and clinicians as a tool with the ability to replace clinical experiments. Much of the hesitancy towards physiologically based modeling originates from doubt regarding the degree of accuracy and reliability of its input. This skepticism is understandable since a PBPK model prediction is only as accurate as the quality of its input and the mechanisms described. Therefore, if the incorporated data contain errors, inconsistencies or miscalculations, the resulting simulations may not truly emulate *in vivo* conditions and performance. Inaccuracies in input arise from the high intrinsic variability of biological systems, imperfect experimental instrumentation, misinterpretation of collected data, knowledge gaps surrounding certain aspects of physiology and anatomy, or a fundamental misunderstanding of the drug compound [24,25]. Additionally, the severe lack of detailed databases for physiological parameters, requires input data to be drawn from several sources [26].

Often times, the available physiological information describes a generic population or an average physiology that is not truly representative of individual subjects [27]. Therefore, sourcing sufficient information to generate appropriate parameter subspaces to reflect the desired physiologies can be resource intensive, especially for highly specialized physiologies [28]. Studies aiming to tease out the effects of patient covariates on pharmacokinetics and pharmacodynamics require carefully designed protocols, highly controlled patient recruitment, and large populations considering inter-individual variability. Therefore, modeling dedicated to address specific subpopulations is a critical interest within the US FDA's Office of Clinical Pharmacology [29]. The literature contains several examples of pharmacokinetic models assessing clinical phenotype, sex, age, and

disease effects [17,26,30-35], paving the way towards reaching the ultimate goal of personalized or individualized medicine [36]. Yet, significant challenges remain for PBPK modeling for special populations due to limited experience to draw conclusions for the effects of pregnancy, ethnicity, geriatrics, obesity, and disease states on drug exposure [6,37,38].

While empirical compartment models rely directly on clinical data to statistically determine the model structure and input parameters [7,39], physiologically based pharmacokinetic models leverage physiological data determined *a priori* and independent of clinical data [40]. Therefore, a critical step in the development of pharmacokinetic models, particularly those that are physiologically based, involves a thorough analysis of the model inputs [41]. Parameter sensitivity and uncertainty analyses inform model development by explaining mechanisms contributing to variability in patient responses, identifying potential clinical consequences, and verifying assumptions [42]. Such analyses are highly informative when PBPK predictions are extrapolated to different populations, when the PBPK model poorly predicts clinical data, or when its development is based on limited experimental data [41]. In these scenarios, conducting a sensitivity analysis to establish the influence of certain parameters on the predicted drug exposure can help to understand the strength of the model [43-46]. The selection of a sensitivity method depends on several factors: (1) computational cost; (2) the ability to account for interactions amongst parameter inputs; (3) the ability to explain nonlinearities and non-monotonicities; (4) the ability to appropriately explore model input space; and (5) the ability to understand and apply the sensitivity results for model development and refinement [47].

1.4 Model parametrization for special populations

The success of PBPK modeling in personalized medicine relies heavily on proper identification of patient-specific covariates that explain the observed pharmacokinetic parameters of individuals or subpopulations of individuals [48,49]. Models are parameterized to explain physiological differences related to specific patient factors, such as sex differences, given sufficient data to describe the population of interest (i.e. male and female physiology) or to assess a complex clinical scenario (i.e. pregnancy). Depending on the complexity and flexibility of the model, system-dependent parameters (gastric emptying rate, gastrointestinal fluid pH, intestinal transit and mobility, secretion and reabsorption, intestinal blood flow, bile secretion rate, intake of food and fluids, etc.) can be adjusted to describe virtually any physiology or clinical condition [32]. In addition to intrinsic patient factors such as organ dysfunction, age, and genetics, physiologically based predictions can also reflect extrinsic influences such as drug-drug interactions, environmental effects, and lifestyle choices on absorption and drug disposition [6,50]. The following sections highlight the impact of sex and biological rhythms on PBPK model development, although several additional covariates exist beyond those discussed.

1.4.1 Sex

For the same dosing regimen, women may respond differently to therapies than males, both in regards to the effectiveness of a particular treatment as well as in the extent of observed adverse effects [51,52]. The occurrence of adverse events is 50 to 75% higher in females than males [53]. Sex differences in responses are not always consistently reported in clinical studies given the influence of sex hormones during development, the menstrual cycle and contraceptive use [54]. Fluctuating levels of hormones contribute to a

wider distribution in pharmacokinetic responses for females compared to males. Pregnancy further affects patient response [54]. As a result, females were typically excluded from Phase I and II clinical trials by the US FDA prior to 1993 because of the risk to unborn children and the influence of the menstrual cycle [55]. However, the inclusion of women into clinical studies has become a key consideration in the design of more recent studies given the high frequency of adverse events amongst female populations. The use of virtual or simulated clinical trials for proper dosage selection is especially favorable to sex-dependent pharmacokinetics, as this approach enables the evaluation of patient risk and benefit without engaging actual patients.

Females typically have reduced body weight relative to males. Thus, pharmacokinetic parameters (clearance, volume of distribution) and bioavailability are often normalized by body weight or body surface area to account for differences between male and female subjects. Many times sex-differences are minimized by this correction and deemed statistically insignificant [56]. However, corrections for anatomical differences are not always sufficient to eliminate sex differences completely in both animal and human studies [56-59]. Thus, physiological differences between sexes beyond body size drive these variations in the rates and extent of absorption and drug distribution, revealing sex-specific bioavailability patterns. Signaling pathways are believed to be structurally similar between males and females, but differentially expressed and regulated by sex hormones [55].

There are several documented physiological differences between sexes, such as gastrointestinal pH, transit time, and volume, along the gastrointestinal tract that drive differences in the bioavailability of oral dosage forms [53-55,60-63]. In general, the

influence of sex hormones can be separated into three considerations: (1) passive diffusion which is dependent on gastrointestinal tract physiology, (2) active transport which is affected by expression and activity of intestinal drug transporters such as P-glycoprotein, and (3) gut metabolism which is driven by expression and activity of gastric enzymes and cytochrome P450 isoforms (CYPs) located in enterocytes lining the gastrointestinal lumen [64]. Ultimately, these physiological differences drive the rate and extent of absorption from the gastrointestinal tract. Further sex differences are observed in transport protein expression due to regulation by sex hormones [34,54,65]. For example, P-glycoprotein (P-gp) is a plasma membrane-bound transporter, which is present in drug-eliminating organs, mainly the liver and to a lesser extent in the intestine [66,67]. Many drugs are substrates of P-gp and thus an important consideration for drug product development is understanding its influence on bioavailability [34,66,68]. This protein has higher expression in males [34,54,65]. Similarly, multidrug-resistant protein transporters (MRPs), organic anion transporters (OATs), and organic cation transporters (OCTs) exhibit sex-specific expression due to differential regulation by sex hormones [21,64]. Incorporation of enzyme and transporter activity into PBPK models is complex for general populations with even greater difficulty for sex-specific mechanisms where little to no data are available.

Similarly, the extent of plasma protein binding is also affected by sex hormones, driving wider distributions in female patient responses during menses [54,55,61]. Women also have a greater proportion of adipose tissue than men. As such, lipophilic drugs may accumulate and have a longer duration of action in women, requiring smaller doses to achieve the same therapeutic effect [53]. Metabolism also leads to variability between male and female oral bioavailability due to differing expression levels of hepatic enzymes

[53,69]. The isoforms of the cytochrome P450 (CYPs) or Phase I enzymes in the liver and intestine have marked differences in expression and activity between sexes, further affected by the menstrual cycle, oral contraceptive use, and pregnancy as a result of regulation by sex hormones [51,54,61-63,66,70]. Many marketed drugs are substrates for CYP3A4, which is the primary isoform of cytochrome P450, making this enzyme a key contributor to sex-dependent metabolism and ultimately drug clearance. Excretion also plays a role in personalized medicine due to the high variability in renal clearance between males and females. In general, renal clearance is known to be higher in men compared to women [53], decrease with age [10,71], correlate with body weight [72], and can be strongly impaired by certain diseases [73].

1.4.2 Circadian rhythms

Daily biological or circadian rhythms are recognized as another key contributor to pharmacokinetic variability in clinical studies. These effects are minimized by controlling the time and frequency of administration. Circadian influences on efficacy have been demonstrated for anticancer, cardiovascular, respiratory, anti-ulcer, anti-inflammatory, immunosuppressive, and antiepileptic drugs [74-85]. To date, several therapies have been synchronized with biological rhythms to maximize patient benefit and minimize risk [74,86]. As an example, the synchronization of corticosteroid therapy with the circadian pattern of various cytokines and hormones influencing rheumatoid arthritis disease activity has been well documented [87,88]. In general, chronopharmacokinetics studies the interdependent relationship between disease symptoms, risk factors, pharmacologic sensitivity, and ADME processes such that the action (or release) of the drug fluctuates with the circadian rhythm of the morbidity [86]. In addition to influencing the dose-exposure

relationship of a drug, circadian rhythms can affect the dose-response relationship and so time-of-day must be taken into consideration when modeling pharmacodynamics [89]. Circadian-driven variability is a result of fluctuations in several biochemical processes controlling absorption and drug disposition, leading to changes in physiology. Gastric pH, acid secretion, motility, and gastric emptying demonstrate circadian rhythms which influence absorption from the gastrointestinal tract [74,90,91]. In practice, tablets administered at night time were shown to have longer gastric residence times and longer colonic residence times than tablets administered during the day time due to patterns of bowel movement [17]. Blood flow, peripheral resistances to drug transport, and protein levels and binding also demonstrate fluctuations that alter distribution. Activity and rest periods relative to drug administration can also influence the distribution of the drug throughout the body [74]. Metabolism and elimination are altered by biological rhythms due to changes in perfusion, glomerular filtration rate, urine excretion rate, urine pH, and electrolyte balances [74,90,91]. Furthermore, circadian rhythms may modulate carrier-mediated transport activity significantly, leading to differences in absorption, intestinal metabolism, or even renal clearance [76,92,93].

Synchronization of drug concentration to rhythms in disease or morbidity activity is usually achieved by carefully timing administration of formulated tablets or through special drug delivery systems with controlled release profiles [94,95]. For example, lipophilic drugs are likely to absorb faster following morning administration relative to evening. Similarly, pharmacokinetic exposure is influenced by the extent of plasma binding which fluctuates differently for acidic or basic drugs [74]. Biological rhythms are likely more important for controlled-release formulations that result in sustained, rapid or

pulsatile release depending on time of administration relative to biological cycles [96]. Controlled release for oral dosage forms is achieved through various drug delivery mechanisms including layered systems, enteric coatings, and press coated systems [86]. Drug release from such systems can be predicted through PBPK modeling, considering the physicochemical properties of the drug, the *in vivo* release profile, and physiological state of virtual patients. Thus, PBPK modeling is a critical tool in chronopharmacokinetics to determine the influence of circadian rhythms on dose-exposure-response relationships by treating model input variables with time-dependent values in accordance with physiological changes associated with internal biological rhythms or environmental influences (i.e. light). Peng et al. successfully demonstrated how PBPK modeling could be utilized to predict the plasma concentration of melatonin, a compound with strong circadian rhythms [97]. This goal was achieved by de-lumping tissues (salivary and pineal gland) into individual compartments on the basis of strong circadian effects due to light. The model demonstrated how delivery of exogenous melatonin as a controlled release formulation could mimic the endogenous rhythms [97].

1.5 Outline of dissertation

Personalized medicine strives to deliver the ‘right drug’ at the ‘right dose’ by considering inter-person variability, one of the causes for therapeutic failure in specialized populations of patients. PBPK modeling is a key tool in the advancement of personalized medicine to evaluate complex clinical scenarios, making use of physiological information as well as physicochemical data to simulate various physiological states to predict the distribution of pharmacokinetic responses. Chapter 2 demonstrates how global sensitivity analysis can reveal physiologically meaningful relationships between model input and

pharmacokinetic output, and how this behavior is highly dependent on the parameter space, highlighting the importance of proper model calibration for accurate predictions. A 2-staged analysis will be applied to GastroPlus™, a commercially available physiologically based pharmacokinetic (PBPK) platform, using four different model compounds with unique physical chemical properties.

Chapter 3 shows how the underlying physiological mechanisms driving differences in pharmacokinetics across populations can be revealed using Monte Carlo simulations even when model input for the desired physiological states are not known *a priori*. Several statistical techniques, including a support vector machine, principal component analysis, and global sensitivity analysis, will be applied to study the isolated parameter subspaces for a compartment model. Simulations reveal unique parameter combinations are associated with male and female phenotypes, while individual parameters contribute to variability within each population. Chapter 4 demonstrates the importance of considering pharmacokinetics and pharmacodynamics simultaneously to achieve personalized medicine using chronopharmacology to demonstrate this concept. Finally, Chapter 5 extends these concepts by accounting for inter-sex and inter-individual variability to understand how the ‘right dose’ and ‘right time’ differs across individuals or patient subgroups.

Completion of this work enables an in-depth analysis of pharmacokinetic and pharmacodynamic models for the purpose of personalized medicine showing (1) how model behavior and variability in model output is highly dependent on the input parameter space, (2) how clinical phenotypes arises due to relationships in model input, (3) how drug exposure and response must be considered simultaneously to optimize patient safety, and

(4) how accounting for differences in underlying regulatory mechanisms across patient groups can further improve treatment options. Together, this work validates the understanding that personalized medicine can only be achieved when the interconnectivity between dose, drug exposure and response are recognized. The novelty of this work lies in how modeling and advanced statistical approaches are uniquely integrated to study the personalized medicine paradigm of delivering the ‘right drug’ at the ‘right dose’ at the ‘right time’.

CHAPTER 2: A framework for 2-stage global sensitivity analysis of GastroPlus™ compartment models

2.1 Introduction

In recent years, there has been a growing interest by the United States Food and Drug Administration (US FDA) and the European Medicines Agency (EMA) to include parameter sensitivity and uncertainty analysis in regulatory submissions containing physiologically based pharmacokinetic (PBPK) models [42,98,99]. Both the US FDA and EMA draft guidance documents state the need for proper regulatory assessment of the intended use and appropriateness of the model through parameter sensitivity analysis [42,98,99], but leave room for interpretation on the extent and timing as best practices have yet to be defined [100]. The draft guidelines recommend focusing on “parameters of concern” including experimentally determined parameters, parameters with discrepancies between reported values, and parameters that are difficult to estimate [99,101].

Sensitivity analyses for PBPK models often employ local One-At-a-Time (OAT) approaches in which sensitivity indices are reported as a change in the output relative to a small change in the input [23,43,102,103]. These local approaches are useful during model building and calibration to identify input factors which have the greatest influence on model predictions when simulated data do not match clinical observations [6,104], but are most effective when there is confidence in the model input [105,106]. In contrast, global methods place the sensitivity measures in the context of the multidimensional input space by accounting for the impact that other parameter values have on the resulting sensitivity measures and exploring model behavior through a scenario that better matches the

stochastic nature of pharmacokinetics and pharmacodynamics. Global sensitivity analysis can provide physiologically meaningful relationships between model input and variability in pharmacokinetic output, and are acceptable for use with models that have wide parameter ranges due to physiological variability [107]. Furthermore, local methods may not fully evaluate PBPK models as these approaches are not designed to explore nonlinear and complex behaviors [108,109], such as metabolism and the underlying physiology that leads to correlations between input parameters [43,110]. As such, global sensitivity methods are better matched to study PBPK models [111], especially as the complexity of the model increases throughout development [105]. These methods may reveal behaviors that are not obvious or intuitive, and would otherwise be missed by local methods [47]. Regulatory need for such an extensive analysis in submissions containing PBPK models remains undecided despite the additional insight provided by global analysis towards model behavior [100]. These methods have been successfully implemented in biomedical research [107,112-114] including several published PBPK models [43,115-117]. In general, the number of published models incorporating global sensitivity analysis has grown significantly over the last ten years [118].

Computational cost is often the limiting factor for the application of global methods, especially when the model contains hundreds of parameters [47]. Global sensitivity analyses, particularly decomposition of variance methods, are often not computationally feasible for large PBPK models. However, this challenge can be overcome by implementing a qualitative analysis to screen for unimportant factors before executing a computationally expensive methodology for variance decomposition [43,111,119-121]. Global screening methods are computationally advantageous compared to variance-based

approaches with fewer simulations required to evaluate parameter effects [122]. The Morris Method has been shown to be an effective screening design that enables both main and total effects to be studied, providing an overall indication of the presence of interactions, but not exact-order interactions [43,107,123,124]. Sobol's sensitivity method is a commonly used variance-based method that offers the advantage of exploring all orders of effects (primary, pairwise or higher-order interactions and total effects) while also being amenable to sophisticated sampling strategies [122]. Both the Morris and Sobol Methods are independent of the model structure and assumptions related to linearity or monotonicity [107,125].

Although the US FDA does not enforce the use of a commercial PBPK software [98], global sensitivity analysis will be applied to GastroPlus™, a well-established and widely accepted platform across academia and industry. GastroPlus thoroughly incorporates physiological understanding and first principles to predict drug exposure for several species (human, monkey, dog, etc.) in both the fasted and fed states. GastroPlus uses the Advanced Compartmental Absorption and Transport (ACAT) model to study the absorption of orally administered drugs, coupling this highly sophisticated mechanistic model to either a compartmental model (basic distribution model) or a whole-body PBPK model for in-depth analysis in individual tissues or organs [126]. The granularity by which gastrointestinal physiology and absorption processes are mathematically described in the ACAT model is a key advantage of using GastroPlus. Given the ability of this model to describe several processes in parallel, global sensitivity analysis is well-suited to study the behavior of GastroPlus. Currently, the software contains a built-in local parameter sensitivity tool [126], but to our knowledge, global sensitivity analysis has not been

performed for this platform. Consequently, the objective of the current study is to establish a framework for 2-stage global sensitivity analysis of GastroPlus using the Morris and Sobol Methods. The analysis will be demonstrated for four drugs (acetaminophen, risperidone, atenolol, and furosemide) to show how parameterization of physiochemical properties can influence the relationships between model input and output according to the Biopharmaceutical Classification System (BCS).

2.2 Global sensitivity methods

2.2.1 Morris method

The Morris Method sensitivity measures are calculated from the elementary effects, which are obtained by taking a step in the input space and then determining the corresponding change in model output. The elementary effect (EE_i) is calculated by **Equation 1**, where $Y(x_1, \dots, x_k)$ and $Y(x_1, \dots, x_{i-1}, x_i + \Delta_i, x_{i+1}, \dots, x_k)$ are the model outputs associated with the parameter sets before and after a step change in the x_i coordinate while all other parameters remain the same. As such, the Morris Method is a one-at-a-time approach to global sensitivity. The difference in model output is taken relative to the difference in parameter values (Δ_i) when scaled from 0 to 1, enabling the elementary effects to be compared across factors with different orders of magnitude.

$$EE_i = \frac{Y(x_1, \dots, x_{i-1}, x_i + \Delta_i, x_{i+1}, \dots, x_k) - Y(x_1, \dots, x_k)}{\Delta_i} \quad \text{Eq. 1}$$

The elementary effects are calculated for several starting points (or samples) within a defined input space. The average elementary effect for a set of r samples is referred to as μ , and is an indicator of the direct influence that an input factor has on the model output

(**Equation 2**). The effect of nonlinearities and interactions between input parameters is determined by calculating the variance (σ^2) in elementary effects across samples (**Equation 3**). When a model is non-monotonic due to the presence of parameter interactions or nonlinear behavior, using μ to rank parameters in order of significance may result in a Type II error; that is, the failure to capture a parameter that has a significant influence on the model output [127]. Thus, a third sensitivity measure, μ^* , was proposed using the absolute values of the elementary effects (**Equation 4**). When μ and μ^* are similar, the model output is monotonic with respect to that parameter, indicating the absence of nonlinearities and parameter interactions. When μ^* is greater than μ , elementary effects have opposing signs across samples, indicating the presence of nonlinearities and/or interactions with respect to that parameter [119]. Therefore, the sensitivity measure μ^* is an indicator of the total effects associated with each parameter, and may serve as a surrogate for the variance-based methods when computational efficiency is a concern [127].

$$\mu_i = \frac{1}{r} \sum_{j=1}^r EE_i^j \quad \text{Eq. 2}$$

$$\sigma_i^2 = \frac{1}{r} \sum_{j=1}^r (EE_i^j - \mu_i)^2 \quad \text{Eq. 3}$$

$$\mu_i^* = \frac{1}{r} \sum_{j=1}^r |EE_i^j| \quad \text{Eq. 4}$$

The computational cost for the Morris Method is $N_t = r(k + 1)$ where N_t is the total number of simulations, r is the number of samples, and k is the number of studied parameters [124].

2.2.2 Sobol sensitivity analysis

The Sobol Method quantitatively relates the contribution of each parameter and interactions between parameters to the overall variability in model output [119,128,129]. The sensitivity coefficient for the first-order effect of parameter x_i is given by **Equation 5** and describes the expected reduction in variance when x_i is fixed relative to the total variance in model output, $V(Y)$, given by **Equation 6** [129]. The inner expectation operator corresponds to the mean scalar model output, Y , taken while all factors but x_i are varied (denoted by X_{-i}). The outer variance is then determined over all possible values of x_i . The sensitivity measure calculated by **Equation 5** indicates the contribution that varying x_i has directly on output variability.

$$S_i = \frac{V_{x_i} \left(E_{X_{-i}}(Y|x_i) \right)}{V(Y)} \approx \frac{\frac{1}{N} \sum_{j=1}^N f(\mathbf{B})_j \left(f(\mathbf{A}_B^{(i)})_j - f(\mathbf{A})_j \right)}{V(Y)} \quad \text{Eq. 5}$$

$$V(Y) = V_{x_i} \left(E_{X_{-i}}(Y|x_i) \right) + E_{x_i} \left(V_{X_{-i}}(Y|x_i) \right) = \frac{1}{N} \sum_{j=1}^N f(\mathbf{A})_j^2 - \left(\frac{1}{N} \sum_{j=1}^N f(\mathbf{A})_j \right)^2 \quad \text{Eq. 6}$$

The sensitivity coefficient for the total effects of parameter x_i is given by **Equation 7** and corresponds to the expected variance remaining if all factors but x_i are fixed relative to the total variance in model output [129]. The mean variance in model output (Y) is determined when all factors but x_i are fixed, over all possible values of X_{-i} . These sensitivity coefficients represent the total contribution that x_i has on the model output variability, that is its direct or first order influence (given by S_i) and the additional contribution due to parameter interactions involving x_i .

$$S_{Ti} = \frac{E_{X_{\sim i}} \left(V_{x_i} (Y | \mathbf{X}_{\sim i}) \right)}{V(Y)} \approx \frac{\frac{1}{2N} \sum_{j=1}^N \left(f(\mathbf{A})_j - f(\mathbf{A}_B^{(i)})_j \right)^2}{V(Y)} \quad \text{Eq. 7}$$

The sensitivity coefficient for the combined total effect of a parameter pair, x_i and x_j , is given by **Equation 8** and describes the expected variance that would remain if all parameters but x_i and x_j were fixed relative to the total variance in model output [129]. The total effect for a parameter pair is used to determine the contribution of all parameter interactions involving x_i and x_j by removing the first order effects as shown in **Equation 9**. Since higher-order interactions are generally negligible, these coefficients are interpreted as describing the portion of variability attributed primarily to the second-order or pairwise interaction between x_i and x_j . For that reasoning, the values calculated by **Equation 9** are referred to as the second-order sensitivity measures in this manuscript.

$$S_{Tij} = \frac{E_{X_{\sim ij}} \left(V_{x_i x_j} (Y | X_{\sim ij}) \right)}{V(Y)} \approx \frac{\frac{1}{2N} \sum_{w=1}^N \left(f(A_B^{(i)})_w - f(A_B^{(j)})_w \right)^2}{V(Y)} \quad \text{Eq. 8}$$

$$S_{ij} = S_{Tij} - S_i - S_j \quad \text{Eq. 9}$$

In practice, the sensitivity coefficients are computed simultaneously from a single set of simulations using estimators of the variance operators and expectation operators that have been established as the most computationally efficient, requiring the fewest number of samples to uniformly explore the input domain [129]. Briefly, these estimators rely on the triplet matrices $(\mathbf{A}, \mathbf{B}, \mathbf{A}_B^{(i)})$ as indicated by the approximations in **Equations 5, 7, and 8**. First, a sampling space of $(N \times 2k)$ is created using Sobol's quasi-random sampling algorithm to generate parameter values, where N is the number of samples and k is the

number of studied parameters. This sample space is then separated into two matrices each with dimensions of $(N \times k)$ where the left half corresponds to the base matrix (**A**) and the right half to the auxiliary matrix (**B**). Next, the resampling matrices [$\mathbf{A}_B^{(i)}$] are generated by replacing the i^{th} column of Matrix **A** with the corresponding Column of Matrix **B** such that there are k resampling matrices. Because the uniformity of the samples within each column decreases as the number of sampled parameters increases, Matrix **A** is considered more uniformly distributed than Matrix **B**, and so the selected estimators rely on Matrices **A**, $\mathbf{A}_B^{(i)}$, and **B** rather than Matrices **A**, $\mathbf{B}_A^{(i)}$, and **B** [129]. Each row in Matrices **A**, $\mathbf{A}_B^{(i)}$, and **B** corresponds to a parameter set for which the model is evaluated, indicated by $f(\mathbf{A})$, $f(\mathbf{A}_B^{(i)})$, and $f(\mathbf{B})$. Readers are directed to [129] for additional details related to development of **Equations 5-9**. Computational cost for the Sobol Method is $N_t = N(k + 2)$ where N_t is the total number of simulations, N is the number of samples, and k is the number of evaluated parameters.

2.3 Approach

2.3.1 GastroPlus setup for selected drugs

Four model compounds were selected based on the Biopharmaceutical Classification System (BCS) for orally administered drugs: acetaminophen (I - high solubility/high permeability), risperidone (II - low solubility/high permeability), atenolol (III - high solubility/low permeability), and furosemide (IV - low solubility/low permeability). Chosen drugs were not intended to describe the exact behavior of each drug class, but to show variability in model sensitivities for drugs with different physicochemical properties. All simulations were performed using GastroPlus™ Version

9.0. The ACAT model was set to “Human – Physiological – Fasted”, which described the fasted state physiology of the human gastrointestinal tract. The Absorption Scale Factor (ASF) model was set to the default option: “Opt logD Model SA/V 6.1”. Default ASF coefficients were used except for risperidone for which the ASF Coefficient C_2 was adjusted until the calculated t_{\max} matched clinical data. Drug-specific GastroPlus input is provided in the **Supplementary Table 1**. Unless noted, the physicochemical properties were predicted by the GastroPlus ADMET Predictor™. Default settings for particle size were assumed for all drugs.

Pharmacokinetic compartmental model parameters were sourced from literature. Clinical data were extracted from their respective sources using the WebPlot Digitizer online application (<http://arohatgi.info/WebPlotDigitizer/>). To ensure the baseline predictions sufficiently described clinical data, the GastroPlus models were calibrated based on the US FDA criteria for bioequivalence [130]. For acetaminophen, the parameters were used directly as reported in the clinical study [131], requiring no further calibration of the GastroPlus model. For risperidone, a 3-compartment model was determined using PKPlus™. The calculated clearance and central compartment volume were adjusted by the reported bioavailability of 70% [132]. First-pass extraction in the liver was also considered for risperidone (fitted using GastroPlus) to ensure the predicted bioavailability matched clinical data. For atenolol, a 2-compartment model was fitted to the clinical data. The reported clearance ($CL/F = 15.2$ L/h [133]) was adjusted using an estimated bioavailability of 72% given intravenous data from Mason et al. [134], and then used to determine the central compartment volume. For furosemide, an acceptable prediction was obtained using

the renal clearance for healthy subjects in the population study and the reported parameters for the 3 compartment model [135].

2.3.2 Morris Method for GastroPlus

The Morris Method was performed for all four drugs with 42 ACAT model parameters and 4 ASF model coefficients. Correlations between small intestine subcompartments were considered such that the jejunum 1 pH, total length of the small intestine, nominal radius of the small intestine, and the total transit time of the small intestine were sampled and then used to calculate the parameter values of the other small intestine subcompartments accordingly. All other parameters within the ACAT model were sampled independently. The number of pharmacokinetic compartment parameters included in the Morris Method varied slightly depending on the structure of the pharmacokinetic model sourced from the literature (2 or 3 distribution compartments) as well as the inclusion of any known drug behaviors (i.e. first-pass extraction or renal clearance). As such, the total number of parameters included in the Morris Method varied from $k = 54$ to 57 parameters. For acetaminophen, the Morris Method was performed using $r = 1, 2, 5, 10, 20, 30,$ and 40 samples to understand how the sample space influenced the resulting sensitivity measures. Computational cost for acetaminophen ($k = 55$) varied from 56 to 2,240 simulations depending on sample size. For all other drugs, twenty samples were used for the Morris Method with computational cost varying from 1,100 simulations ($k = 54$) to 1,160 simulations ($k = 57$). Sampling bounds were set to $\pm 20\%$ of the baseline values and were not based on physiology for the preliminary exploration of the GastroPlus model.

An advanced sampling strategy for global sensitivity analysis guaranteed the input space was thoroughly studied while minimizing the number of samples required to do so

[127]. Sobol's quasi-random sampling algorithm was selected due to its ability to uniformly sample the unit hypercube by minimizing sample discrepancy and maximizing the distance between sampling points [136]. Thus, quasi-random sequences required fewer samples to fill the hypercube than random sampling methods for improved computational efficiency. Sampling was performed using MATLAB® R2017a with the commands 'sobolset', 'scramble', and 'net' to generate and scramble the initial quasi-random Sobol unit hypercube before selecting r samples [137,138]. The Matousek-Affine-Owen algorithm was added to reduce the likelihood of correlations between samples through a random linear scramble and digital shift of the initial Sobol set [139,140]. The scrambler ensured independent parameter sets were obtained for replicate calculations of sensitivity measures to confirm whether the sampling conditions were appropriate to cover the input domain and to evaluate the robustness of the Morris Method. It should be noted that the sampling method did not account for the probability of certain parameter combinations occurring at higher frequencies [141].

The maximum concentration (C_{\max}), the time to maximum exposure (t_{\max}), and the area-under-the-curve (AUC_{0-t}) were used as model output to calculate sensitivity measures, consistent with sensitivity analyses for other PBPK models [142-144]. Sensitivity measures for the maximum concentration and AUC_{0-t} provided an indication of the underlying physiology affecting maximum and cumulative drug exposure of orally administered drugs while t_{\max} offered insight into which parameters affected the rate of appearance in systemic circulation. Factors with μ^* greater than 10% of the maximum value for each model output were considered to have a significant effect on that output. Significance was based on μ^* because this measure accounted for parameter interactions.

2.3.3 Sobol sensitivity analysis for GastroPlus

Given the number of parameters included in the GastroPlus model, only the important factors determined by the Morris Method were explored further using the Sobol Method while all unimportant parameters were fixed at the baseline values. The Sobol sensitivity analysis utilized the same sampling method as described for the Morris Method, and considered the same model output for comparison between methods. For the Sobol Method, the sampling bounds were set to $\pm 20\%$ of the baseline values. Parameters were considered significant if sensitivity measures were greater than 0.05 [128], corresponding to at least 5% of the variability explained by a given parameter and/or its interactions.

The number of samples (N) required for convergence of the Sobol sensitivity analysis depended on the model complexity and the number of parameters considered for analysis. Convergence was determined using confidence intervals for the sensitivity indices derived from the bootstrap method. Convergence was achieved when the 95% confidence interval represented less than 10% of the calculated sensitivity index for the most sensitive parameters, consistent with the methods reported by others [120,145,146]. Furthermore, the sensitivity results for GastroPlus met the following criteria for non-additive models with interactions: (1) $S_{ti} > S_i$, (2) $\sum S_i < 1$, and (3) $\sum S_{ti} > 1$ [119,120]. The first criterion held true due the fact that S_{ti} is the sum of direct effects (S_i) and non-zero interactions between parameters. The second criterion indicated that the variability in model output was not apportioned to only direct effects. The third criterion accounted for the fact that S_{ij} and any non-zero higher-order interactions were accounted for in the total effects of multiple parameters. The number of samples varied from 3,000 to 5,000 depending on the number of parameters and the drug evaluated by the Sobol Method.

2.3.4 Development of the automated GastroPlus framework

Given the number of simulations required to perform global sensitivity analysis for GastroPlus, particularly for the Sobol Method, management of the GastroPlus input and output needed to calculate the sensitivity measures was not feasible manually. As such an integrated framework was developed to enable GastroPlus to interface with MATLAB. The framework for GastroPlus facilitated the efficient transfer of parameter values into the GastroPlus interface for thousands of simulations, and transfer of GastroPlus output back to MATLAB for rapid integration with downstream analysis of model predictions and calculation of sensitivity measures. AutoIt was used to automate GastroPlus by replicating the keystrokes, mouse movements, and window/tab manipulations needed to run simulations in the user interface. In this manner, GastroPlus was transformed into a callable function by MATLAB, enabling the commercial software to be incorporated into a broader modeling framework without any modification to the GastroPlus software. The integrated framework for global sensitivity analysis of the GastroPlus model is given in **Figure 1**. The framework was structurally the same for both stages of global sensitivity analysis, requiring the number of samples (r or N), parameters studied (k), and sensitivity calculations (μ , σ^2 and μ^* or S_i , S_{ij} and S_{ii}) to be updated to reflect the use of the Morris or Sobol methods.

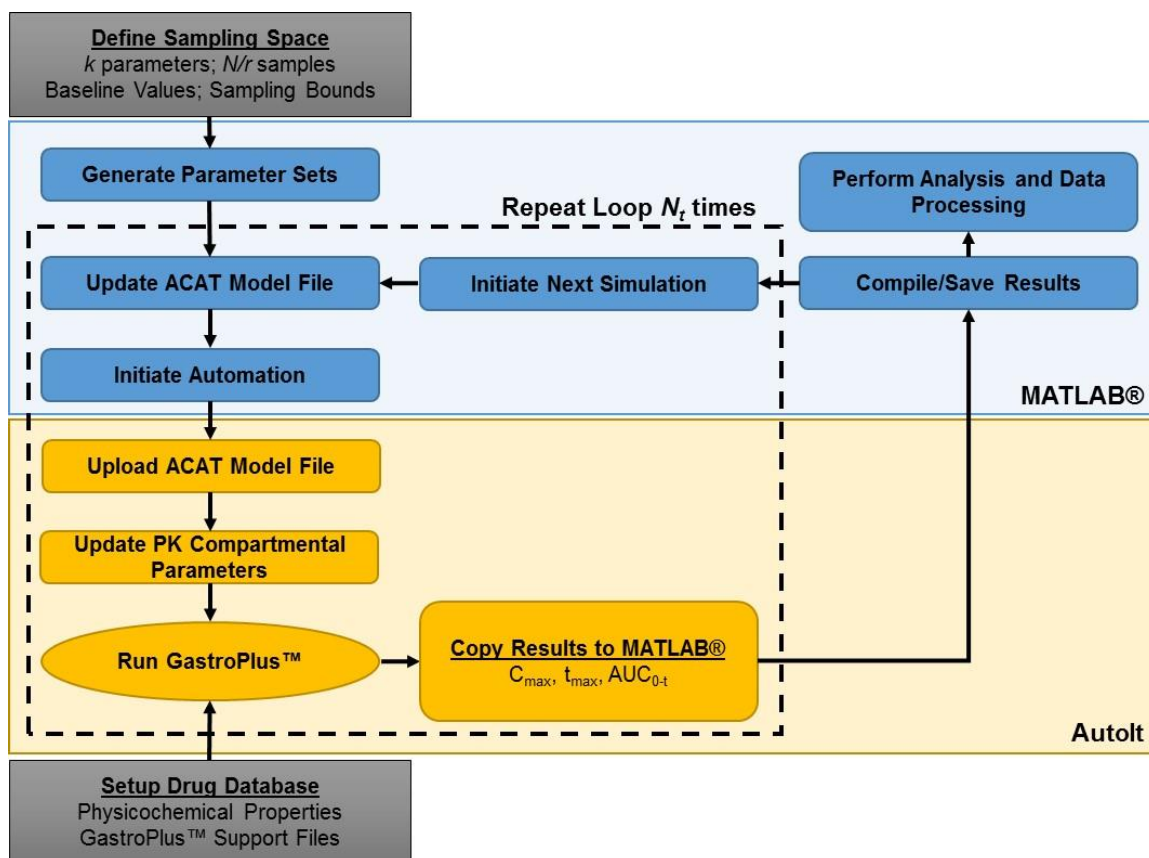


Figure 1: Automated GastroPlus framework for global sensitivity analysis. GastroPlus parameter sets were generated in MATLAB and then AutoIt was used to update the parameters in the GastroPlus interface according to the sample space, to run simulations for each parameter set, and to transfer GastroPlus predictions back to MATLAB for calculation of sensitivity measures.

The automation framework was deployed using Intel® Xeon® E5-1620 v3 @ 3.50GHz and Intel® Core™ i5-6600 @ 3.30GHz processors. On either computer, the total time per iteration was approximately 30 seconds, which encompassed the time to update the ACAT model file through transferring GastroPlus results back to MATLAB for each simulation. The time for each analysis is given in **Supplementary Table 2**.

2.4 Results

GastroPlus was calibrated against clinical data for acetaminophen, risperidone, atenolol, and furosemide prior to implementing global sensitivity for each of these drugs.

Baseline predictions are given in the **Supplementary Figure 1**, showing the GastroPlus models described the clinical data reasonably well.

Global sensitivity was implemented in two stages using the Morris Method followed by the Sobol Method for each drug. As part of screening, the suitability of the Morris Method for GastroPlus was assessed by grouping model input according to Absorption-Distribution-Metabolism-Elimination (ADME) processes to understand whether the sensitivity analysis was broadly aligned with physiological understanding. Furthermore, the influence of the sampling space on the resulting sensitivity measures, and thus the interpretation of results, for the Morris Method was evaluated using different sampling bounds to understand how the input space could influence screening and the identified relationships between model input and output.

2.4.1 Stage 1: Screening for significant parameters

2.4.1.1 Selection of sample size for the Morris Method

The ability of the Morris Method to rank parameters reproducibly and determine those with the greatest influence using different sampling sizes (r) was evaluated for acetaminophen. Sensitivity measures were determined for three independent sample sets at each r as shown in **Figure 2** for C_{\max} and in **Supplementary Figure 2** and **Supplementary Figure 3** for t_{\max} and AUC_{0-t} , respectively. The number of samples used in the Morris Method had limited influence on the resulting sensitivity measures when sampling bounds were $\pm 20\%$, with μ^* and σ (standard deviation of μ^* across triplicate analyses) stabilizing at 20 samples. These sampling conditions were also selected for use with the risperidone, atenolol, and furosemide GastroPlus models, which indicated similar

robustness to sample size (data not shown). Optimization of sample size guaranteed that the randomly selected samples from the Sobol quasi-random point set in MATLAB were sufficient to minimize the likelihood of Type I or II errors during screening. The use of $r = 20$ in the Morris Method ensured all significant parameters were identified for further evaluation by the Sobol Method when the sampling bounds were $\pm 20\%$.

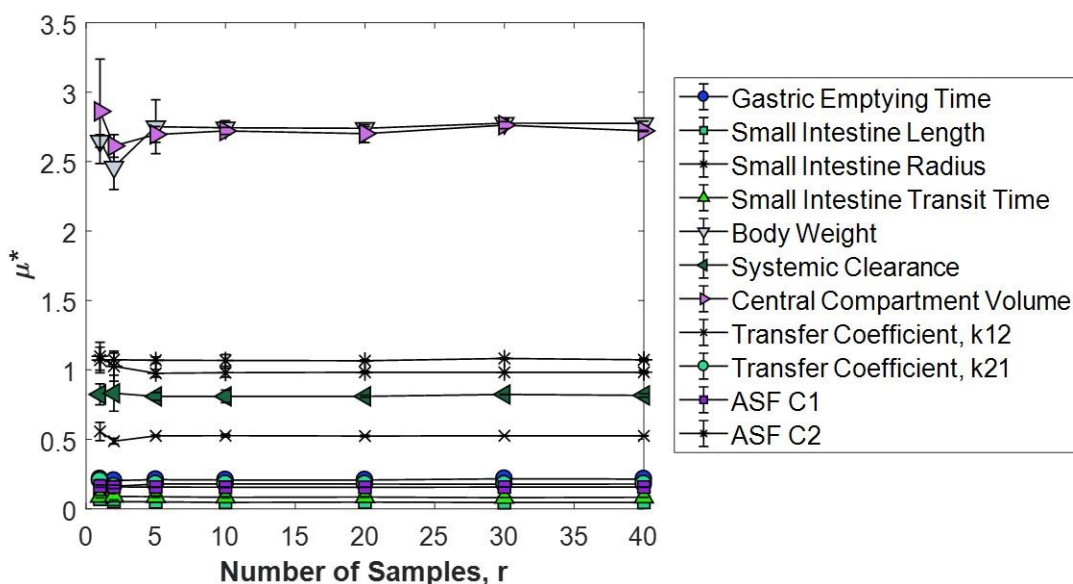


Figure 2: Morris Method results for acetaminophen C_{\max} using $r = 1$ to 40 and sampling bounds of $\pm 20\%$. The error bars represent the standard deviation in μ^* from 3 independent analyses at each sample size.

2.4.2 Identification of significant GastroPlus parameters by the Morris Method

Representative Morris Method results for acetaminophen, risperidone, atenolol, and furosemide using sampling bounds of $\pm 20\%$ and $r = 20$ are given in **Figure 3** and **Figure 4** for μ^* values associated with C_{\max} . Morris Method results for t_{\max} and AUC_{0-t} are given in **Supplementary Figure 4** to **Supplementary Figure 7**. These results demonstrated that sensitivity was apportioned to a subset of GastroPlus parameters which varied both in the number of sensitive parameters as well as the relative ranking of parameters across model outputs and for each drug.

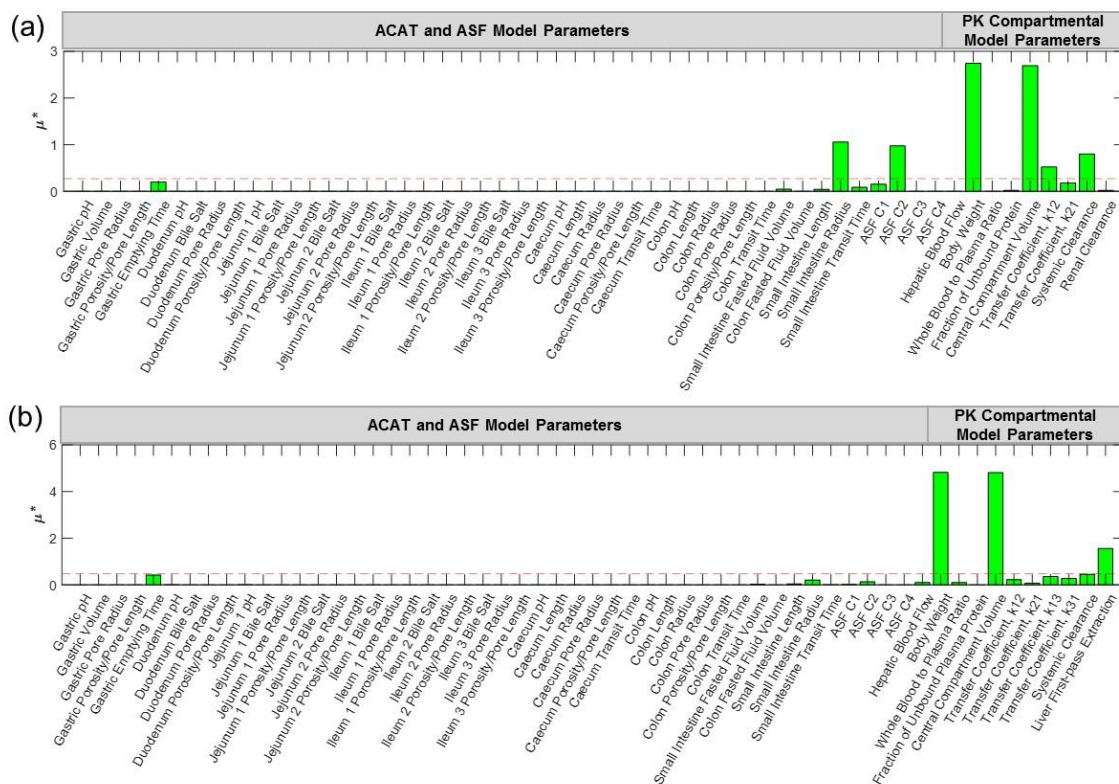


Figure 3: Representative Morris Method results for acetaminophen and risperidone C_{max} . The values of μ^* were determined using $r = 20$ and sampling bounds of $\pm 20\%$. The cutoff for significance (indicated by dotted red line), corresponded to 10% of the maximum μ^* for C_{max} associated with each drug.

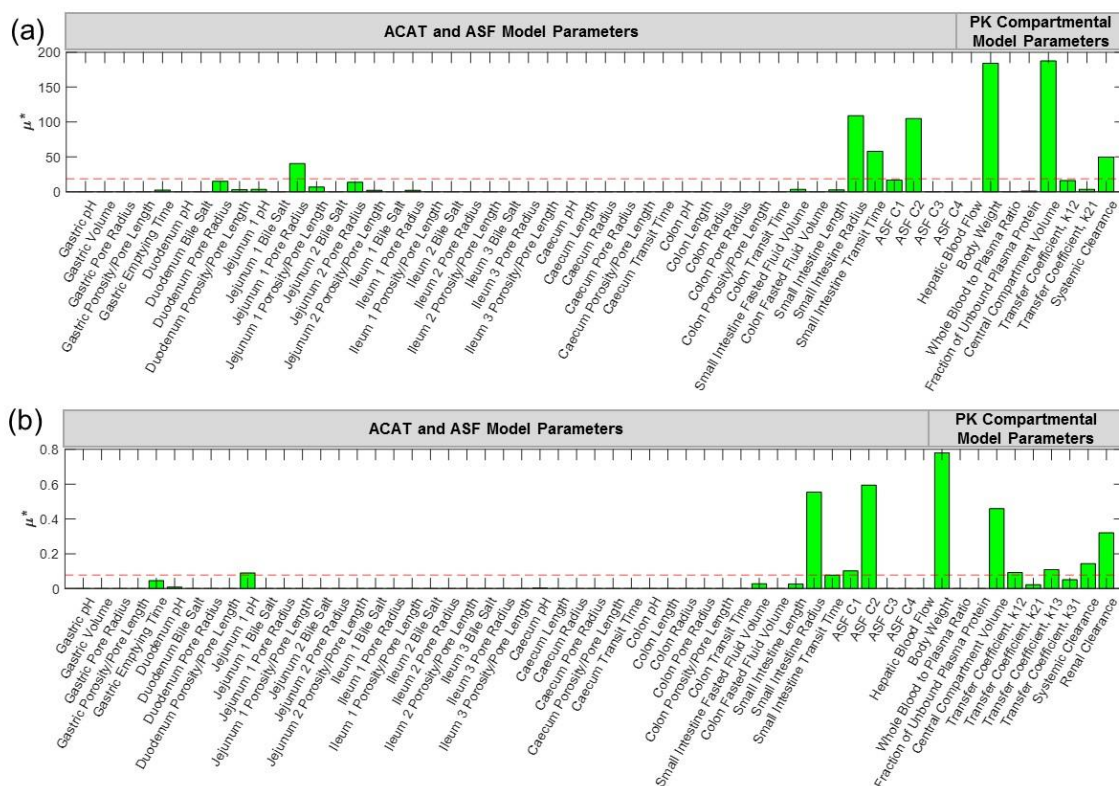


Figure 4: Representative Morris Method results for atenolol and furosemide C_{max} . The values of μ^* were determined using $r = 20$ and sampling bounds of $\pm 20\%$. The cutoff for significance (indicated by dotted red line), corresponded to 10% of the maximum μ^* for C_{max} associated with each drug.

The significant parameters based on μ^* for each drug are summarized in **Table 1**. Many significant parameters were common to all drugs, regardless of its physicochemical properties, such as the gastric emptying time, small intestine radius, and ASF C2, as well as compartmental model parameters. For poorly permeable drugs (atenolol and furosemide), additional ACAT model parameters related to the small intestine were also significant, while only the gastric emptying time and small intestine radius were significant for highly permeable drugs (acetaminophen and risperidone). Fasted fluid volume, length, and transit time were significant for both atenolol and furosemide, whereas pore radius and porosity per pore length were only important for atenolol, and gastrointestinal pH was significant for furosemide. Across all four drugs, the significant ACAT and ASF model

parameters were primarily associated with the stomach and small intestine compartments, corresponding to the fact that these formulations were modeled as immediate release and the primary site of absorption was the upper region of the gastrointestinal tract. Thus, parameters related to the caecum and colon were largely insignificant. Body weight, systemic clearance, central compartment volume, and transfer coefficients were significant for all drugs, while the significance of other pharmacokinetic parameters varied. The significance of transfer coefficients (k_{12} , k_{21} , k_{13} , and k_{31}) supported the need for at least one compartment to describe drug distribution to peripheral tissues.

Table 1: Significant parameters determined by the Morris Method for the GastroPlus models

GastroPlus Parameters		Acetaminophen	Risperidone	Atenolol	Furosemide
ACAT Model	Gastric Emptying Time	+	+	+	+
	SI Radius	o, +, x	+	o, +, x	o, +, x
	SI Fasted Fluid Vol.	[]	[]	+	+
	SI Length	[]	[]	+	+
	SI Transit Time	[]	[]	o, +, x	o, +, x
	Duodenum Pore Radius	[]	[]	+	[]
	Duodenum pH	[]	[]	[]	+
	J1 Pore Radius	[]	[]	o, +, x	[]
	J1 Porosity/Pore Length	[]	[]	+	[]
	J1 pH	[]	[]	[]	o
	J2 Pore Radius	[]	[]	+	[]
Colon pH	[]	[]	[]	x	
ASF Model	ASF C1	+	[]	+	o, +
	ASF C2	o, +, x	+	o, +, x	o, +, x
Compartment Model	Body Weight	o, +, x	o, +, x	o, +	o, +, x
	Systemic Clearance	o, +, x	+, x	o, +, x	o, +, x
	Central Compartment Vol.	o, +, x	o, +, x	o, +	o, +
	Transfer Coefficient, k ₁₂	o, +, x	[]	+	o
	Transfer Coefficient, k ₂₁	+, x	[]	[]	[]
	Transfer Coefficient, k ₁₃	NA	+	NA	o
	Transfer Coefficient, k ₃₁	NA	+	NA	+
	Hepatic Blood Flow	[]	+	[]	[]
	Whole Blood to Plasma Ratio	[]	+	[]	[]
	Renal Clearance	[]	NA	NA	o, +, x
Liver First-pass Extraction	NA	o, x	NA	NA	

Abbreviations: SI = Small intestine; J1 = Jejunum 1; J2 = Jejunum 2; Vol. = Volume

Symbols: o = C_{max}; + = t_{max}; x = AUC_{0-t}; [] = No significant output; NA = Not Applicable

2.4.3 Morris Method results in the context of ADME processes

To validate the observed relationships between model input and output, the sensitivity measures determined by the Morris Method were organized according to ADME properties to evaluate how the GastroPlus model responded to parameterization of drug-

specific physicochemical properties. Sensitivity measures were separated into three groups describing absorption, distribution, and excretion (including metabolism and elimination) to determine the pooled effect of each biological process on the model output as shown in **Figure 5**. GastroPlus parameters included in each group are given in **Supplementary Table 3**. Sensitivity measures were determined for each parameter individually (see previous section) and then pooled to determine the total significance as opposed to determining the grouped effects directly, which risked concealing the significance of parameters with opposing influences [119]. Distribution-related parameters had the greatest influence on C_{\max} for highly permeable drugs while both absorption and distribution parameters had similar significance for the C_{\max} of poorly permeable drugs. The t_{\max} values for acetaminophen and furosemide were primarily driven by absorption-related parameters, while the t_{\max} values for risperidone and atenolol were affected by both absorption and distribution parameters. Interestingly, the Morris Method results revealed different physiological processes across C_{\max} and t_{\max} , despite the relationship between these model outputs. Together C_{\max} and t_{\max} provided an indicator of parameters influencing both the rate and/or extent of absorption. For highly permeable drugs formulated as immediate release, absorption was both rapid and complete, such that drug transport by way of the portal vein to the liver and finally systemic circulation would be the rate-limiting steps to maximum exposure. For poorly permeable drugs, gastrointestinal physiology would have a greater influence on the rate and extent of absorption. The relationship between input parameters and AUC_{0-t} was less clear across the four drugs. For risperidone, systemic clearance and first-pass extraction in the liver were the primary indicators of AUC_{0-t} . First-pass extraction was not considered for the other drugs included

in the study, which may have contributed to the differences observed with risperidone relative to acetaminophen, atenolol, and furosemide. For all four drugs, the time scale for elimination was far longer than absorption when treated as immediate release. Yet, the AUC_{0-t} was significantly influenced by more than just elimination-related parameters, such as systemic clearance, and instead showed contributions across all ADME processes for drugs of very different physicochemical properties. These results reflected the complicated structure of the GastroPlus model and its ability to capture several physiological processes in parallel.

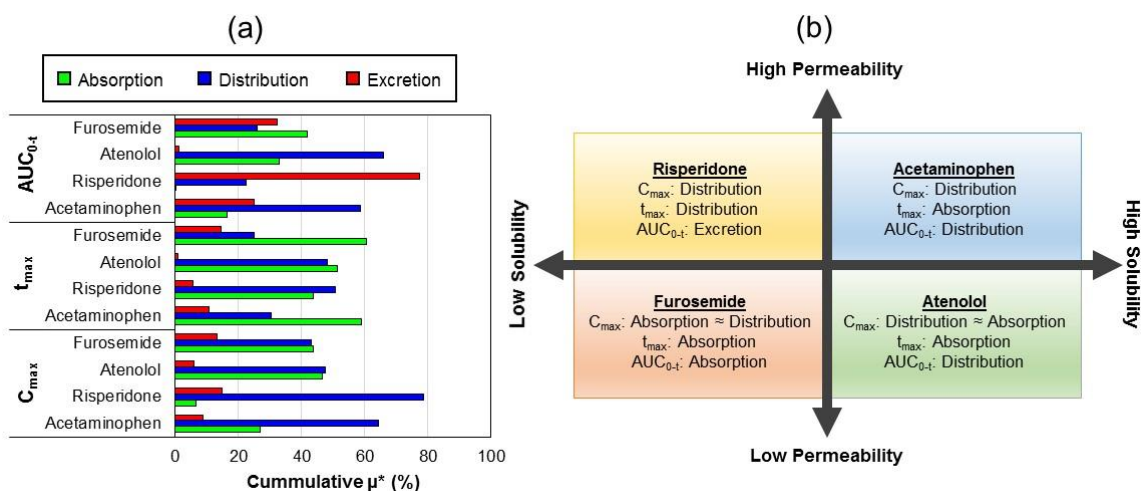


Figure 5: Influences of ADME processes according to the Morris Method. The percent contributions in (a) were determined by the sum of μ^* associated with parameters in each group relative to the sum of all μ^* for all groups. These contributions were then used to identify the key process influencing each model output in (b). Parameters contained in each group are provided in Supplementary Table 3.

2.4.4 Stage 2: Quantitative assessment of output variability

Considering that sensitivity measures do not converge at the same number of samples for all model outputs and an algorithm to determine the number of samples needed for convergence *a priori* does not exist, the Sobol Method was performed only for those parameters that were significant for C_{max} . The 2-stage approach to global sensitivity

analysis resulted in a reduction in computational cost by at least 86% for acetaminophen, 92% for risperidone, 84% for atenolol and 78% for furosemide compared to studying over 50 parameters directly by the variance-based method.

2.4.5 Sobol Method for acetaminophen

Six significant parameters for acetaminophen C_{\max} based on the Morris Method were further evaluated by Sobol sensitivity analysis using 4,000 samples, requiring a total of 32,000 simulations. Sensitivity measures are given in **Figure 6**. The calculated values met the criteria for convergence (see Methods section), indicating that 4,000 samples were sufficient to perform the analysis. Body weight was the most significant parameter for acetaminophen C_{\max} , followed closely by the central compartment volume. Together, body weight and the central compartment volume explained approximately 85% of the variability in C_{\max} with relatively low contributions from their interactions. While small intestine radius, ASF C2, k_{12} , and systemic clearance had negligible first-order effects on C_{\max} ($S_i < 0.05$), the small intestine radius and ASF C2 indicated significant interactions with other parameters and the most significant between these two parameters. Small intestine radius and ASF C2 influenced the rate and amount of drug absorbed and transferred to the central compartment, interacting with the compartmental model parameters to influence the calculated plasma concentration. All other interactions were negligible.

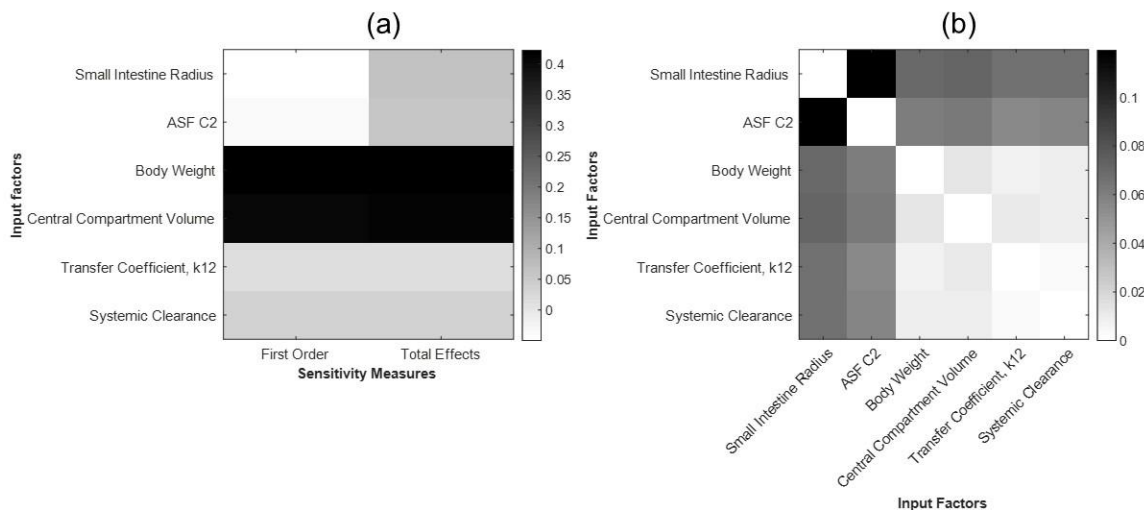


Figure 6: Sobol Method for acetaminophen C_{max} . The sensitivity measures were determined using $N=4,000$ for parameters identified by the Morris Method based on μ^* . The first-order and total effects are given in (a). The second-order interactions are given in (b).

2.4.6 Sobol Method for risperidone

Significant parameters for risperidone C_{max} identified by the Morris Method were assessed by the Sobolj Method using 3,000 samples and a total of 15,000 simulations, which was sufficient for method convergence. Sensitivity measures are provided in **Figure 7**. Similar to the results for acetaminophen, body weight was the most significant parameter for risperidone C_{max} , followed by the central compartment volume, with the strongest interaction between these parameters. Together, these parameters explained approximately 90% of the variability in C_{max} . While the fraction of first-pass extraction in the liver had negligible first-order effects ($S_i < 0.05$), approximately 5% of the variability in C_{max} ($S_{ii} \approx 0.05$) was attributed to interactions with this parameter. First-pass extraction in the liver accounted for drug loss in the central compartment due to metabolism, interacting with both the central compartment volume and body weight to influence the calculated plasma concentration.

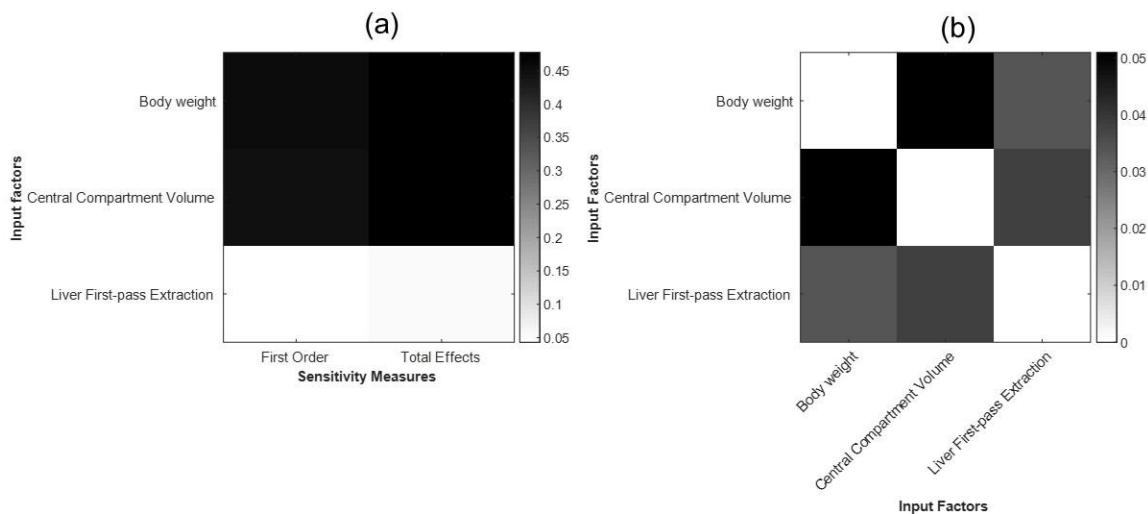


Figure 7: Sobol Method for risperidone C_{max} . The sensitivity measures were determined using $N=3,000$ for parameters identified by the Morris Method based on μ^* . The first-order and total effects are given in (a). The second-order interactions are given in (b).

2.4.7 Sobol Method for atenolol

Seven significant parameters for atenolol C_{max} based on screening were investigated further by Sobol's method, requiring 4,000 samples for method convergence with $N_t = 36,000$ simulations. Sensitivity measures are given in **Figure 8**. Central compartment volume was the most significant parameter for C_{max} followed by body weight, accounting collectively for approximately 70% of the variability in C_{max} . While the first-order effects of other parameters were negligible ($S_i < 0.05$), the small intestine radius and ASF C2 had significant interactions with all other parameters. The strongest pairwise interaction was between these parameters, echoing the behavior of GastroPlus for acetaminophen. Other physiological parameters and compartmental model parameters had negligible interactions.

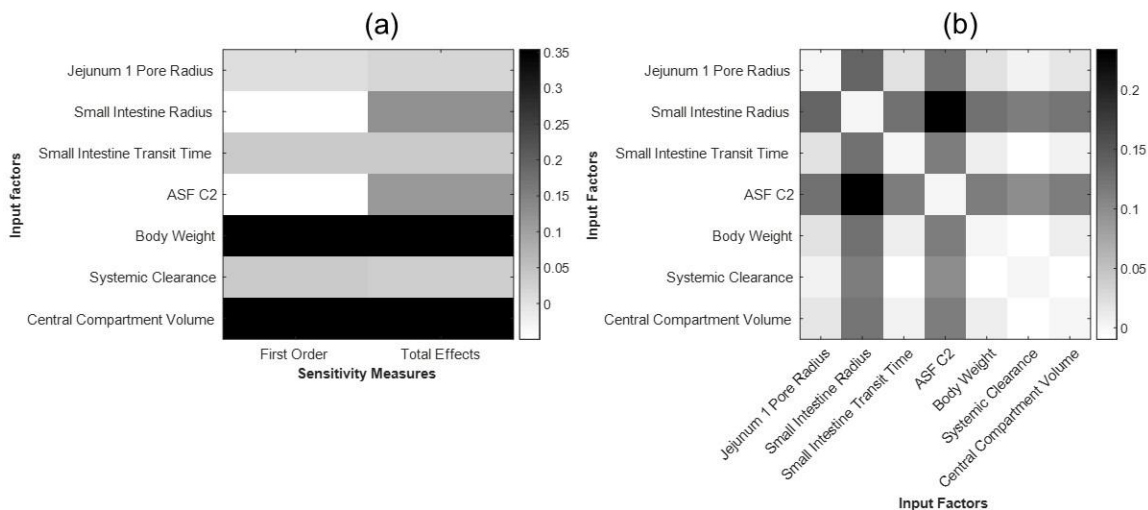


Figure 8: Sobolj Method for atenolol C_{max} . The sensitivity measures were determined using $N=4,000$ for parameters identified by the Morris Method based on μ^* . The first-order and total effects are given in (a). The second-order interactions are given in (b).

2.4.8 Sobolj Method for furosemide

Sobolj's method was implemented with 5,000 samples ($N_t = 65,000$ simulations) for furosemide C_{max} using the eleven significant parameters determined from the Morris Method. Sensitivity measures are shown in **Figure 9**. The most important parameter influencing furosemide C_{max} directly was body weight, which had the highest first-order effect and moderately weak interactions with other parameters. Variability in C_{max} was distributed as follows for furosemide: approximately 33% for body weight, 10% for central compartment volume, and 6% for renal clearance, while the remaining variability was attributed to parameter interactions. ASF C2, which indicated almost no direct influence on C_{max} ($S_i \approx 0.05$), showed significant interactions with all other parameters. Similarly, the small intestine radius had strong interactions, but a negligible first-order effect. The strongest pairwise interaction was observed between the small intestine radius and ASF C2, consistent with the behavior of GastroPlus for acetaminophen and atenolol. Furosemide was the only studied drug without the majority of variability apportioned to

first order effects. This observation was likely due to the stronger influence that gastrointestinal physiology has on the rate and extent of absorption for a poorly soluble and permeable drug, reflecting the added complexity of developing an accurate PBPK model for a BCS IV drug.

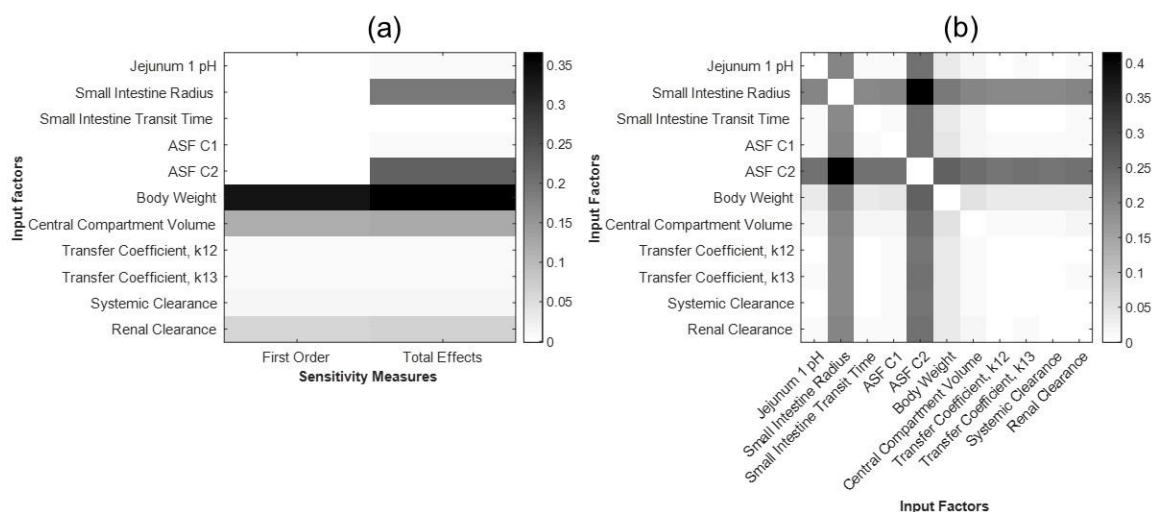


Figure 9: Sobolj Method for furosemide C_{max} . The sensitivity measures were determined using $N=5,000$ for parameters identified by the Morris Method based on μ^* . The first-order and total effects are given in (a). The second-order interactions are given in (b).

2.4.9 Parameter rankings by the Morris and Sobolj methods were consistent

A comparison of parameter ranking and significance determined by the Morris and Sobolj Methods for parameters included in both stages is given in **Table 2**. The number of significant parameters for C_{max} was overestimated by the Morris Method when a cutoff of 10% of the maximum μ^* was used, leading to several of these parameters explaining less than 5% of the variability in model output according to the Sobolj Method.

Table 2: Parameter ranking determined by the Morris and Sobol sensitivity methods for C_{\max}

Parameter	Acetaminophen		Risperidone		Atenolol		Furosemide	
	S_{ii}	μ^*	S_{ii}	μ^*	S_{ii}	μ^*	S_{ii}	μ^*
SI Radius	3*	3	NA	NA	3*	3	3*	3
SI Transit Time	NA	NA	NA	NA	5	5	11	11
J1 pH	NA	NA	NA	NA	NA	NA	10	10
J1 Pore Radius	NA	NA	NA	NA	7	7	NA	NA
ASF C_1	NA	NA	NA	NA	NA	NA	8	8
ASF C_2	4*	4	NA	NA	4*	4	2*	2
Body Weight	1*	1	1*	1	1*	1	1*	1
Central Compartment Vol.	2*	2	2*	2	2*	2	4*	4
Transfer Coefficient, k_{12}	6	6	NA	NA	NA	NA	9	9
Transfer Coefficient, k_{13}	NA	NA	NA	NA	NA	NA	7	7
Systemic Clearance	5	5	NA	NA	6	6	6	6
Renal Clearance	NA	NA	NA	NA	NA	NA	5*	5
Liver First-pass Extraction	NA	NA	3*	3	NA	NA	NA	NA

Abbreviations: SI = Small intestine; J1 = Jejunum 1; J2 = Jejunum 2; Vol. = Volume; NA = Not Applicable (Parameter not included in Sobol Method for particular drug.)

Note: Parameters with $S_{ii} < 0.05$ were negligible. Parameters with $S_{ii} > 0.05$ were considered significant (indicated by *).

2.4.10 Quality of 2-stage global sensitivity analysis depends on screening with the Morris Method

Global sensitivity analysis was performed by sampling from uniform distributions that did not account for physiological distributions or sampling bounds. To understand how the sampling bounds influenced the sensitivity measures and the established relationships between model input and output, sampling bounds were increased to $\pm 50\%$ of the nominal values. Values of μ^* (mean of elementary effects) and σ (standard deviation of elementary effects) for triplicate analysis at sampling bounds of $\pm 20\%$ and $\pm 50\%$ with $r = 20$ are given in **Figure 10a** for acetaminophen C_{\max} . The ratio σ/μ^* was considered to be an indicator of higher-order effects as originally proposed by Garcia-Sanchez et al. [125,147]. The

Morris Method revealed parameter sensitivities for sampling bounds of $\pm 20\%$ fell within the monotonic and linear regions according to the boundaries defined by Garcia-Sanchez et al., largely failing to capture the presence of potential nonlinearities and/or parameter interactions as shown in **Figure 10b**. When the sampling bounds were widened to $\pm 50\%$, sensitivity analysis detected the presence of higher-order effects between GastroPlus input and output. The distribution of elementary effects for body weight, the most significant parameter for acetaminophen C_{\max} , given in **Figure 10c** showed large differences in variance between sampling bounds.

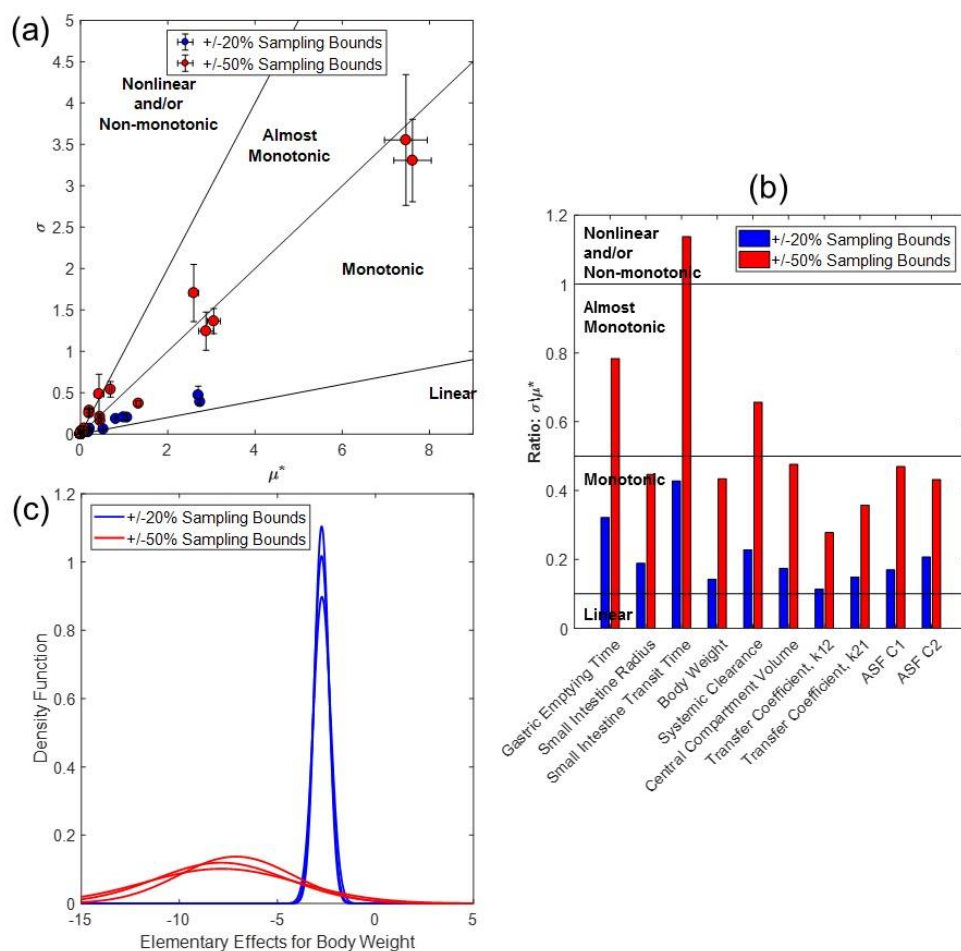


Figure 10: Relationships between model input and output for acetaminophen C_{max} . The values of μ^* and σ determined using $r = 20$ and the average ratio σ/μ^* from triplicate analysis are plotted in (a) and (b), respectively, for sampling bounds of $\pm 20\%$ and $\pm 50\%$. Error bars in (a) represent the standard deviation associated with μ^* and σ for triplicate analyses. The distribution of elementary effects for each replicate analysis are given in (c) for body weight.

The plasma concentration profiles from GastroPlus are provided in **Figure 11** when body weight (significant parameter for all model outputs) and gastric pH (low significance for all model outputs) were set to the upper limit (+20% or +50%) and lower limit (-20% or -50%). This comparison showed how parameter significance according to the Morris Method corresponded to noticeable differences in model output. While the upper and lower sampling bounds produced similar changes in model output from the baseline at $\pm 20\%$, the elementary effects for the wider sampling bounds were not equal at the upper and lower

limits. This observation was likely due to a nonlinear relationship between body weight and plasma concentration that was not detected by the narrower sampling bounds. Thus, sampling failed to fully evaluate the relationship between model inputs and outputs if the sampling bounds were too narrow. However, the input space for global sensitivity can be amended according to the objective of the analysis, such as wider bounds for model understanding and preliminary studies or biologically relevant distributions/bounds for exploration of underlying physiological mechanisms.

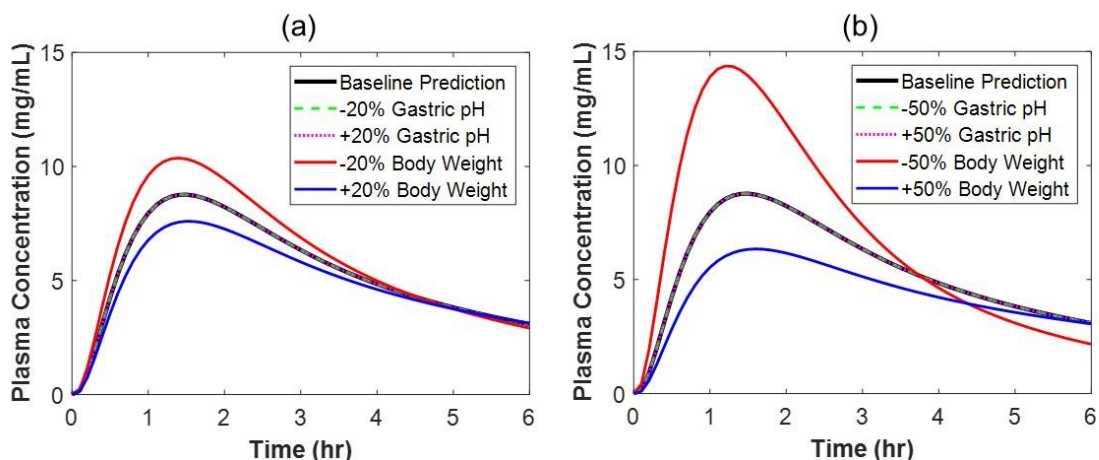


Figure 11: GastroPlus predictions for acetaminophen at the sampling bounds. The plasma concentration profiles predicted by GastroPlus when body weight and the gastric pH were set to the upper and lower limits are given in (a) and (b) for sampling bounds of $\pm 20\%$ and $\pm 50\%$, respectively.

2.5 Discussion

The decision to integrate GastroPlus into a framework for global sensitivity was based on the advantages of utilizing an established model employed by industry, academia, and regulatory agencies. While the ACAT and ASF models of GastroPlus allowed for a comprehensive analysis of absorption-related parameters, the physical meaning and interpretation of the sensitivity results were limited using the basic compartmental models. Nevertheless, the current study was sufficient to demonstrate the capabilities of the

automation framework for managing thousands of simulations, and to validate the appropriateness of the 2-stage global sensitivity approach for use with GastroPlus models. The framework represented an attractive and immediate solution for the application of global sensitivity analysis to existing versions of GastroPlus, serving as a useful tool to generate further interest in such methods. AutoIt circumvented the issues of automating closed code, proprietary applications by instead utilizing graphical user interface automation. The greatest limitation for the existing framework was the added computational time associated with automation compared to a fully integrated script-based workflow within the GastroPlus interface. While the Morris Method was executed within hours, the Sobol Method took longer for completion despite limiting the number of evaluated parameters with the 2-stage approach. However, the behavior of AutoIt scripts was reliable across different computers. Therefore, both the Morris and Sobol Methods were amenable to parallel processing to ease implementation. Various tests were performed during development of the framework to validate its use and confirm that data was correctly transferred between MATLAB and GastroPlus. An advantage of the automation framework was the relative ease at which additional model parameters and other features of GastroPlus were incorporated as needed for each of the studied drugs.

The Biopharmaceutical Classification System for oral dosage forms was used to identify model compounds belonging to each class for use with the Morris and Sobol Methods. These compounds were not intended to describe the true behavior of each drug class, but to guide the selection of drugs in this study. From these four representative compounds, one can appreciate how parameter significance might vary with physicochemical properties, such as permeability and solubility. Sensitivity results alluded

to underlying physiological mechanisms that influenced absorption and were grossly consistent with the challenges faced for each class, both in terms of PBPK model development [148,149] and formulation strategies [150,151]. Sensitivity results for furosemide provided an example, albeit high level, of how the Morris Method was used to determine the underlying physiology driving variability in pharmacokinetics. Renal clearance of furosemide was found to be significant for all model outputs, consistent with the population study which revealed differences in renal function were the key indicator of pharmacokinetic response, separating healthy subjects, and those with hepatic cirrhosis and congestive heart failure [135].

The Morris Method indicated ASF C2 was significant for acetaminophen, atenolol, and furosemide for all model outputs when the default ASF coefficients were used as the baseline. In the risperidone model, calibration of ASF C2 to 5-fold greater than the default value was needed to match the predicted t_{\max} with clinical data and was found to be significant for only t_{\max} during screening by the Morris Method. Since these coefficients do not have an exact physiological meaning, the interpretation of ASF sensitivities was limited to a lumped change in drug physicochemical properties influencing permeability in each of the gastrointestinal compartments. Further interpretation would require more knowledge of the drug properties and behavior *in vivo*. Nonetheless, the Morris Method results supported the common practice of using the ASF model to calibrate GastroPlus against clinical observations [152,153], considering its significant influence on model output. However, calibration of the ASF model coefficients may mask the importance of other gastrointestinal parameters on the absorption rate. The risperidone model, which was the only model that required calibration of an ASF coefficient, had fewer gastrointestinal

parameters with significance in comparison to furosemide, the other poorly soluble drug. It is unclear whether this behavior is true for all BCS II drugs or unique to risperidone due to model calibration.

The 2-staged approach to global sensitivity analysis offered the key advantage of significantly reducing computational cost without sacrificing insight into model behavior, overcoming one of the major hurdles for implementing such an extensive analysis for a larger PBPK model. The 2-stage approach resulted in a reduction in computational cost by at least 75% for all drugs compared to using the Sobol Method to screen over 50 parameters. Despite the relative improvement in computational efficiency, global sensitivity analysis continues to require far more simulations than a local method. However, the Morris and Sobol Methods revealed nonlinearities and parameter interactions, indicating that more complex relationships exist between model input and output than can be detected by the local method, requiring a global analysis to fully evaluate the GastroPlus model. Furthermore, the cutoff for parameter significance (10% of maximum μ^* for each output) during screening led to several parameters which contributed insignificantly to output variability (less than 5%) according to Sobol's analysis. Tightening the selection criteria during screening would reduce the computational cost of the Sobol Method by minimizing the number of parameters evaluated quantitatively, but at the risk of missing parameters that significantly contributed to variability in C_{\max} . Therefore, further work is needed to optimize the cutoff for parameter significance to balance the risk of Type I and Type II errors with computational cost. The actual need for the quantitative method following screening depends on the objective and intended use of the sensitivity analysis. Both methods converged to the same parameter rankings given a

sufficient number of samples. Therefore, μ^* of the Morris Method may serve as a surrogate of the computationally expensive S_{ii} from the Sobol Method when the objective is to rank parameters, consistent with the analysis of other models [154]. While the Morris Method would be appropriate for factor fixing or model simplification, the Sobol Method enables the modeler to determine which pairwise interactions drive model behavior and how variability in model output is apportioned to model input, the latter of which may be highly informative for drug development and explaining clinical observations.

Global analysis places sensitivity measures in the context of the entire input space, accounting for the impact of other parameter values on the resulting sensitivity measures in contrast to local methods which evaluate sensitivity indices one-at-a-time using a fixed baseline. As such, global sensitivity results and their interpretation often depend on the sampled input space [155]. When model input changes, the corresponding output may change as well, influencing the calculated sensitivity measures accordingly. **Supplementary Figure 8** and **Supplementary Figure 9** show how different input spaces influence the total effects determined by the Morris Method when both physiological and uniform distributions are used for the GastroPlus model. Physiological distributions constrain the sampling space to biologically meaningful model input and output while wider distributions enable the model structure to be fully explored. The selection of the input space may be of particular interest to PBPK modeling for special populations (i.e. young vs. elderly, male vs. female, healthy vs. disease state, pregnant female vs. non-pregnant female) due to the uncertainty associated with model input for these physiologies [106,156,157]. In this manner, global sensitivity analysis could thoroughly evaluate the most influential parameters using a physiologically relevant input space, providing

direction for future experimental studies, and improving confidence in PBPK predictions for special populations that may otherwise be limited by incomplete and inconsistent physiological data [148].

The effectiveness of the automated framework for managing thousands of GastroPlus simulations were demonstrated specifically for global sensitivity analysis, but the potential use of such a framework extends beyond the scope of the current study. An application that has yet to be fully explored is large scale sampling for model re-parameterization. Paralleling the sophisticated methods implemented for systems biology models [158], the framework can be used to explore the highly dimensional input spaces of GastroPlus to identify parameter sets that predict a target response profile or clinical output. Additionally, the existing framework can be expanded to perform global sensitivity analysis on a whole-body PBPK model, a scenario that will introduce many new parameters into the framework and benefit extensively from the 2-staged global sensitivity analysis.

CHAPTER 3: Exploration of sexual dimorphism and inter-individual variability in multivariate parameter spaces for a pharmacokinetic compartment model

3.1 Introduction

The development of sex-specific PBPK models is dependent on proper calibration of the model to account for the intrinsic differences in physiology between male and female populations across all ADME processes. However, quantitative differences between genders are rarely discussed in the literature and instead are often presented as a relative comparison (males > females, males < females, males = females). Thus, identifying and estimating sex-specific parameters is at the liberty of the researcher. Monte Carlo simulations provide an alternative approach to generate combinations of parameters which can be restricted to only those parameter sets that adequately describe the target pharmacokinetic output to establish the biologically plausible parameter distributions when physiological data are not readily available [40,158,159]. A key advantage of this methodology is that precise physiological data for a particular population is not needed as a starting point, instead available information for a general population can be utilized to inform the sampling bounds whenever available, such that sampling is not completely random. Furthermore, parameter distributions obtained from sampling encompass variability in parameter values that cannot be attributed only to patient differences, and instead account for random variability and uncertainty [160]. Such methodologies also enable additional subjects to be simulated by re-sampling from the biologically plausible population distributions [27], creating larger virtual populations which may be analyzed by

various statistical techniques. Global sensitivity analysis further aids model development and guides future experimental studies for determination of model parameters [106,156,157], and has previously been implemented for pharmacokinetic models for special populations [148,161].

Our approach utilizes a published pharmacokinetic compartmental model to demonstrate how sampling in conjunction with global sensitivity analysis can be used to differentiate model behavior and output between male and female phenotypes. These observations are well cited in the literature, indicating that physiological differences between sexes can translate to large differences in pharmacokinetic parameters and to further variability in pharmacodynamics [56-58,62,162]. Sex differences have yet to be consistently and reproducibly incorporated into clinical trials, considering the ethical concerns associated with testing during pregnancy and the increased variability in female populations due to influence of the menstrual cycle [31,55]. As such, sexual dimorphism has been selected to demonstrate the benefits of the model-based approach to establishing male and female parameter subspaces. This analysis is achieved using a stochastic approach to generate random combinations of several physiological parameter values *in silico* [163,164], leading to a wide distribution of model outputs from which predictions matching clinical data were selected for further analysis. Through global sensitivity analysis, the importance of differences can be studied to identify parameters that have the greatest influence of model output in relationship to parameter subspaces associated with male and female physiologies.

3.2 Approach

3.2.1 Overview of model-based methodology

The model-based methodology, summarized in **Figure 12**, was demonstrated for a compartmental model selected from the literature that described the pharmacokinetics of valproic acid following a single dose of a delayed release tablet [68]. The approach relied on stochastic sampling to generate thousands of potential parameter sets from initial parameter distributions that depicted a generic human population, and then isolating parameter sets that matched clinical data for male and female phenotypes. Physiological parameters are intrinsically correlated through underlying physiology and so resulting parameter combinations from random sampling may be unrealistic [110]. Biologically implausible parameter sets were discarded by enforcing selection criteria to isolate parameter sets that only produced the target model outputs. Parameter sensitivity analysis was implemented using the male and female parameter subspaces to understand how model behavior differed between phenotypes.

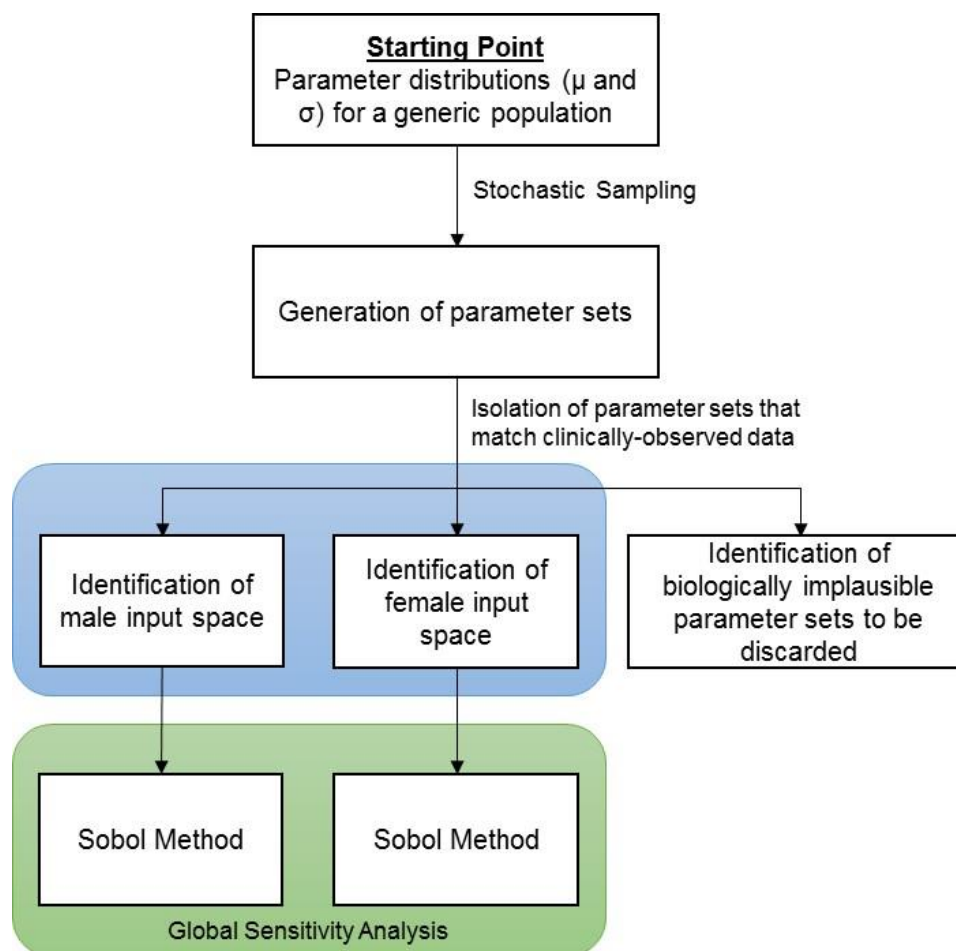


Figure 12: Schematic outlining the model-based approach for isolation of male and female model parameter subspaces using stochastic sampling and global sensitivity analysis. Random samples are drawn from each parameter distribution with mean (μ) and standard deviation (σ) for the mixed sex population. Parameter sets associated with model output within the acceptable male or female ranges are specified as male or female accordingly. The isolated male and female parameter subspaces are then used for the global sensitivity analysis to identify parameters with the greater influence on model output. Parameter sets associated with model output outside the acceptable ranges are considered biologically implausible and discarded.

3.2.2 Overview of the selected model

Purely predictive modeling as implemented in this study may be cross-validated by comparing the *in silico* results against data collected from real subjects [165]. For this reasoning, a published compartment model describing sexual dimorphism in valproic acid pharmacokinetics was selected to demonstrate how special populations may be studied *in silico* when physiological and clinical data are lacking for the population of interest. The

literature model described the pharmacokinetics of valproic acid using four compartments: gastrointestinal tract (GI), central (C), peripheral (P), and gallbladder (GB). The model parameters were lag time (t_{lag}), apparent absorption rate constant (k_a), distribution clearance (CL_D), peripheral compartment volume (V_P), central compartment volume (V_C), elimination clearance (CL), reabsorbed fraction (F_E), time of reabsorption (T_{EHC}), and reabsorption rate constant (k_{EHC}). The system of differential equations that comprises the model and describes the mass (or amount, A) of valproic acid in each of the four compartments are given in **Equations 10-13** prior to the onset of enterohepatic recirculation ($t < T_{EHC}$), and in the central and gallbladder compartments after the onset of reabsorption ($t > T_{EHC}$) in **Equations 14-15** [29]. The plasma concentration was calculated by $C_p = A_C/V_C$.

3.2.2.1 Before Reabsorption ($t < T_{EHC}$)

Gastrointestinal Tract:

$$\frac{dA_{GI}}{dt} = -k_a \cdot A_{GI} \quad \text{Eq. 10}$$

Central Compartment:

$$\frac{dA_C}{dt} = k_a \cdot A_{GI} - \frac{CL}{V_C} \cdot A_C + \frac{CL_D}{V_P} \cdot A_P - \frac{CL_D}{V_C} \cdot A_C \quad \text{Eq. 11}$$

Peripheral Compartment:

$$\frac{dA_P}{dt} = \frac{CL_D}{V_C} \cdot A_C - \frac{CL_D}{V_P} \cdot A_P \quad \text{Eq. 12}$$

Gallbladder Compartment:

$$\frac{dA_{GB}}{dt} = F_E \cdot \frac{CL}{V_C} \cdot A_C \quad \text{Eq. 13}$$

3.2.2.2 After Reabsorption ($t \geq T_{EHC}$)

Central Compartment:

$$\frac{dA_C}{dt} = k_a \cdot A_{GI} - \frac{CL}{V_C} \cdot A_C + \frac{CL_D}{V_P} \cdot A_P - \frac{CL_D}{V_C} \cdot A_C + k_{EHC} \cdot A_{GB}$$

Eq. 14

Gallbladder Compartment:

$$\frac{dA_{GB}}{dt} = -k_{EHC} \cdot A_{GB}$$

Eq. 15

3.2.3 Identification of initial parameter estimates for a generic population

In the original population study, the model structure was identical for males and females with sex differences reflected only in model parameterization [68]. The parameter estimates for the compartment model were adapted to represent a mixed sex or general human population to demonstrate the model-based approach shown in **Figure 12** because sex-specific parameter estimates are often unavailable, especially for more complex physiologically based models. The mean parameter values and sampling bounds describing the generic population are given in **Supplementary Table 4**. The Wilcoxon rank sum test, a nonparametric method for comparison of population medians, was used to compare model input for the simulated male and female populations when the assumption of normality was not accurate for one or both populations. The two-sided Smirnov-Kolmogorov test, a nonparametric method for comparison of population distributions, was also used to evaluate sexual dimorphism in model input. The Wilcoxon rank sum test was used to determine whether median parameter values obtained from sampling matched the corresponding values determined in the original population study.

3.2.4 Identification and analysis of male and female parameter subspaces

Random samples were drawn from the normal distributions generated in MATLAB® using the mean (μ) and standard deviation (σ) for the generic population and sampling bounds of $\pm 3\sigma$. Parameters were treated independently during sampling to maximize the variability in predicted pharmacokinetic outputs [166]. The compartment model was run for each parameter set and the model output was used to identify whether the parameter set could be classified as male, female or discarded when biologically implausible. The selection criteria for inclusion of a parameter set were based on the non-compartmental analysis determined from the 14 subjects [68], where acceptable parameter sets were associated with model output that was within 1 standard deviation of the mean values reported for C_{max} and area-under-the-curve (AUC), and within the observed minimum and maximum reported values for t_{max} and t_{lag} . Parameter sets associated with model output within the acceptable range for females or males were included in the male or female population accordingly. Parameter sets with some or all model output outside the acceptable range were discarded and not used for further analysis. The male and female model outputs from the clinical study are given below in **Table 3** with statistically significant sex differences for C_{max} and AUC_{0-48} . The data for all 7 female subjects was used, including the two subjects using contraceptive therapy. The Wilcoxon rank sum test was used to compare the model outputs identified for the simulated male and female populations against those reported by the clinical study.

Table 3: Target male and female pharmacokinetic model output for selection of parameter sets from stochastic sampling

	C_{max} (mg/L) ^a	T_{max} (hr) ^b	AUC_{0-48} (mg h/L) ^a
Clinical Male Subjects	35.6 (5.2)	3-5	496.6 (55.2)
Clinical Female Subjects	55.3 (9.4)	3-6	809.4 (148.4)
Sex Differences ^c	p-value<0.001	NS	p-value<0.01

^aThe mean and standard deviation (values in parentheses) were reported directly by the original clinical study and determined using a noncompartmental analysis.

^b The minimum and maximum values for t_{max} were determined using the plasma concentration profiles given in the original clinical study. These values considered the time from administration until maximum drug exposure, including the initial lag time.

^c Sex differences were reported by the original clinical study, where NS corresponds to a non-significant difference between male and female model output.

3.2.5 Support vector machine for binary classification

A support vector machine (SVM) was used to determine the equation of the hyperplane that defined the separation between the simulated male and female multivariate parameter spaces. The separating hyperplane was defined by **Equation 16**, where \mathbf{x} corresponds to the matrix of input parameters, $\boldsymbol{\beta}$ represents the matrix of the best-fit hyperplane coefficients, and b is the bias determined while fitting the optimal separating hyperplane for the training data set.

$$f(x) = \mathbf{x}' \cdot \boldsymbol{\beta} + b = 0 \quad \text{Eq. 16}$$

The classifier was trained using a subset of parameter sets, selected by random sampling from the simulated populations for 1,000 virtual male subjects and 1,000 virtual female subjects. The function ‘fitcsvm’ was used in MATLAB® to determine the equation of the separating hyperplane for the 9 model parameters. Data were preprocessed by calculating the z-scores for each observation (i.e. the difference between the mean and individual parameter values divided by the standard deviation). Bootstrapping was

implemented to understand the sensitivity of the hyperplane parameters to the selected subset of parameter sets using 1,000 replicates.

3.2.6 Principal component analysis

A principal component analysis (PCA) was used to identify the existence of any parameter dependencies associated with the biologically plausible model output, revealing trends in parameter combinations that contribute to observed phenotype. PCA was implemented in MATLAB® using z-scored data for 1,000 bootstrapped samples of 1,000 virtual female subjects and 1,000 virtual male subjects randomly selected from the original simulated populations. PCA condensed the multi-dimensional data set into fewer principal components, thereby representing the original data as linear combinations of the parameter values for each virtual subject. The PCA was performed using the same number of observations for males and females such that the PC scores were not skewed by the number of samples contained in each population. Bootstrapping was used to ensure the resulting principal components for the selected subset of virtual subjects were representative of the simulated populations. Following transformation of data into its principal components, a support vector machine was trained using the principal component scores.

3.2.7 Sobol sensitivity analysis

The Sobol sensitivity method was implemented using the sex-specific parameter distributions identified from stochastic sampling for all model parameters ($k = 9$). The Sobol method is described in more detail in Chapter 2 as well as Scherholz et al. [161]. Briefly, the Sobol sensitivity analysis relies on random sampling to generate parameter sets ($N = 6,000$) from the male and female parameter spaces for calculation of the sensitivity measures. Although physiologically representative normal distributions were considered

for individual parameters, the sampling method did not account for the probability that certain parameter combinations occur at higher frequencies [141]. For each sex, the analysis was repeated ten times. The total computational cost for each analysis was $N_t = N(k + 2)$ or 66,000 simulations. The sensitivity measures for direct effects (S_i) were determined for all parameters included in the model using the maximum concentration (C_{\max}), the time to maximum exposure (t_{\max}), and AUC_{0-48} as the model output. Sensitivity measures for the maximum concentration and AUC_{0-48} indicated which factors affected maximum and cumulative drug exposure whereas sensitivity measures for t_{\max} showed which parameters affected the rate of appearance in systemic circulation. Parameters were deemed significant if sensitivity measures were greater than 0.05 [128], such that at least 5% of the total model output variability was explained directly by each parameter.

3.3 Results

3.3.1 Identification of simulated male and female populations

From the 200,000 parameter combinations generated by stochastic sampling, 3,905 sets were consistent with male clinical data and 27,492 for female clinical data. The remaining parameter sets resulted in model output that was neither male or female and were discarded. The density distributions of all 9 model parameters associated with the simulated male and female populations as well as the initial sampled population are given in **Figure 13**. Sex differences were statistically significant (p -value < 0.05) except for the reabsorption rate constant (k_{EHC}) based on the two-sided Kolmogorov-Smirnov tests for comparison of population distributions and the Wilcoxon rank sum test for comparison of population medians. The greatest sex differences between the simulated populations were observed for the univariate parameter distributions of the central compartment volume (V_C)

and elimination clearance (CL). Furthermore, the median parameter values obtained by sampling were statistically similar to the values determined in the original population study for both males and females. The results of the statistical analyses are given in the **Supplementary Table 5 to Supplementary Table 7**.

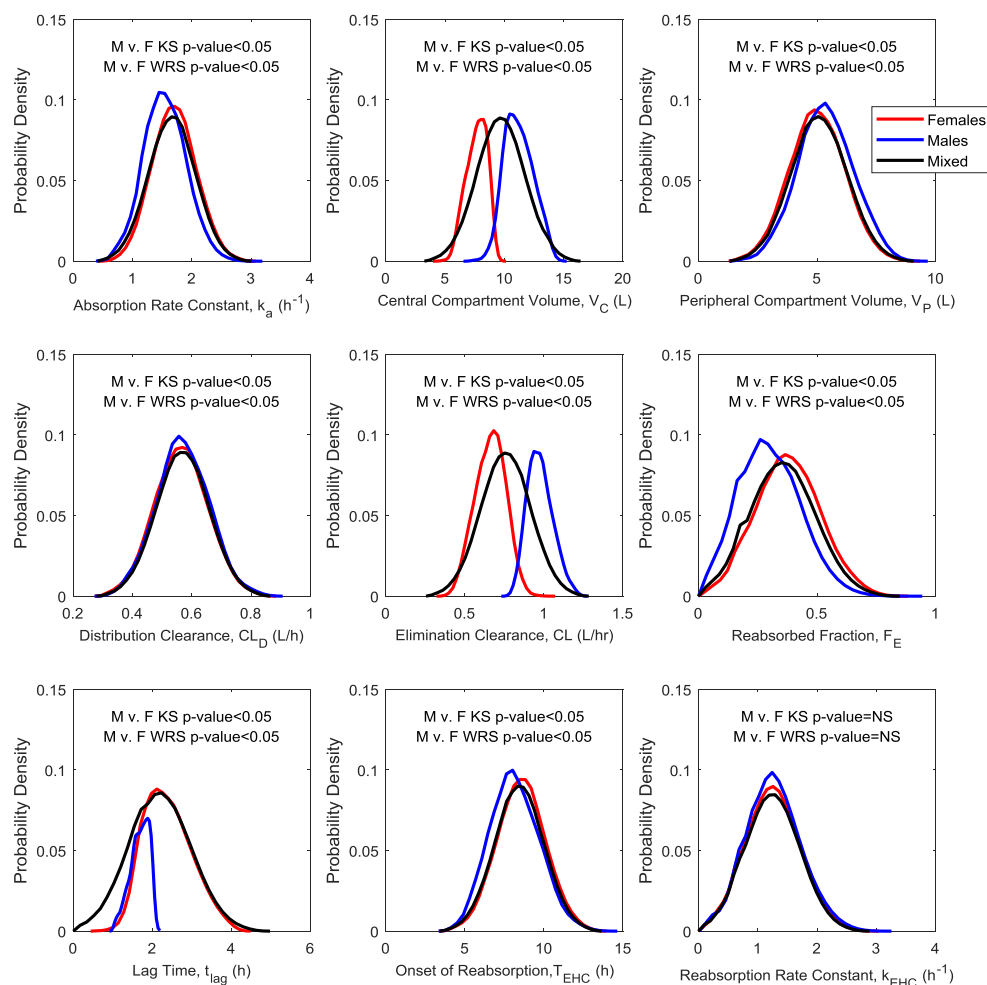


Figure 13: Probability density distributions of model input parameters for the simulated male and female populations. The probability density distributions are given for the simulated male and female populations isolated from sampling (blue and red lines, respectively) and the original mixed sex population used as the starting point for sampling (black line). The p-values are reported for the comparison of population distributions according to the Kolmogorov-Smirnov (KS) test and the comparison of population medians according to the Wilcoxon Rank Sum (WRS) test. Sex differences that were not statistically significant were indicated by NS (not significant).

The model output for the simulated male and female populations are given in **Figure 14** with statistically significant sex differences for all model outputs (C_{max} , t_{max} , and

AUC₀₋₄₈). Differences between the simulated population and the corresponding clinical population were not statistically significant for either male or female subjects based on a comparison of the population medians (p-values < 0.05 for the Wilcoxon rank sum test). The results of the statistical analysis are given in **Supplementary Table 8**. Furthermore, the plasma concentration profiles associated with the male and female parameter sets were in qualitative agreement with the experimentally observed plasma concentration profiles as shown in **Figure 15**. Thus, the simulated populations were considered to be representative of the original clinical subjects.

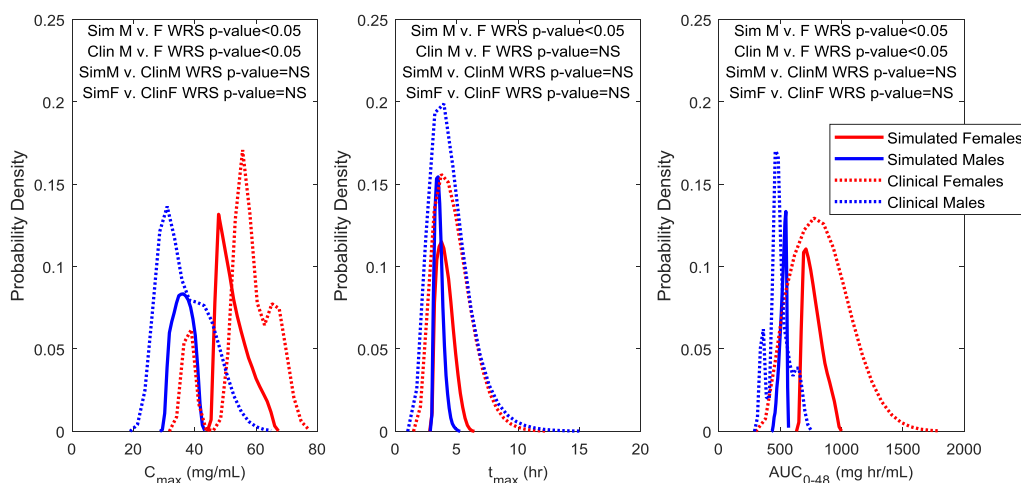


Figure 14: Probability density distributions of model output for the simulated male and female populations. The probability density distributions are given for the simulated male and female populations isolated from sampling (blue and red solid lines, respectively) and the original clinical populations (blue and red dotted lines). The p-values are reported for the comparison of the population medians according to the Wilcoxon Rank Sum (WRS) test. Sex differences that were not statistically significant were indicated by NS (not significant).

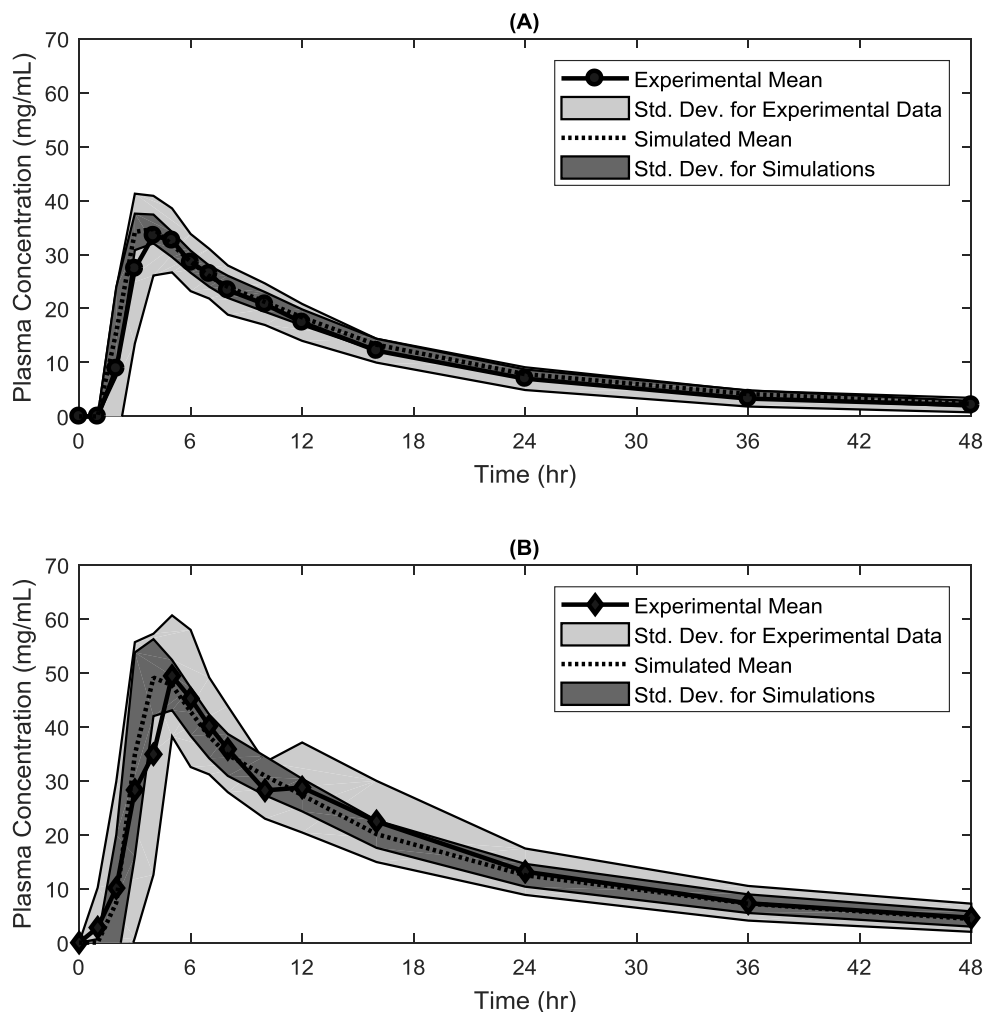


Figure 15: Plasma concentration profiles for the simulated and clinical populations. The mean plasma concentration profiles for the male and female populations are given in subplots (A) and (B), respectively. The light shaded area represents the experimentally observed standard deviation whereas the darker shaded area represents the standard deviation associated with model predictions corresponding to the isolated male and female parameter sets.

3.3.2 Separation of model input into male and female parameter subspaces

A support vector machine was used to establish the equation of the separating hyperplane for identification of the model input that dictated whether a parameter set was identified as male or female. The hyperplane coefficients are given in **Figure 16** for 1,000 bootstrapped samples, where each β corresponded to an input parameter. Elimination clearance (CL) and the central compartment volume (V_C) were the most important

parameters for separation of male and female model input, whereas the reabsorption rate constant or initial lag time were not significant indicators of phenotype.

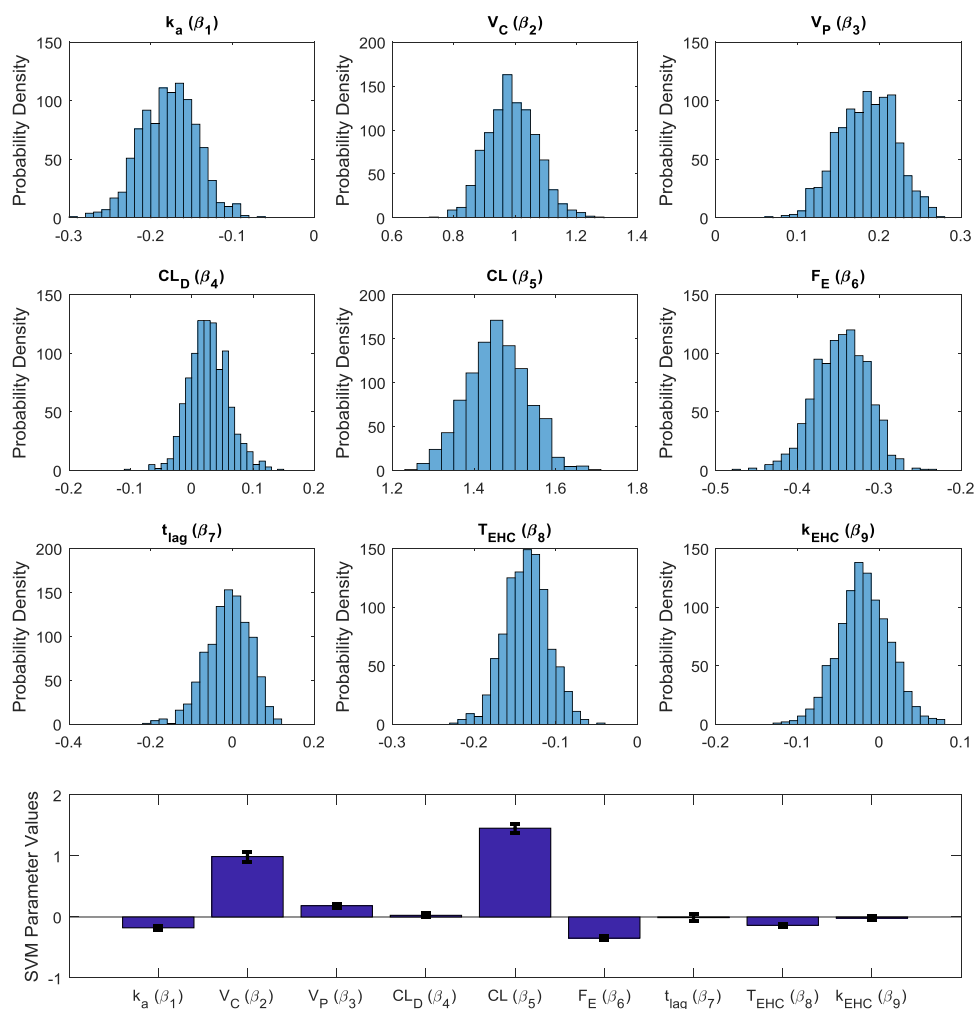


Figure 16: Separating hyperplane coefficients using model input as support vector machine (SVM) predictors. A binary classifier was developed using a randomly selected subset of 1,000 male and 1,000 female parameter sets for 1,000 bootstrapped samples to identify which parameters separated model output into the two phenotypes. The distributions of hyperplane coefficients for the bootstrapped samples are given in subplots (A) through (I) with the mean values of hyperplane coefficients reported in subplot (J).

When the separating hyperplane was approximated by the top two predictors of sex, a clear boundary was observed between male and female parameter combinations for elimination clearance (β_5) and the central compartment volume (β_2), whereas significant overlap was observed when the parameters with the lowest β values were used (**Figure 17**).

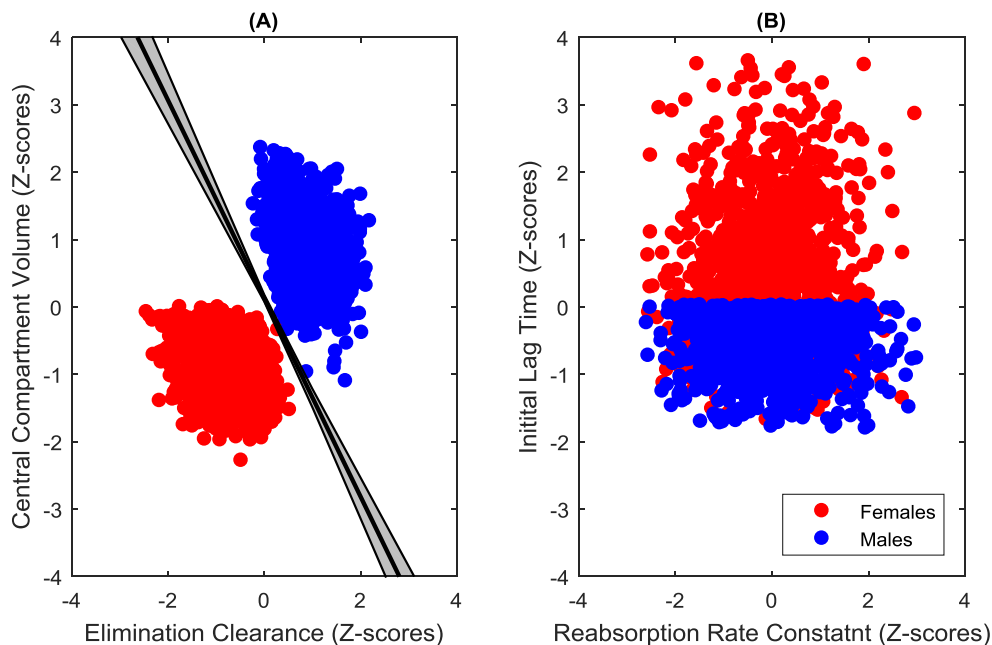


Figure 17: Approximation of the separating hyperplane between male and female model input using two predictors. The hyperplane using the most significant predictors (highest β_i values) and the least significant predictors (lowest β_i values) are given in subplots (A) and (B), respectively. The black line in (A) corresponds to the mean hyperplane for the 1,000 bootstrapped samples. The shaded area represents the potential location of the boundary between males and females when the separating hyperplane parameters were within 1 standard deviation of the mean values. The scatter plot shows the z-scores for the given parameters associated with male subjects (blue) and female subjects (red) from one representative bootstrapped sample.

3.3.3 Identification of parameter correlations in model input

The model input for the simulated populations were transformed into its principal components to understand how correlations between parameters differentiated male and female phenotypes. The resulting scores plot for the first three principal components is given in **Figure 18a**, showing clustering of the simulated male and female populations into two distinct regions. A principal component score of zero corresponded to the mean score of all observations (both male and female populations), whereas a positive score indicated a value above the overall mean and a negative score indicated a value below the overall mean. On average, the first component captured 26% of the total variability in parameters with the second and third components each describing 12%. The separating hyperplane

parameters that defined the boundary between male and female principal component scores are given in **Figure 18b** for the 1,000 bootstrapped samples. Only the first principal component was important for separation of male and female parameter subspaces. The PC loadings are given in **Figure 18c** for the first component, where the magnitude indicated the relative contribution of a model parameter towards the component score and the sign indicated how parameters were related. Elimination clearance (CL), central compartment volume (V_C) and the initial lag phase (t_{lag}) had the highest loadings for the first principal component. When considered independently, t_{lag} was not a key identifier of phenotype based on the support vector machine in the untransformed data. Conversely, clearance and the central compartment volume were important for both the untransformed and transformed data. Simulated females had negative scores for the first component, corresponding to longer initial lag times, and reduced values for the central compartment volume and elimination clearance than the simulated males, consistent with the results observed clinically [29]. The loadings for the second and third component show greater variability between bootstrapped samples than observed for the first principal component (data not shown).

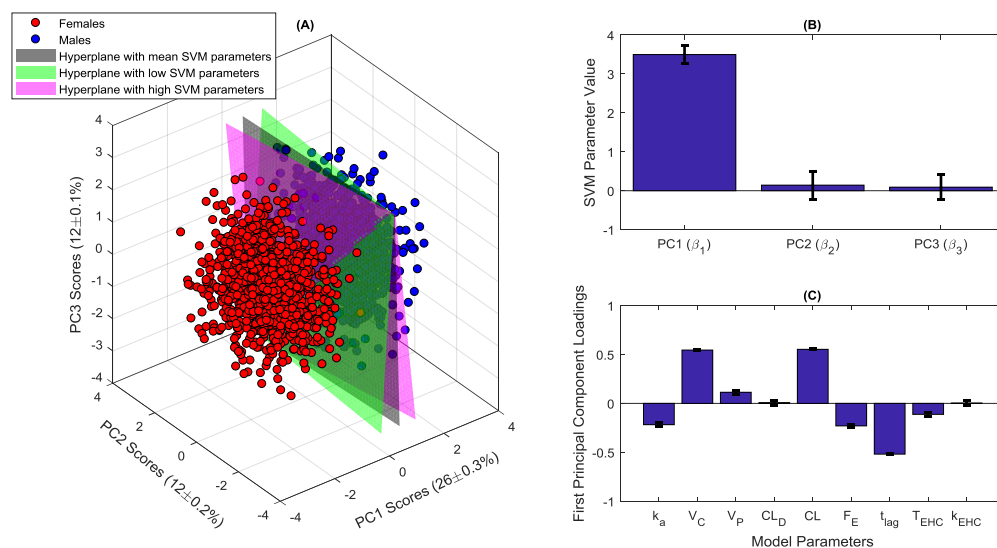


Figure 18: Separating hyperplane between male and female populations using principal components. The 3D scores plot in (A) shows the separating hyperplane using the first three principal components. The percentage of variability explained by each principal component is indicated in the axis labels. The black surface corresponds to the mean boundary of the 1,000 bootstrapped samples. The pink surface corresponds to the boundary when the separating hyperplane are $+1\sigma$ of the mean values. The green surface corresponds to the boundary when the separating hyperplane are -1σ of the mean values. The scatter plot shows the principal component scores for the male subjects (blue) and female subjects (red) from one representative sample. The mean separating hyperplane parameters for the support vector machine (SVM) are given in (B) where the error bars represent the standard deviation of the 1,000 bootstrapped samples. The mean loadings for the first principal component are given in subplot (C) with error bars that represent the standard deviation for the 1,000 samples.

3.3.4 Identification of model input driving inter-individual variability within each population

The Sobol sensitivity analysis was performed by randomly sampling the normal distributions established in Section 3.1 with sampling bounds set to $\pm 3\sigma$ and $N=6,000$, requiring a total of 66,000 simulations to calculate sensitivity indices in each analysis. The mean first order effects for C_{max} , t_{max} , and AUC_{0-48} determined by the Sobol sensitivity analysis are given for the simulated male and female populations in **Figure 19**. For the simulated male population, variability in C_{max} was attributed to the central compartment volume (77%) followed by the absorption rate constant (19%). Similarly, variability in C_{max} in the simulated female population was explained by the central compartment volume

(78%) and the absorption rate constant (15%). For t_{\max} values in males, the absorption rate constant accounted for 64% of the total variability and the initial lag time for 24%, whereas 17% and 78% of total variability in females were explained by k_a and t_{lag} , respectively. Interestingly, the first order sensitivity measures differed appreciably between the simulated populations considering AUC_{0-48} as the model output. In the simulated male population, the elimination clearance primarily explained variability in the AUC_{0-48} (61%), followed by the fraction reabsorbed (22%), central compartment volume (6.2%), peripheral compartment volume (5.9%), and time of reabsorption event (5.3%). Variability in AUC_{0-48} associated with the simulated female population was largely apportioned to the elimination clearance (77%) and to a lesser extent by the fraction reabsorbed (9.8%) and the peripheral compartment volume (6.3%). In summary, the sensitivity analysis indicated that variability in pharmacokinetics was primarily apportioned to the subset of parameters that captured the key features of pharmacokinetic profile: onset and rate of absorption (t_{lag} and k_a), disappearance of the drug from systemic circulation ($k_E = CL/V_C$), and the reabsorption event (F_E and T_{EHC}). Second order and higher interactions did not contribute significantly towards variability in model output (data not shown) such that variability in model output was almost entirely explained by the first order effects of these parameters.

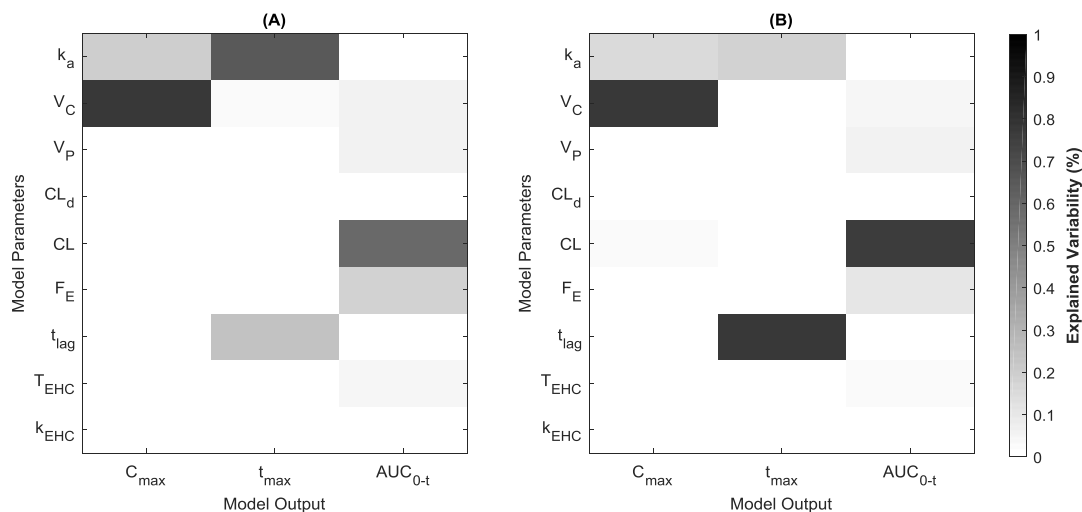


Figure 19: Sobolj sensitivity analysis for male and female parameter subspaces. The first order sensitivity measures for male and female parameter subspaces are given in subplots (A) and (B), respectively using C_{max} , t_{max} , and AUC_{0-t} as the model output. A higher value corresponds to a parameter which explains a greater proportion of the variability in model output.

3.3.5 Relating sexual dimorphism and inter-individual variability

The parameters for the separating hyperplane and the loadings for the principal components provided an indication of which parameters were critical for separation of the model input into distinct phenotypes while the Sobolj sensitivity measures explained which parameters contributed to variability in model output within each population. The importance of parameters for the support vector machine and the principal component analysis were largely similar with the exception of the initial lag time (**Table 4**). The difference between methods can be attributed to the fact that the support vector machine in the untransformed parameter space ranked parameters purely on the ability to separate male and female phenotypes based on univariate parameter distributions while the principal component analysis considered parameter dependencies. Generally, parameters that were important for separating male and female phenotypes were also significant for at least one model output whereas parameters that significantly influenced model output, such as the absorption rate constant or the initial lag time, did not necessarily distinguish phenotype.

Table 4: Summary of Parameter Rankings for Support Vector Machine, Principal Component loadings, and Sobol sensitivity analysis

Model Input Parameters	SVM Ranking	PC1 Loading	Sobol Sensitivity Male Parameter Space			Sobol Sensitivity Female Parameter Space		
			C _{max}	t _{max}	AUC ₀₋₄₈	C _{max}	t _{max}	AUC ₀₋₄₈
			Elimination Clearance, CL	1	1	4	4	1*
Central Compartment Vol., V_C	2	2	1*	3	4*	1*	3	4
Reabsorption Fraction, F_E	3	4	7	7	2*	9	7	2*
Peripheral Compartment Vol., V_P	4	6	5	8	3*	5	9	3*
Absorption Rate Constant, k_a	5	5	2*	1*	7	2*	2*	7
Onset of Reabsorption, T_{EHC}	6	7	6	6	5*	8	8	5
Distribution Clearance, CL_D	7	8	3	5	9	4	5	8
Reabsorption Rate Constant, k_{EHC}	8	9	9	9	8	7	6	9
Initial Lag Time, t_{lag}	9	3	8	2*	6	6	1*	6

Abbreviations: Vol. = Volume

Symbols: * = Significant parameter (greater than 5% contribution to variability in model output)

3.4 Discussion

As researchers and clinicians strive for personalized medicine, pharmacokinetic modeling is an important tool to identify exposure risks for individuals and patient subgroups. To support this goal, the concept of a pharmacokinetic model that represents an average individual or a generic population is replaced by models adapted to the physiology or clinical scenario of interest with an understanding that patient covariates, such as sex, can significantly affect the pharmacokinetic response. Today, there remains a high level of uncertainty and missing information associated with special populations that hinders the usefulness and predictive power of such models [106,148]. Unfortunately, generating this knowledge may be both time and cost prohibitive and so, several initial assumptions are often needed to generate preliminary pharmacokinetic predictions for specialized physiological states. However, the analytical framework herein has the potential to explore the underlying physiology leading to clinically observed responses using limited data and

minimal assumptions. The insight gained from the support vector machine, principal component analysis, and global sensitivity analysis guides future *in vitro* studies to improve confidence in estimates for the critical model parameters, enabling the model input to be amended accordingly.

Our approach draws from concepts in both top-down and bottom-up approaches to identify the parameter subspaces associated with the male and female phenotypes for the selected pharmacokinetic model. Drawing from bottom-up methodologies, existing knowledge of physiology, or in this case model input for a mixed sex population, was used as the starting point for sampling. Paralleling top-down methodologies, the current study used the observed clinical behavior to identify parameter combinations that predicted plasma concentration profiles associated with the male and female phenotypes. Rather than obtaining the best-fit parameter values for the individual profiles, the collection of parameter sets that produced plasma concentration profiles within an acceptable range of the mean male and female profiles were identified. Despite limiting the plasma concentration profiles to a relatively narrow range, male and female phenotypes were associated with wide variability in both individual parameter values and combinations of parameters. That is, the parameter sets within a sex-specific region qualitatively produced similar model output, yet, large quantitative differences between model input were observed. As such, the isolated parameter subspaces revealed inter-individual variability within each sex as well as population differences.

The acceptance criteria for the simulated parameter combinations could be further refined such that the likelihood of a particular model output is considered to better match the population distributions to the clinical study rather than accepting parameter sets that

generate outcomes within an acceptable range with equal probability. The general conclusions drawn from the sampling-based approach regarding sexual dimorphism in pharmacokinetics paralleled the findings from the published population study, thus validating the methodology outlined herein against the well-accepted methodologies of population pharmacokinetics. Although the original study identified male and female parameterization for the statistical model, this information is largely not available for more complex physiologically based models [27]. As such, the starting point for the sampling-based methodology was a generic population that represented a mix of both sexes to demonstrate that the parameter values, as well as the multivariate parameter combinations, associated with male and female phenotypes can successfully be isolated from the mixed population given prototypical model output for the subpopulations of interest. The sampling-based approach parallels the techniques used to implement virtual clinical trials where a large number of subjects were generated from limited data [167-169]. In contrast to these virtual trials in which parameter dependencies were known *a priori*, the relationships between model input may not be previously established for special populations. The approach enables these potential underlying mechanisms to be identified as a preliminary step in virtual clinical trials when not available from existing *in vitro* data.

While the combination of parameters that gave rise to the male or female phenotypes were unique to either population, univariate distributions revealed overlapping values between male and females. Such overlap is unsurprising considering that physiological data are usually associated with a relatively narrow range of plausible values [27]. Thus, phenotype was not dictated by an individual parameter, but instead, by unique combinations across populations. Together, the elimination clearance, central compartment

volume, and the initial lag phase constituted the main differences between males and females. These findings were consistent with the fact that several physiological mechanisms contribute to observed phenotype such as differences in the gastrointestinal physiologies reflected in the initial lag time and absorption rate constant or differences in drug disposition and excretion reflected in the elimination clearance and central compartment volume for this compartment model. Augmenting analysis of the model input with global sensitivity analysis enabled an understanding of both sexual dimorphism and inter-individual variability in pharmacokinetics. The approach revealed that specific combinations of parameters gave rise to a certain phenotype, while individual parameters (negligible higher order effects) influenced the plasma concentration profile within the population. Furthermore, the sensitivity analysis revealed differences in significant parameters as a function of parameter subspace, particularly for AUC_{0-48} , which captured the influence of model parameters on the cumulative drug exposure. This finding highlighted the dependency of the sensitivity measures on the sampled input space and the need to explore model behavior using appropriate model input, consistent with previous implementations of global sensitivity analysis [155,161].

The interpretation of the underlying physiological differences between males and females was limited by the use of the compartment model as the model input were highly lumped terms describing several physiological processes through a limited number of parameters. However, the use of a simple model enabled the methodology to be validated before applying this technique to a more complex physiologically based pharmacokinetic model where there may be very limited or incomplete physiological and clinical data that serves as model input for the physiologies of interest. Given a more detailed

physiologically based model, the sampling-based approach can be used to gain insight into the underlying physiological mechanisms responsible for the observed sex differences. While the current model input was separated based on sex, similar differences for other patient factors, such as age, disease state, etc., would also be expected and could be evaluated by the described methodology.

CHAPTER 4: Modeling the influence of chronopharmacological administration using an integrated semi-mechanistic PKPD model

4.1 Introduction

Natural glucocorticoids (GC) are a class of cholesterol-derived hormones secreted from the zona fasciculata of the adrenal glands [170]. These hormones mediate a wide array of physiological functions with potent modulatory effects on metabolic, anti-inflammatory, immunosuppressive and cognitive signaling [170,171]. The synthesis of natural glucocorticoids, primarily cortisol in humans, is regulated by the hypothalamic-pituitary-adrenal (HPA) axis, which along with the sympathetic nervous system constitutes the primary physiological stress response mechanism. HPA axis activity is mediated through a signaling cascade involving the sequential release of corticotrophin-releasing hormone (CRH), adrenocorticotrophic hormone (ACTH) and cortisol (CORT). Cortisol transduces its physiological functions by binding to glucocorticoid receptors [172]. Upon cortisol binding, the glucocorticoid receptor complex translocates to the nucleus where it can regulate gene expression by binding to glucocorticoid response elements that subsequently activate or repress gene transcription [173]. Importantly, the basal activity of the HPA axis hormones exhibits pronounced circadian variation, with a peak in glucocorticoid secretion during the early morning hours in humans [172]. Cortisol is critically involved in the appropriate synchronization of peripheral circadian clock genes, which further coordinate the functions of their residing tissues and promote homeostasis [174]. Therefore, the

maintenance of homeostatic cortisol circadian rhythms is critical to overall host survival [175].

Since the discovery of the immunosuppressive and anti-inflammatory properties of cortisone (a closely related natural analog of cortisol) by Hench and Kendall in 1948 [176], synthetic GCs have been extensively used in the treatment of chronic inflammatory conditions including asthma, skin infections, and rheumatoid arthritis as well as for their immunosuppressive effects in patients undergoing organ transplantation [177-179]. Synthetic glucocorticoids have complex genomic action, similar to cortisol, with anti-inflammatory effects largely mediated by transrepression of regulatory genes involved in human immunology [180,181]. Although structurally similar to natural GCs, synthetic GCs can significantly differ in their potency and metabolic clearance to their endogenous analogs [181,182]. Despite the vast pharmacological benefits of synthetic GC administration, chronic use is associated with serious systemic adverse effects, especially during high-dose administration [183-186]. Adverse effects are attributed to the transactivation of pathways involved in diabetes and glaucoma, as well as the transrepression of the HPA axis [180,181,187]. Consistent with clinical manifestations due to cortisol exposure outside the normal physiological range, patients receiving synthetic GCs are at an increased risk of developing psychiatric disorders like depression, drug-induced hyperglycemia, long-term diabetes mellitus, osteoporosis, gastritis and cardiovascular disease [185,188-191]. Considering the diverse and complex effects of synthetic GCs, the relationship between pharmacological dosing and the biochemical, physiological and behavioral processes influenced by chronic administration of synthetic glucocorticoids has yet to be fully elucidated [173,192].

Given the central regulatory function of the endogenous glucocorticoids, chronic disruption of cortisol rhythmicity is thought to result in the subsequent misalignment of peripheral circadian clocks, thus leading to the development of systemic complications [174,193]. Therefore, there is a great deal of interest in the development of novel dosing regimens that can minimize the disruption of homeostatic circadian activity of cortisol and still maintain the pharmacological benefits of long-term synthetic GC therapy [194]. While significant progress has been made in the development of selective glucocorticoid receptor agonists that minimize transactivating properties to avoid adverse effects [181], a number of studies have investigated the influence of administration time of exogenous GCs on the endogenous cortisol rhythm with the aim of identifying chronopharmacological dosing regimens that minimize the disruption of the endogenous cortisol rhythm and the incidence of adrenal suppression. For example, healthy subjects administered synthetic GCs in the morning were found to exhibit the least suppression of the endogenous cortisol rhythm, while evening administration, resulted in maximal suppression of cortisol secretion and thus, found to be less physiologically compatible [87,179,184,195]. Additional studies aimed to replicate the endogenous cortisol activity for patients suffering from adrenal insufficiency [196]. While these studies showed that the administration time could likely be tailored to minimize disruption or to replicate the endogenous GC rhythm in the short-term, comprehensive studies on the longer-term influences of chronic dosing of synthetic GCs on the rhythmic characteristics of endogenous HPA axis activity are currently lacking.

Along with time-of-dosing, the influence of dose strength and different administration routes on endogenous HPA axis activity in the context of chronic exposure to synthetic GCs has yet to be elucidated. Adequately accounting for such factors in

exploratory experimental studies can be exceedingly expensive as clinical designs grow in complexity and size. In such cases, a model-based approach can be a particularly useful tool for efficiently generating and evaluating experimentally-verifiable hypotheses related to the dose-exposure-response relationship for synthetic GCs. Through mathematical modeling, the impact of pharmacokinetics (dose, administration time, route of administration, duration of treatment, etc.) in accordance with internal circadian rhythms and external environmental influences, such as light and feeding, can be thoroughly investigated [81,83,106,197]. For example, physiologically based modeling was previously implemented to understand how endogenous melatonin, a compound with strong circadian dependence, was influenced by the administration of exogenous melatonin and to elucidate the chronopharmacokinetics of exogenous melatonin for replication of the endogenous rhythm of melatonin [97].

In this study, a mathematical model was developed to explore the influence of exogenous GC dosing on the endogenous cortisol rhythm for a generic synthetic GC, considering both an intra-venous bolus and once-daily oral dosing. For these administration routes, the HPA axis activity was compared as indicated by changes in the cortisol rhythm due to a bolus of drug in systemic circulation with the pharmacological response following slower appearance rates in systemic circulation considering absorption after oral dosing. Furthermore, differences in the response to short term and chronic treatment were determined. As such, the goal of this study was to elucidate how long-term chronopharmacological dosing regimens influenced the basal cortisol activity using a model-based approach. Within the context of personalized medicine, this study emphasized

how delivering the ‘right dose’ at the ‘right time’ minimized the impact to normal biological functioning using a dynamic, semi-mechanistic PKPD model.

4.2 Approach

4.2.1 Description of the HPA axis model

A schematic of the model is depicted in **Figure 20**. The underlying form of the oscillator was originally developed by Goodwin [198], and has since been modified to include the Michaelis-Menten type degradation kinetics, which obviates the need to use unrealistically large Hill coefficients [199]. Given an appropriate choice of parameters, the model equations are able to produce circadian (24-hour periodic) oscillations [77,83,200].

The primary mediators of the HPA axis, CRH, ACTH and cortisol (CORT) are represented by nonlinear ordinary differential equations (ODEs). CRH induces the release of ACTH from the pituitary gland, which subsequently induces the release of CORT from the adrenal glands (**Equation 23-25**). The synthesis of CRH in the hypothalamus is described by zero-order kinetics, while ACTH and CORT synthesis is described by first-order kinetics. Moreover, the model accounts for the binding of CORT to the glucocorticoid receptor (GR) [77] as well as the pharmacodynamics of the cortisol-bound receptor complex (**Equation 26-29**).

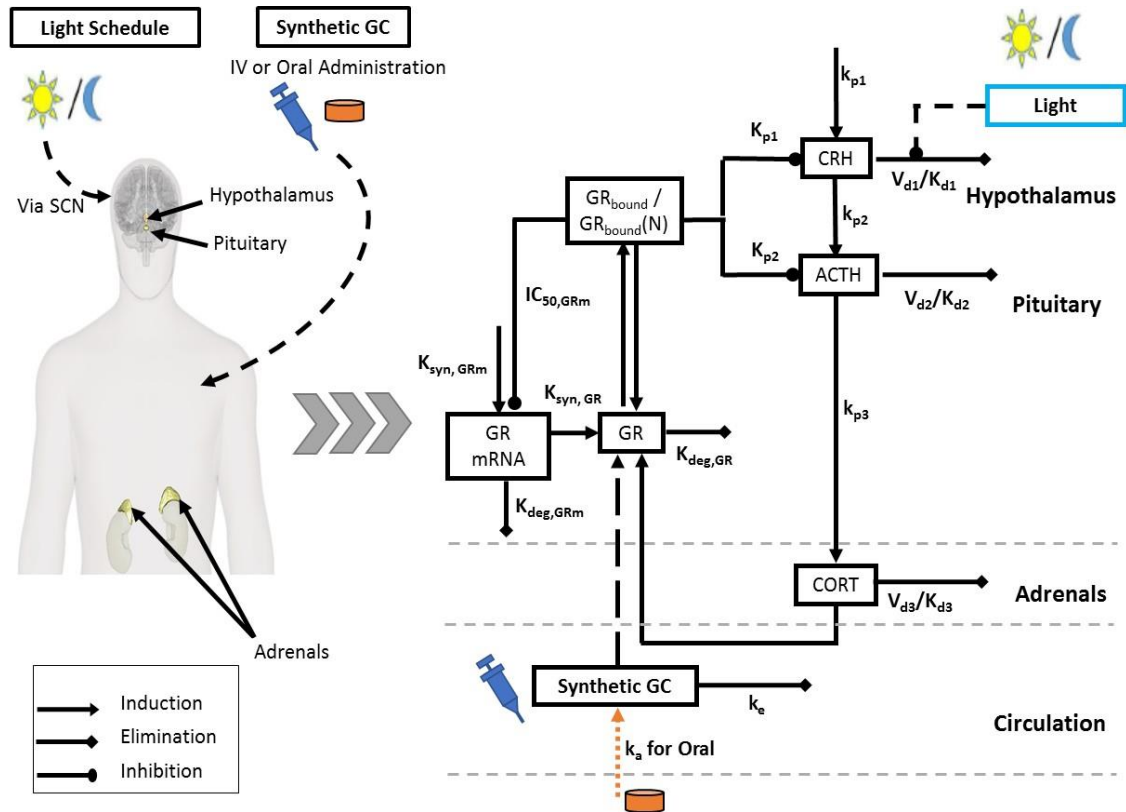


Figure 20: Model Schematic: A schematic of the model depicting the primary interactions in the hypothalamus-pituitary-adrenal (HPA) axis. The synthetic glucocorticoids (GC) competitively bind to the glucocorticoid receptor and contribute to the negative feedback arm of the HPA axis. Synthetic GCs are administered by either a bolus injection directly into systemic circulation or by oral administration. Appearance in systemic circulation following oral administration is indicated by the orange line.

Briefly, the model accounts for the transcription of GR mRNA (GR_{mRNA}), (**Equation 26**) and the subsequent translation of GR protein (GR) (**Equation 27**). CORT forms a complex with cytoplasmic GR, (GR_{bound}). A fraction of this complex translocates to the nucleus, $GR_{bound}(N)$. Upon translocation, the hormone-receptor complex, (GR_{bound}) is known to negatively regulate the expression of (GR_{mRNA}), which is accounted for in **Equation 26**. Finally, **Equations 23-24** account for inhibitor influence of the nucleated CORT-bound receptor complex, $GR_{bound}(N)$, on the release of CORT and ACTH.

Furthermore, the entraining influence of light on the HPA axis via the suprachiasmatic nucleus (SCN) was considered. Light is assumed to have an inductive

influence on CRH in diurnal animals by inhibiting its degradation [201]. A symmetric light schedule (12-hour light/12-hour dark) was used to entrain the HPA axis model. Such a light schedule has been used previously in mathematical modeling studies to investigate the influence of light entrainment on the behavior of the endogenous circadian clock and the HPA axis hormones [81,83,202,203]. While a simple 12-hour light/12-hour dark schedule was used in the present study, more complex light schedules could be considered to investigate the influence of factors such as seasonality on the pharmacodynamic response of synthetic GCs. The model considers a 1 to 2-hour delay between the start of light exposure and the onset of the photo-induced effects in the HPA axis, denoted by the term $light_{effect}$ [204]. This delay in the photo-inductive effect on the HPA axis was modeled using a series of transit compartments. Finally, a step function is used to model the light profile, while a Hill function is used to describe the dynamics of the phototransduction pathways (**Equation 17-22**). All simulations were implemented in MATLAB 2017b. Model equations were integrated using MATLAB's built-in ode45 routine.

4.2.1.1 HPA Axis Mediators

$$light = \begin{cases} 1 & 6:00 \leq t \leq 18:00 \\ 0 & 18:00 < t < 6:00 \end{cases} \quad \text{Eq. 17}$$

$$\frac{dlight_{TCsynth1}}{dt} = k_t(light - light_{TCsynth1}) \quad \text{Eq. 18}$$

$$\frac{dlight_{TCsynth1i}}{dt} = k_t(light_{TCsynth1i-1} - light_{TCsynth1i}), i = \{1,2,3\} \quad \text{Eq. 19}$$

$$\frac{d\text{light}_{TCdeg1}}{dt} = k_t(\text{light}_{deg} - \text{light}_{TCdeg1}) \quad \text{Eq. 20}$$

$$\frac{d\text{light}_{TCdeg i}}{dt} = k_t(\text{light}_{TCdeg i-1} - \text{light}_{TCdeg i}); i = \{1,2,3\} \quad \text{Eq. 21}$$

$$\begin{aligned} \frac{d\text{light}_{effect}}{dt} = & k_{us} \frac{\text{light}_{TCsynth i}^n}{K_{M,us}^n + \text{light}_{TCsynth i}^n} - k_{deg,us} \text{light}_{effect} (1 \\ & + k_{eff} \text{light}_{TCdeg i}) \end{aligned} \quad \text{Eq. 22}$$

$$\frac{dCRH}{dt} = \frac{k_{p1} \cdot K_{p1}}{K_{p1} + GR_{bound}(N)} - V_{d1} \cdot \frac{CRH \cdot \left(1 - \frac{\text{light}_{effect}}{1 + \text{light}_{effect}}\right)}{K_{d1} + CRH} \quad \text{Eq. 23}$$

$$\frac{dACTH}{dt} = \frac{k_{p2} \cdot K_{p2} CRH}{K_{p2} + GR_{bound}(N)} - V_{d2} \cdot \frac{ACTH}{K_{d2} + ACTH} \quad \text{Eq. 24}$$

$$\frac{dCORT}{dt} = k_{p3} \cdot ACTH - V_{d3} \cdot \frac{CORT}{K_{d3} + CORT} \quad \text{Eq. 25}$$

4.2.1.2 Glucocorticoid Receptor Pharmacodynamics

$$\frac{dGR_{mRNA}}{dt} = k_{synGRm} \cdot \left(1 - \frac{GR_{bound}(N)}{IC_{50GRm} + GR_{bound}(N)}\right) - k_{deg} \cdot GR_{mRNA} \quad \text{Eq. 26}$$

$$\begin{aligned} \frac{dGR}{dt} = & k_{syn,GR} \cdot GR_{mRNA} + r_f \cdot k_{re} \cdot GR_{bound}(N) - k_{on} \cdot (CORT) \cdot GR \\ & - k_{deg,GR} \cdot GR \end{aligned} \quad \text{Eq. 27}$$

$$\frac{dGR_{bound}}{dt} = k_{on} \cdot (CORT) \cdot GR - k_T \cdot GR_{bound} \quad \text{Eq. 28}$$

$$\frac{dGR_{bound}(N)}{dt} = k_T \cdot DR - r_f \cdot k_{re} \cdot GR_{bound}(N) \quad \text{Eq. 29}$$

4.2.2 Description of pharmacokinetic models for synthetic GC administration

Once-daily dosing is described using pharmacokinetic models that qualitatively captured the experimentally observed features of the drug exposure profile, such as the absorption rate and half-life, for a generic synthetic GC. While some synthetic GCs demonstrate complex pharmacokinetics due to competitive binding of the corticosteroid binding globulin (CBG) and interconversion between pharmacologically active and inactive forms by 11β -hydroxysteroid dehydrogenase type1/2 [182,184,205], linear pharmacokinetics are assumed for the model drug. Disruption of endogenous cortisol circadian rhythmicity following dosing may be evaluated under the assumption of linear pharmacokinetics to understand qualitative changes in the dose-exposure-response relationship.

To assess how the endogenous cortisol rhythm is influenced by the rate of appearance of drug into the system, pharmacokinetic models describing an intra-venous (IV) and oral dosing are used assuming absorption and elimination follow first-order rate processes. Disposition of synthetic GCs was previously described by 1 or 2 compartment models depending on the drug, administration route and dose [182]. For this preliminary dosing study, a 1-compartment model is assumed to describe drug distribution within the body. The rate of disappearance of drug from systemic circulation following an injection is described by **Equation 30**. Disappearance from the gastrointestinal tract (GIT) after oral administration is described by **Equation 31** and the amount of drug in systemic circulation is given by **Equation 32**. These equations are simplified from those developed by Xu et al.

for IV and oral dosing of prednisolone using a 1-compartment model [205], neglecting first pass extraction and interconversion between prednisolone and prednisone for the arbitrary synthetic GC. Since the displacement of cortisol from plasma protein, metabolic enzymes, and GR binding sites due to competition with synthetic GCs is not considered, the loss of endogenous cortisol and drug from the system are independent in this model.

The 1-compartment model (**Equation 32**) was amended to simulate extended release of an oral dose using a series of five transit compartments (TC) as shown in **Equations 33-35**. The use of transit compartments has previously been implemented to delay the absorption rate in pharmacokinetic models [206,207]. In this study, the number of transit compartments and absorption rate constants for the slow-acting synthetic GC were selected to delay the absorption rate by approximately 3-fold while maintaining the same elimination rate constant as the fast-acting GC, and ensure drug was cleared from the body within 24 hours. The pharmacokinetics of synthetic GCs as described by **Equations 33-35** will herein be referred to as slow-acting synthetic GCs whereas the behavior described by **Equation 32** will be referred to as the fast-acting synthetic GCs.

4.2.2.1 IV administration

$$\frac{dGC}{dt} = -k_E \cdot GC \quad \text{Eq. 30}$$

4.2.2.2 Oral administration

$$\frac{dGC_{GIT}}{dt} = -k_a \cdot GC_{GIT} \quad \text{Eq. 31}$$

$$\frac{dGC}{dt} = k_a \cdot GC_{GIT} - k_E \cdot GC \quad \text{Eq. 32}$$

$$dGC_{TC1} = k_{at,1} \cdot (GC_{GIT} - GC_{TC1}) \quad \text{Eq. 33}$$

$$dGC_{TC,i} = k_{at,i} \cdot (GC_{TC,i-1} - GC_{TC,i}), i = 2,3,4,5 \quad \text{Eq. 34}$$

$$\frac{dGC}{dt} = k_a \cdot GC_{TC5} - k_E \cdot GC \quad \text{Eq. 35}$$

4.2.2.3 Glucocorticoid receptor pharmacodynamics after GC dosing

Upon dosing synthetic GCs, the equations describing the glucocorticoid receptor dynamics are modified to consider binding of the synthetic GC, as well as cortisol, to the glucocorticoid receptor, resulting in increased negative feedback to the HPA axis precursors, CRH and ACTH. GR is assumed to have the same affinity for endogenous and synthetic GCs.

$$\begin{aligned} \frac{dGR}{dt} = & k_{syn,GR} \cdot GR_{mRNA} + r_f \cdot k_{re} \cdot GR_{bound}(N) - k_{on} \cdot (CORT + GC) \cdot GR \\ & - k_{deg,GR} \cdot GR \end{aligned} \quad \text{Eq. 36}$$

$$\frac{dDR}{dt} = k_{on} \cdot (CORT + GC) \cdot GR - k_T \cdot GR_{bound} \quad \text{Eq. 37}$$

4.2.2.4 Parameterization of the model

The model is calibrated to qualitatively match the early morning peak in the endogenous cortisol circadian rhythm in healthy human subjects [172] in order to understand how the endogenous cortisol rhythm is modified by drug administration in the

absence of chronic inflammation. The model input parameters are given in **Supplementary Table 9**.

4.2.3 Dosing experiments

Several chronopharmacological dosing regimens are simulated to understand how administration time, dosing strength, administration route, and duration of treatment of synthetic GCs disrupted HPA axis activity. The once-a-day administration time of the IV bolus or oral dose of synthetic GCs is varied by 1-hour intervals throughout the simulated day. Different doses of synthetic GCs are modeled to evaluate how the strength of negative feedback via the glucocorticoid receptor dynamics influence the endogenous cortisol rhythm. Doses varied from the nominal amount of 1x are classified as low (less than 1x), intermediate (2x to 10x), and high (above 10x). For both administration routes, the pharmacological effects of short term and chronic treatments are simulated using a single dose and multiple doses with a dosing interval of 24 hours for once-a-day administration.

Changes in amplitude, acrophase, and area-under-the-curve (AUC) of the endogenous cortisol rhythm are used as metrics to quantify disruption of the HPA axis activity relative to the baseline activity. Amplitude and acrophase are determined when the cortisol rhythm reached a new stable oscillatory state after chronic once-daily dosing. The relative change in amplitude is calculated by **Equation 38**.

Relative Amplitude (%)

$$= \frac{Amplitude_{treatment} - Amplitude_{baseline}}{Amplitude_{baseline}} \times 100\%$$

Eq. 38

The AUC of the endogenous cortisol profile is determined for the 24-hour period following the first dose and after multiple doses when the cortisol rhythm reaches the new stable state. The change in 24-hour AUC for short and long term pharmacological effects is calculated by **Equation 39**.

$$\begin{aligned} & \text{Relative AUC (\%)} \\ & = \frac{AUC_{[t_{dose} \rightarrow t_{dose}+24hr]}_{treatment} - AUC_{[t_{dose} \rightarrow t_{dose}+24hr]}_{baseline}}{AUC_{[t_{dose} \rightarrow t_{dose}+24hr]}_{baseline}} \times 100\% \end{aligned} \quad \text{Eq. 39}$$

Simulations are compared against various clinical studies that evaluated disruption of the endogenous cortisol rhythm following intra-venous and oral administration of synthetic glucocorticoids [87,178,184,208].

4.3 Results

4.3.1 Pharmacokinetic profiles for the synthetic glucocorticoid

The pharmacokinetic profiles for the representative synthetic glucocorticoid administered by IV and oral administration routes are given in **Figure 21** for the nominal dose of 1x. The faster-acting oral dose resulted in a $C_{max} \approx 40\%$ of the initial dose, $t_{max} = 2.75$ hours, and 100% bioavailability ($AUC_{IV} = AUC_{oral}$). The slow-acting oral GC had a $C_{max} \approx 30\%$ of the initial dose, $t_{max} = 8.4$ hours, and 99% bioavailability.

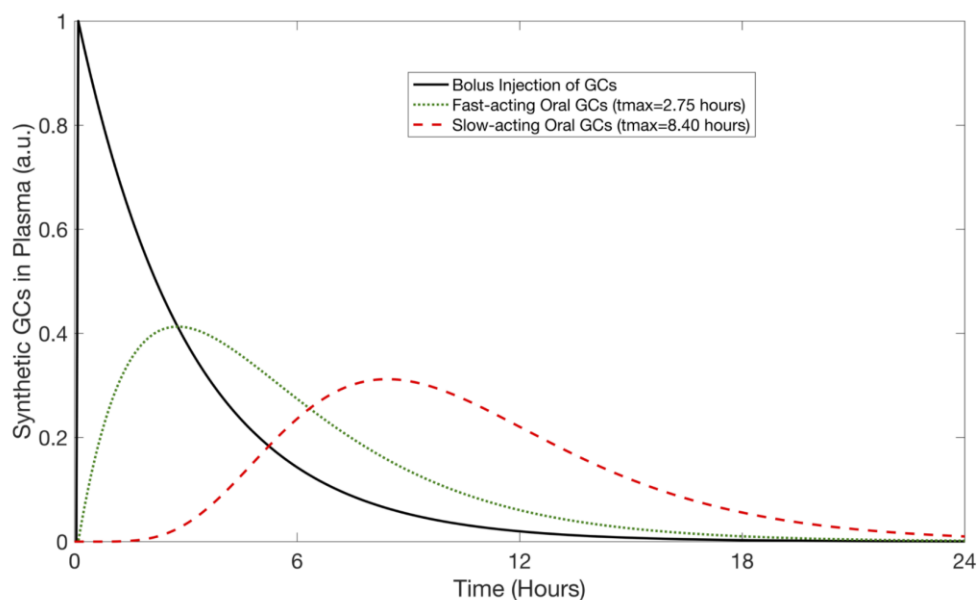


Figure 21: Pharmacokinetic profiles for a bolus injection, a fast-acting oral dose, and a slow-acting oral dose of synthetic GCs. Representative profiles are shown for a nominal dose of 1x. Plasma concentration is given in arbitrary units (a.u.).

4.3.2 Influence of once-daily chronopharmacological dosing of synthetic GCs on the cortisol circadian rhythm

Once-a-day administration of synthetic GCs caused endogenous cortisol activity to evolve to a new stable, regular circadian rhythm (**Figure 22**). Upon termination of treatment, the cortisol rhythm returned to the basal activity observed prior to dosing (**Supplementary Figure 8**).

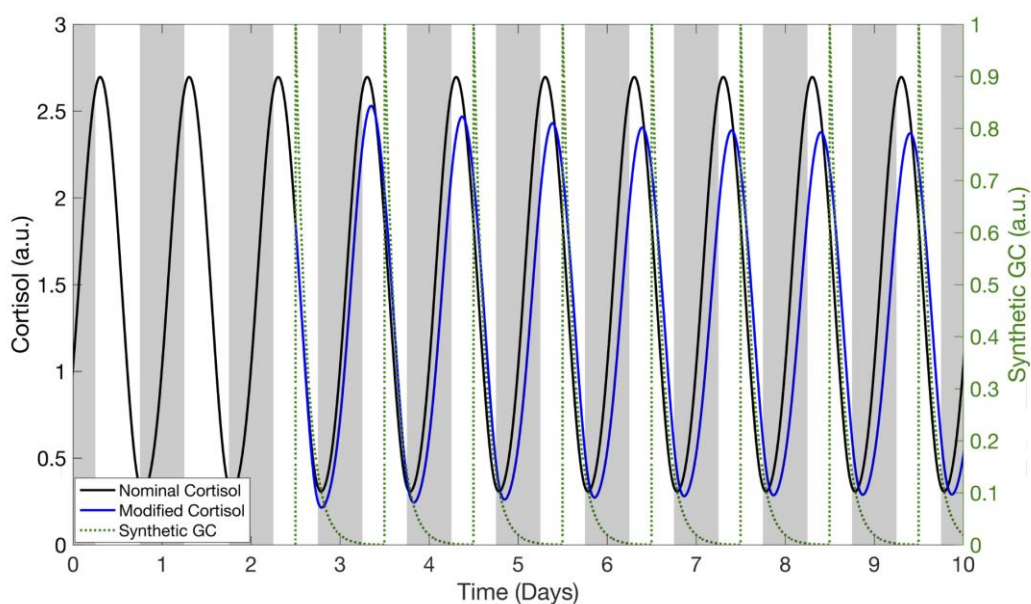


Figure 22: Modified cortisol profiles after dosing of synthetic glucocorticoids (GC) by bolus injection at the nominal amount (1x). The modified cortisol rhythm is indicated by the blue line. The black line corresponds to the nominal cortisol profile based on endogenous HPA axis activity. The pharmacokinetic profiles for the bolus injection are indicated by the dotted green line. The grey shaded areas represent the time at which the system is not exposed to light. Cortisol concentration is given in arbitrary units (a.u.).

The amplitude and acrophase of this new stable cortisol rhythm depended on the time at which the drug was administered as shown in **Figure 23**. Amplitude generally decreased when the daily dosing of synthetic GCs by bolus injection was initiated during the declining phase of the nominal cortisol rhythm (**Figure 23a**). The endogenous cortisol rhythm following once-a-day administration of the fast-acting and slow-acting oral doses qualitatively showed similar changes in amplitude as the bolus injection, but with an advance in dosing times by about 2 hours and 6 hours to produce the same effect on the cortisol rhythm. The shifts roughly correlated with the time needed to reach the maximum pharmacological effect following oral administration due to the absorption rates ($t_{\max} = 2.75$ hours and $t_{\max} = 8.4$ hours). Maximal suppression occurred when synthetic GCs were administered daily at 3:00 PM by bolus injection, 1:00 PM for the faster-acting oral dose, and 9:00 AM for the slow-acting oral dose. For all administration routes, certain once-daily

chronopharmacological dosing regimens resulted in HPA axis induction, corresponding to an increase in amplitude of the endogenous cortisol rhythm. Maximal induction of the endogenous cortisol amplitude largely occurred when synthetic GCs were administered during the simulated night.

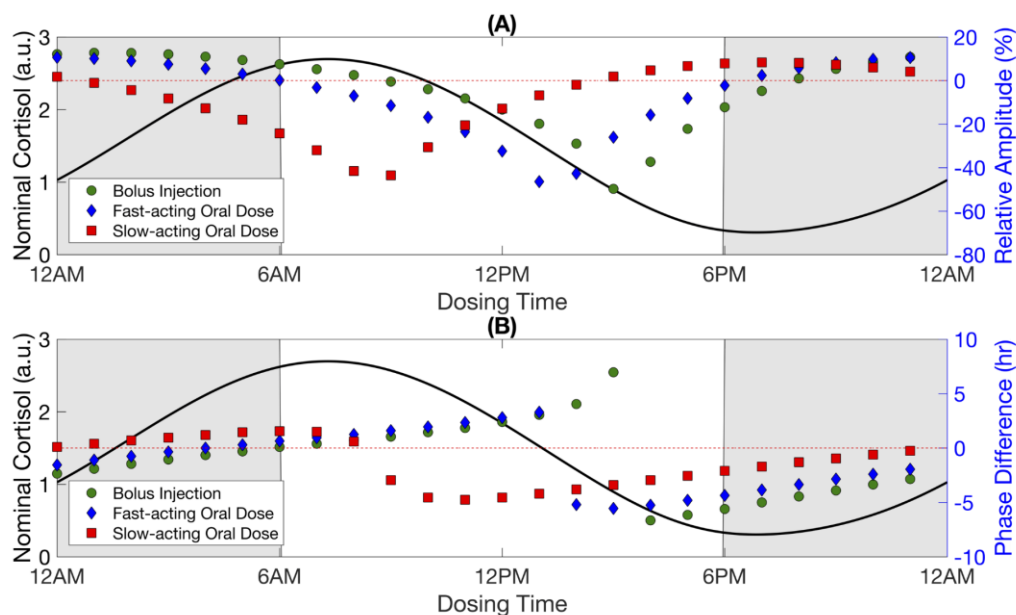


Figure 23: Amplitude and phase of the modified cortisol rhythm after once-daily chronopharmacological dosing of synthetic glucocorticoids. The relative amplitude and difference in the acrophase of the modified cortisol rhythm after a repeated once-a-day administration of a bolus injection, fast-acting oral dose, or slow-acting oral dose are shown in A and B, respectively. The nominal cortisol rhythm (indicated by the black line) is given for reference to show how dosing times align with the baseline circadian rhythm. The shaded areas represent the simulated night, that is the time at which the system is not exposed to light. The change in amplitude is calculated by $\text{Relative Amplitude (\%)} = \frac{(\text{Amp}_{\text{treatment}} - \text{Amp}_{\text{baseline}})}{\text{Amp}_{\text{baseline}}} \times 100\%$. A negative value for phase difference indicates an advance in the acrophase (i.e. peaks earlier in the simulated day relative to the nominal cortisol rhythm) while a positive value indicates a delay in the acrophase (i.e. peaks later in the simulated day). Cortisol concentration is given in arbitrary units (a.u.).

A once-daily bolus injection introduced near the nadir or during the rising phase of the nominal cortisol rhythm predicted an advance in the acrophase of the cortisol rhythm, whereas initiating dosing near the peak or descending phase of the cortisol rhythm resulted in a delay of the acrophase (**Figure 23b**). For both administration routes, the change in acrophase was most sensitive when synthetic GCs were administered at dosing times

associated with greatest amplitude suppression for all routes of administration. Furthermore, while the change in acrophase for the bolus injection and fast-acting oral doses exhibited a discontinuity (termed Type 0 [209]), the acrophase response varied more smoothly (continuous, termed Type 1 [209]) for the slow-acting oral dose, which had a lower maximal plasma concentration. The relationship between amplitude and phase are shown **Figure 24** for the bolus injection and the slow-acting oral dose. The fast-acting oral dose revealed similar behavior to the bolus injection (data not shown). Depending on the time of synthetic GC administration, the acrophase of the new stable rhythm was found to adopt two different values for a given change in its amplitude with the difference between acrophases increasing with greater amplitude suppression as observed for the bolus injection (**Figure 24a**). Similar behavior was observed for the slow-acting GC, but to a lesser extent (**Figure 24b**).

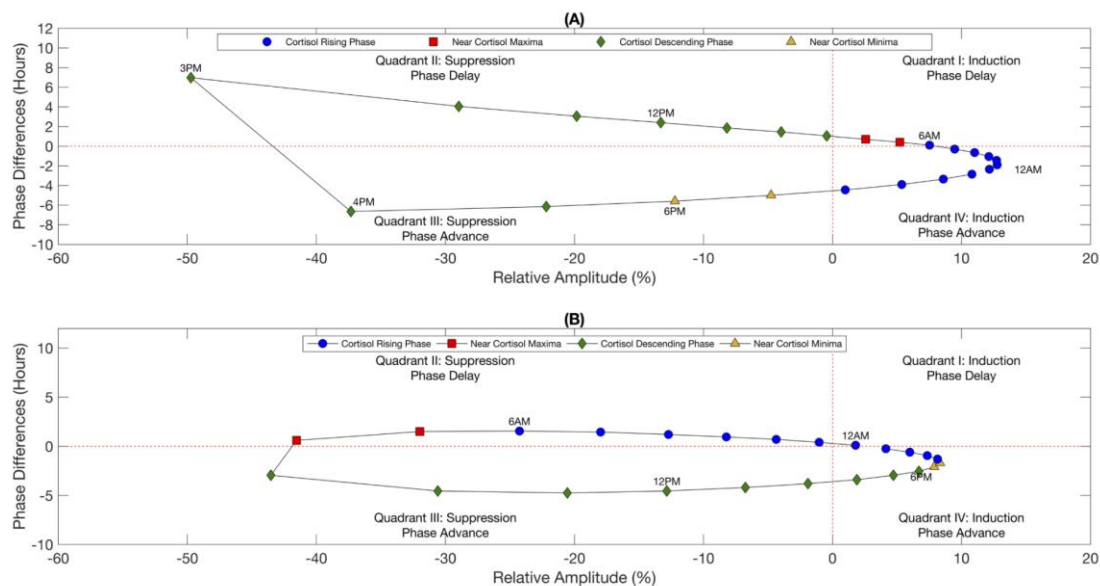


Figure 24: Relationship between the relative amplitude and phase difference of the modified cortisol rhythm after long-term once-daily chronopharmacological dosing of synthetic glucocorticoids. Amplitude and phase for the modified cortisol rhythms after chronic administration of a daily bolus injection and the slow-acting oral dose are shown in A and B, respectively. Marker labels correspond to the time of administration. Marker color indicates the administration time relative to the nominal cortisol rhythm where blue circles correspond to dosing times from 8:00 PM to 6:00 AM (ascending phase of baseline rhythm), red squares correspond to dosing times from 7:00 AM to 8:00 AM (near peak of baseline rhythm), green diamonds correspond to dosing times from 9:00 AM to 5:00 PM (descending phase of baseline rhythm), and yellow triangles correspond to dosing times from 6:00 PM to 7:00 PM (near nadir of baseline rhythm).

Importantly, simulations indicated that specific chronopharmacological regimens of synthetic GC administration can minimize the disruption of the nominal GC rhythm. For example, daily administration of a nominal dose of synthetic GCs by bolus injection around 9:00 AM (**Supplementary Figure 8**), resulted in a minimal change to the amplitude and acrophase of the cortisol rhythm relative to the basal activity, whereas a fast-acting oral dose at 6:00 AM or a slow-acting oral dose at midnight resulted in minimal change. Moreover, the amplitude change after a single dose was not indicative of the amplitude change after repeated administration (**Figure 25**) considering that several days to weeks of once-a-day dosing was needed before the endogenous cortisol stabilized to the new rhythm.

Simulations predicted similar behavior following oral administration (**Supplementary Figure 9**).

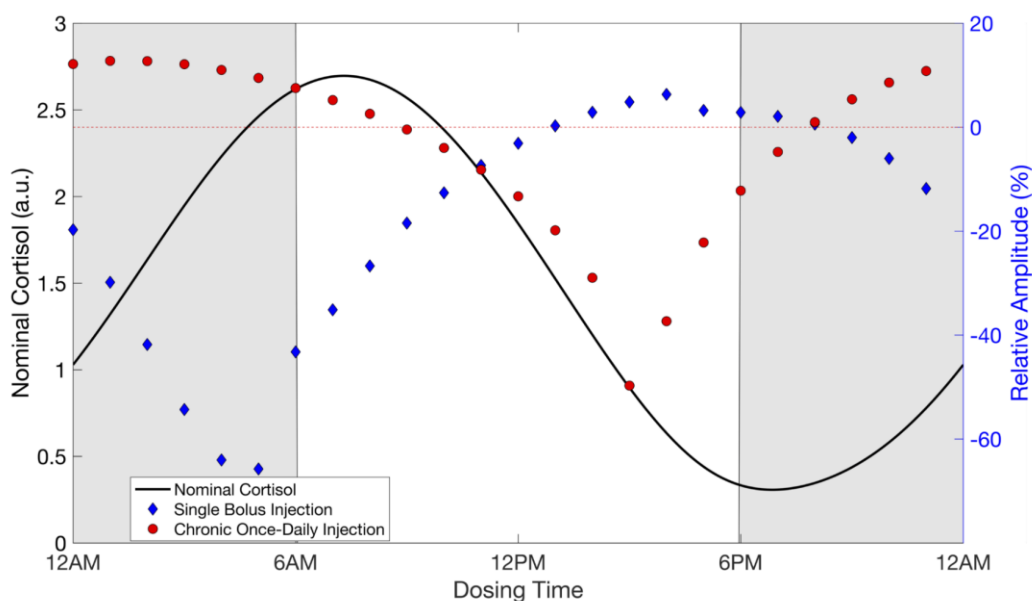


Figure 25: Amplitude of the modified cortisol rhythm after single and repeated once-daily chronopharmacological dosing of synthetic glucocorticoids by bolus injection at the nominal dose. The relative amplitude associated with the modified cortisol rhythm after a single injection and after long-term once-daily IV dosing are shown. The relative change in amplitude is calculated by $\text{Relative Amplitude (\%)} = \frac{(\text{Amp}_{\text{treatment}} - \text{Amp}_{\text{baseline}})}{\text{Amp}_{\text{baseline}}} \times 100\%$. Cortisol concentration is given in arbitrary units (a.u.).

4.3.2.1 Influence of dosing on total cortisol exposure

The induction of the cortisol amplitude in response to once-daily chronopharmacological dosing of synthetic GCs does not necessarily imply an increase in the total cortisol secreted by the adrenal glands in the 24-hour period following dosing, herein referred to as the total cortisol exposure. While the amplitude of the endogenous cortisol rhythm quantified the difference between the altered minima and maxima following once-a-day administration of synthetic GCs, the change in 24-hour AUC indicated how total cortisol exposure differed relative to the basal HPA axis activity. The relationship between amplitude and 24-hour AUC after repeated administration of a once-

daily injection are shown in **Figure 26a**. Long-term dosing during the night between 10:00 PM and 5:00 AM indicated induction of the HPA axis by both the amplitude and 24-hour AUC, while chronic dosing during the day between 9:00 AM and 7:00 PM were associated with HPA axis suppression as shown by the reduced amplitude and 24-hour AUC. Interestingly, simulations showed that dosing between 6:00 to 8:00 AM and 8:00 to 9:00 PM resulted in increased amplitude, but reduced total cortisol exposure (24-hour AUC) relative to the basal cortisol activity without synthetic GCs.

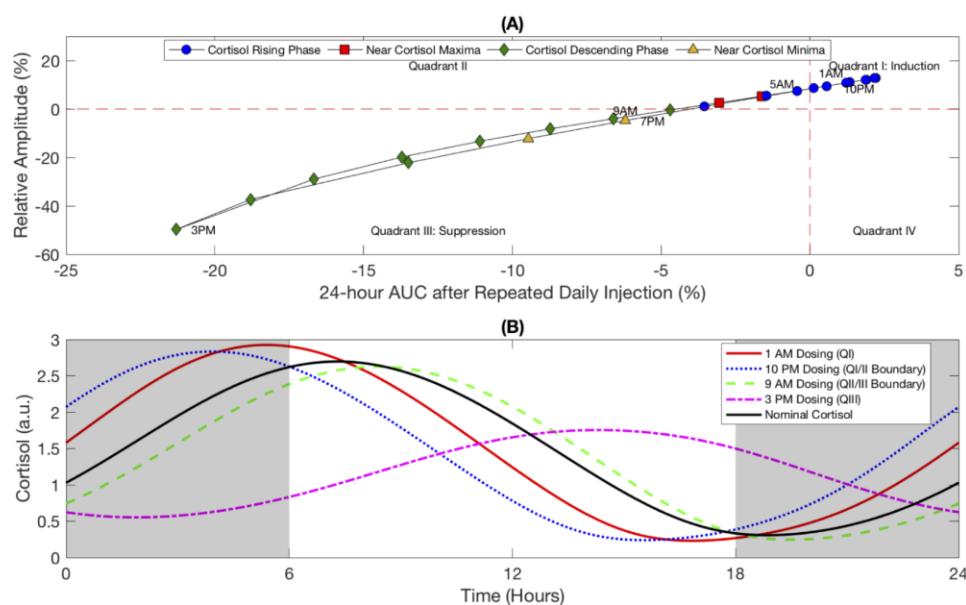


Figure 26: Influence of chronic once-daily chronopharmacological dosing on the total cortisol exposure. The relationship between the 24-hour AUC and amplitude change after long-term dosing of a daily bolus injection at the nominal dose (1x) is shown in A. The modified cortisol profiles after dosing and for the baseline conditions are given in B for selected dosing times. The grey shaded areas represent the simulated night, that is the time at which the system is not exposed to light. Cortisol concentration is given in arbitrary units (a.u.).

Endogenous cortisol profiles are given in **Figure 26b** for selected dosing times. The cortisol rhythm associated with maximum induction (dosing at 1:00 AM) showed increased daily cortisol maxima and reduced daily cortisol minima, in which the shift in maxima was sufficient to increase the total cortisol exposure despite the reduction in minima. In

contrast, the predicted cortisol profile associated with maximum HPA axis suppression (dosing at 3:00 PM) revealed a decrease in daily maxima and an increase in daily minima, leading to an overall reduction in 24-hour exposure. Cortisol profiles that fell within quadrant II of **Figure 26a** showed a decreased daily cortisol nadir and an increased daily cortisol maximum, which was insufficient to overcome the decreased minima, leading to an overall decline in the total cortisol exposure (data not shown). Two additional cortisol profiles are provided in **Figure 26b** characterized by a negligible change in 24-hour AUC following repeated dosing at 10:00 PM (nearest the boundary between quadrants I and II), and negligible amplitude change after repeated dosing at 9:00 AM (nearest the boundary between quadrants II and III). The former scenario showed the increase in daily cortisol was balanced by a reduction in the cortisol nadir such that the 24-hour AUC was maintained, while the latter case revealed the cortisol maxima and nadir were both reduced such that no net change was observed in the peak to trough height relative to the baseline amplitude. Similar behavior was predicted for oral administration (**Supplementary Figure 10**), although no profiles were observed in Quadrant I for the slow-acting oral GC.

4.3.2.2 Influence of dosing strength on the activity of the HPA axis

The amplitude of the cortisol rhythm associated with once-daily chronopharmacological dosing of a bolus injection that predicted the greatest suppressive and inductive effects on the HPA axis activity are given in **Figure 27** for several dosing strengths, where 1x corresponded to the nominal amount.

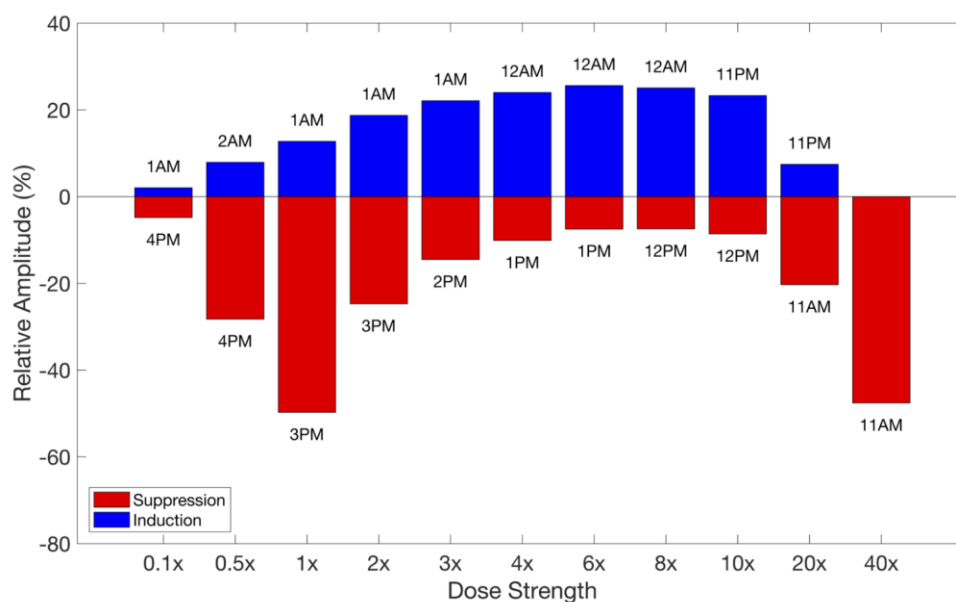


Figure 27: Influence of dosing strength on the relative amplitude after chronic once-daily chronopharmacological dosing of a bolus injection. The relative amplitude for the modified cortisol rhythms are given for the once-daily chronopharmacological dosing regimens that resulted in the greatest inductive and suppressive effects at each strength of the IV dose. The administration times corresponding to these changes in amplitude are indicated in the figure.

The amplitude changes associated with all chronopharmacological injections are given in **Supplementary Figure 11a**. Higher doses led to maximum suppression and induction earlier in the simulated day than low or intermediate doses. As the dose increased beyond the nominal, once-daily dosing during the simulated night led to increased inductive effects while dosing in the simulated day showed reduced suppressive effects up to 6x. Beyond 6x, the inductive effects were reduced and suppression increased until only suppression was observed at all dosing times at 40x. Furthermore, the model predicted that the acrophase of the endogenous cortisol rhythms was also sensitive to the dosing strength as shown in **Supplementary Figure 11b** where low doses of the bolus injection were associated with continuous Type 1 phase response curves, and intermediate and high doses of the bolus injection were associated with discontinuous Type 0 phase response curves. Below the nominal dose, the maximal phase resetting and greatest suppression of the

amplitude were predicted to occur at the same dosing time whereas the maximal phase resetting occurred at dosing times well after maximal suppression of the amplitude was observed for intermediate and high doses.

The dose-response relationship following oral administration of fast and slow-acting synthetic GCs are provided in **Supplementary Figure 12**. The amplitude change associated with all chronopharmacological dosing regimens are given in **Supplementary Figure 13a** and **Supplementary Figure 14a**, respectively. For the nominal and low doses, the bolus injection showed greatest amplitude suppression after chronic once-daily pharmacological dosing compared to the equivalent oral doses of the fast or slow acting GCs. Beyond the nominal amount, greater suppression of the amplitude was predicted for the slow-acting oral dose, while the fast-acting oral dose showed an intermediate effect at all dosing strengths. Differences between administration routes were attributed to the duration at which the synthetic GCs was maintained above a minimum pharmacologically active amount and the maximal concentration achieved at an equivalent dose. Interestingly, the bolus injection resulted in greater induction of HPA axis activity for all dose strengths, which may result due to the very high initial concentrations immediately following the bolus injection. Furthermore, administration of the fast-acting oral GCs resulted in a phase-response relationship that was qualitatively similar to that obtained during IV administration. For the slow-acting oral GCs, discontinuous Type 0 phase response curves were associated with intermediate and high doses with the discontinuity occurring at dosing times during the simulated day, except at very high doses when the phase discontinuity was observed near the start of the simulated night. The phase change associated with all chronopharmacological dosing regimens are given in **Supplementary Figure 13b** and

Supplementary Figure 14b. Moreover, the relationship between 24-hour AUC and amplitude following repeated administration of synthetic GCs by all administration routes are provided in **Supplementary Figure 15** to **Supplementary Figure 17** for several dosing strengths.

4.4 Discussion

Recognizing the functional importance of the circadian regulation underlying the signaling dynamics of complex physiological systems, such as the HPA axis, has led to great interest in the incorporation of chronobiological principles for the development of safer and more efficacious therapies [95,210]. A major concern associated with long-term therapeutic use of GCs is the suppression of endogenous HPA axis activity [174]. However, chronopharmacological delivery of synthetic GCs is a promising approach to minimize the disruption of the endogenous cortisol circadian rhythmicity. In the present work, a semi-mechanistic mathematical model of the HPA axis was used to study the influence of chronic chronopharmacological intervention on endogenous HPA axis activity.

The model predicted that for all simulated dose strengths and routes of administration considered, the endogenous circadian activity of the HPA axis adapted to the repeated daily exposure to synthetic GCs by adopting a new stable circadian rhythm. Moreover, all three routes of administration of synthetic GCs resulted in qualitatively similar alterations of the cortisol circadian rhythm. However, due to differences in the duration for which synthetic GCs were maintained above a minimum pharmacologically active amount, both the oral administration routes considered resulted in a greater suppression of HPA axis activity in comparison to IV administration. For a given dosing

strength, oral administration resulted in a comparable change in the rhythmic characteristics of the cortisol rhythm at earlier dosing times. This shift in response to earlier dosing times was most prominent for slow-acting oral administration, for which the maximal plasma drug concentrations were delayed the longest. Therefore, results suggested that the exposure profile of synthetic GCs might be systematically manipulated in order to optimize the dosing time as well as the pharmacodynamic effect on the cortisol rhythm. An improved characterization of the chronopharmacological influence of synthetic GCs on HPA axis activity can lead to the development of novel dosage forms in order to improve patient compliance and limiting the incidence of adverse effects while maintaining treatment efficacy [211]. Indeed, modified-release (MR) prednisolone tablets that delay the release of drug up to 4 hours after administration have been developed to chronopharmacologically target the late-night (2:00 to 4:00 AM) circadian rise in proinflammatory cytokines in rheumatoid arthritis (RA) patients by enabling the dose to be administered at 10:00 PM, conveniently before the patients slept [178]. The use of MR prednisolone was shown to result in an improvement in clinical symptoms while also preventing the suppression of endogenous cortisol rhythmicity. Furthermore, once-daily dosing of extended release formulations have proven effective for improved pain relief in patients with osteoarthritis of the knee [212] and in studies aiming to replicate endogenous cortisol rhythmicity in patients suffering from adrenal insufficiency [213,214], thereby replacing therapies requiring multiple doses per day. Together, these studies highlight the benefits of novel formulations with systematically manipulated exposure profiles to aide in the development of improved treatment options.

The maintenance of homeostatic circadian rhythms in the HPA axis is dependent on an intricate balance between the temporally-varying feedforward and feedback processes within the HPA network. Given this variation in regulatory dynamics of the HPA axis, chronopharmacological dosing can reduce the disruption of the endogenous cortisol rhythm. Indeed, simulations suggest that once-daily administration of synthetic GCs shortly after the start of the active phase (around 6:00 AM for fast-acting oral GCs or 9:00 AM for a bolus injection) can minimize the suppression of the endogenous cortisol rhythm, by largely preserving its amplitude and acrophase. Moreover, the simulated suppression of the cortisol rhythm after the first dose is in qualitative agreement with experimental findings exploring the short-term influence of the synthetic GC administration of endogenous cortisol rhythmicity. A number of studies have found that administration of a single dose of synthetic GCs by infusion in the morning results in minimal disruption of the endogenous cortisol rhythm, while evening administration is associated with a substantial suppressive effect [87]. Long-term daily administration of synthetic GCs by bolus injection or a fast-acting oral dose in the latter half of the active phase (late afternoon in humans) is predicted to result in maximal suppression of the cortisol rhythm.

In addition to the changes in amplitude, there were substantial alterations in the acrophase of the cortisol rhythm upon long-term once-daily administration of synthetic GCs. The acrophase of the circadian rhythm of critical signaling hormones, such as cortisol, is tightly regulated and is thought to enable the host to optimally separate physiologically incompatible processes to different times of the day [215,216]. Disruptions in the appropriate circadian activity of cortisol are associated with a number of health

problems [217]. Therefore, understanding the influence of dosing on the acrophase of the endogenous cortisol rhythm is particularly important.

Interestingly, model simulations predicted that the time of dosing could be varied such that the acrophase of the cortisol rhythm adopted two different values for roughly the same change in amplitude. The acrophase of the rhythm was most sensitive for chronic dosing regimens that resulted in high plasma concentrations of synthetic GCs towards the end of active phase (late afternoon). The acrophase response exhibited a sharp discontinuity at high doses. Such an acrophase response has been well documented in the study of phase response curves (PRC) for other circadian oscillators, with transition from continuous PRCs (Type 1) to discontinuous PRCs occurring upon exposure of the circadian systems to large perturbations [209]. Moreover, dosing times resulting in maximal amplitude suppression were also associated with the greatest resetting in the acrophase of the rhythm. These observations agree with experimental studies on the phase-resetting behavior, in response to a light pulse, of the mammalian circadian clock in individual fibroblasts [218,219]. Therefore, daily dosing of the bolus injection or fast-acting synthetic GCs near the beginning of the subjective night and at high doses is predicted to be least favorable due to the maximal disruption of the endogenous cortisol rhythm.

Despite synthetic GCs having an apparent inhibitory influence in the short-term, certain chronopharmacological dosing regimens can result in the induction of HPA axis activity after chronic use. Put another way, the activity of the HPA axis following the first dose was not predictive of the HPA axis in response to long-term treatment. At the nominal (1x) dose strength, model simulations predicted that a once-daily bolus injection of synthetic GCs at 3:00 AM, a fast-acting daily oral dose at 12:00 AM, or a slow-acting daily

oral dose at 7:00 PM, during the simulated night, resulted in an induction of HPA axis activity. Moreover, results suggested that the observed induction in HPA axis activity is linked to a regulatory change associated with the repeated administration of the synthetic GCs at only low to moderate doses, since administration at high dose strengths leads to suppression in HPA axis activity regardless of dosing time. Interestingly, such a time-of-day dependent increase in amplitude is in agreement with observations from the study by Kirwan et al., where the daily administration of low dose (5mg) MR-prednisolone such that it was released at 2:00 AM, during the rising phase of the cortisol rhythm, resulted in an increase in the circadian maxima and a decrease in circadian minima of the cortisol rhythm in RA patients after a 2-week dosing period [178,208]. However, an increase in the cortisol amplitude does not necessarily imply an increase in the total endogenous cortisol exposure (as measured by the 24-hour AUC). Once-daily IV administration of a nominal (1x) dose of synthetic GCs near the start of the active phase resulted in a suppression of the total endogenous cortisol exposure, but either increased the amplitude (for dosing between 6:00 to 8:00 AM) or preserved the amplitude of the endogenous cortisol rhythm (for dosing around 9:00 AM). Despite the increased amplitude, the decrease in the 24-hour AUC might still be indicative of an overall suppression of HPA axis activity. On the other hand, the enhanced circadian rhythmicity might also suggest that the chronic chronopharmacological intervention enables the system to more efficiently restrict the high cortisol levels to a given time of the day, and thereby, separate conflicting downstream GC-responsive physiological processes [215].

While previous models have successfully studied the time-dependence of cortisol suppression after a single dose [184], simulations can also explore the adaptability and

responsiveness of the HPA axis following repeated administration. By accounting for a more physiologically relevant representation of the interactions between feedforward and feedback processes in the HPA network, the model predicts that synthetic GCs can have a complex non-trivial influence on HPA axis activity that might not be captured by simpler mathematical representations, which do not account for endogenous circadian rhythmicity. In doing so, the importance of using multiple metrics (circadian amplitude, acrophase, AUC and responsiveness) to comprehensively understand the alterations in HPA axis activity in response to chronopharmacological intervention was emphasized. The current model may be augmented with a physiologically based pharmacokinetic model that accounts for the nonlinear dynamics associated with some synthetic GCs. These complexities arise from competitive binding to the corticosteroid binding globulin (CBG) and to interconversion between pharmacologically active and inactive forms by 11β -hydroxysteroid dehydrogenase type1/2 for both endogenous and synthetic GCs [182,184,205]. Furthermore, these proteins exhibit their own circadian rhythmicity [220,221], which can complicate the chronopharmacological relationship between dose, drug exposure, and response. The feedback mechanisms underlying dysregulation of the HPA axis are thought to be a result of the imbalance between GR and mineralocorticoid receptors [222]. As such, the disruption of the HPA axis following administration of synthetic GCs can be studied more thoroughly considering the activity of both receptors.

CHAPTER 5: Modeling sexual dimorphism and inter-individual variability in response to chronopharmacological administration of synthetic glucocorticoids

5.1 Introduction

Physiological factors, such as chronotype, sex, age, race or disease state, contribute to substantial variability in pharmacokinetics as well as variation in the underlying regulatory mechanisms and responsiveness of the HPA axis [106,188,223-226]. Clinical studies have shown that the duration and extent of cortisol suppression is highly variable across patient subgroups [179,227,228]. Sexual dimorphism in susceptibility to autoimmune and chronic inflammatory disorders has, in part, been attributed to differences in the underlying regulatory mechanisms of the HPA axis across sexes, such as greater adrenal sensitivity and weaker negative feedback in females [200]. Given differential regulatory mechanisms in basal activity of the HPA axis, one would expect differences in the response and activity of the HPA axis following drug administration. One study reported a greater potency of methylprednisolone in female subjects. However, the increased sensitivity to glucocorticoids was balanced by higher methylprednisolone clearance in females such that same overall therapeutic effect was observed across sexes [182]. Another study reported sex differences in prednisolone pharmacokinetics following a single oral dose, which interestingly resulted in similar half-life in women and men [229]. While sex differences were observed for pharmacokinetics but not the pharmacodynamics of prednisolone, the opposite was true when race was treated as the covariate. This

observation suggests that different patient subgroups may be more susceptible to adverse effects due to differences in drug exposure and sensitivity [229].

Accounting for such differences in drug exposure and response due to inter-individual differences provides another opportunity to tailor glucocorticoid therapies to improve patient safety [230]. Yet, efforts to establish the relationship between dose and HPA axis suppression has been hindered by this inherent variability in regulatory mechanisms and the complexity of glucocorticoid activity due to the crosstalk between the neuroendocrine and immune systems [231]. Mechanistic modeling provides an opportunity to explore the behavior of this dynamic network and to help identify the potential mechanisms leading to marked differences in clinical responses across individuals or patient subgroups.

In this study, the model developed in Chapter 4 was modified to account for the underlying differences in the HPA axis activity across individuals and between sexes. The model was adapted to nocturnal species to evaluate the dose-response relationship for synthetic glucocorticoids in rats, extending the previous modeling work by Rao et al. which established the parameter sub-spaces for male and female rat populations [200]. The goal of the current study was to elucidate how long-term chronopharmacological dosing of synthetic glucocorticoid influences endogenous glucocorticoid activity and how the dose-response relationship is linked to the traits of individuals in the male and female rat populations. For these simulations, inter-individual and inter-sex differences in pharmacokinetics were not considered, choosing instead to focus on differences in the regulatory mechanisms of the HPA axis to study the spectrum of the pharmacodynamic responses.

5.2 Approach

5.2.1 Adaptation of the HPA Axis model to nocturnal species

The model used in Chapter 4, which described the HPA axis in a representative healthy human, was re-parameterized to reflect basal differences in the underlying regulatory mechanisms of the HPA axis in previously established male and female rat populations. While cortisol is the primary glucocorticoid in humans secreted by the adrenal glands, corticosterone is the main glucocorticoid in rats. The structure of the model was largely similar to that presented in Chapter 4 Section 4.2 with the following modifications to reflect the behavior of the HPA axis in nocturnal species.

First, the light schedule differed between the human and rat studies. Rats were entrained to a 14-hour light/10-hour dark lighting schedule, to stay consistent with the original animal study from which corticosterone data were taken, and so **Equation 17** was modified accordingly to **Equation 40** [200].

$$light = \begin{cases} 1 & 7:00 \leq t \leq 21:00 \\ 0 & 21:00 < t < 7:00 \end{cases} \quad \text{Eq. 40}$$

Second, the influence of light differed between diurnal and nocturnal species. Light is considered to stimulate the hypothalamic suprachiasmatic nuclei (SCN), which induces vasopressin and subsequently influences the HPA axis. Vasopressin is a hormone synthesized in the hypothalamus and serves as an output signal of the SCN with secretion following a circadian rhythm [201]. Vasopressin induces HPA axis activity in diurnal species and inhibits activity in nocturnal species [232]. Thus, the CRH equation for humans (**Equation 23**) was modified so light had a negative effect on the HPA axis activity of

nocturnal species by increasing elimination when light was on as shown in **Equation 41**. All other equations were consistent with those described in Chapter 4 Section 4.2.

$$\frac{dCRH}{dt} = \frac{k_{p1} \cdot K_{p1}}{K_{p1} + GR_{bound}(N)} - V_{d1} \cdot \frac{CRH \cdot \left(1 + \frac{light_{effect}}{1 + light_{effect}}\right)}{K_{d1} + CRH} \quad \text{Eq. 41}$$

5.2.2 Parametrization of the Model

The nocturnal rat model was previously calibrated by Rao et al. to qualitatively match the endogenous corticosterone rhythmicity in a population of male and female rats [200]. Briefly, the male and female parameter sub-spaces were identified by Sobol sampling. Parameter sets were accepted when the simulated corticosterone profiles matched experimental data within ± 1 standard deviation of the scaled experimental cosinor parameters obtained by the original animal study. Three parameters were necessary to describe the male and female corticosterone rhythms: adrenal sensitivity of corticosterone to ACTH (k_{p3}), the glucocorticoid receptor-mediated negative feedback to the hypothalamus (K_{p1}), and the glucocorticoid receptor-mediated negative feedback to the pituitary gland (K_{p2}). All other HPA axis parameters were common to both male and female rats. The model input parameters are given in **Supplementary Table 10**. The pharmacokinetic compartment models and corresponding parameters described in Chapter 4 Section 4.2.2 for a bolus injection, fast-releasing oral formulation, and slow-releasing oral formulation were used in the animal dosing experiments and were not parameterized specifically for rats.

5.3 Dosing Experiments

The chronopharmacology of a daily dose of synthetic glucocorticoid was simulated by varying the administration time, dosing strength, and administration route. Administration time was varied by 4-hour intervals (12:00 AM, 4:00 AM, 8:00 AM, etc.) throughout the simulated day using a dosing interval of 24 hours for once-a-day administration. Doses of 0.1x, 1x, and 10x were evaluated to understand how the strength of negative feedback via the glucocorticoid receptor dynamics influenced pharmacodynamic differences between individuals and sexes. Changes in the amplitude (**Equation 38**) and acrophase of the endogenous glucocorticoid rhythm were used to quantify the degree of disruption of HPA axis activity relative to the baseline conditions without treatment.

5.4 Results

5.4.1 Male and female rat subpopulations used in dosing experiments

For the dosing experiments, 100 male and 100 female rats were randomly selected from the larger populations established in Rao et al. [200]. The selected rats are shown in **Figure 28** and are well distributed across the male and female parameter subspaces previously identified for the sex-dependent parameters.

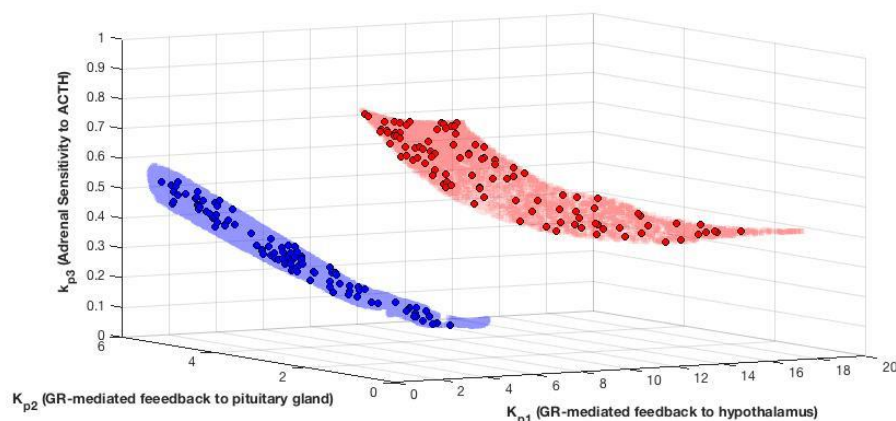


Figure 28: Male and female parameter subspaces for sex-specific parameters used in dosing experiments. The subset of 100 male rats and 100 female rats were selected from the original populations established by Rao et al. [200].

5.4.2 Influence of once-daily chronopharmacological dosing on corticosterone rhythmicity in male and female rats

Basal differences in the circadian rhythmicity of endogenous corticosterone are shown in **Figure 29**, showing that sex-dependent parameterization of the HPA axis model led to unique male and female phenotypes. Following once-a-day administration of synthetic glucocorticoids, the rhythmicity of endogenous corticosterone evolved to new stable oscillations as shown in **Figure 30**. The amplitude and acrophase of the modified rhythm depended on the time at which the drug was administered and the dosage form as shown in **Figure 31** for male and female rats. Similar to the results observed in the human model, the different dosage forms produced qualitatively similar effects on the corticosterone rhythm with an advance in dosing times needed to produce the same effect corresponding to the time for absorption of oral glucocorticoids. However, male rats had a remarkably greater time-of-day dependence than female rats, showing larger differences in the suppressive and inductive effects of synthetic glucocorticoids across dosing times.

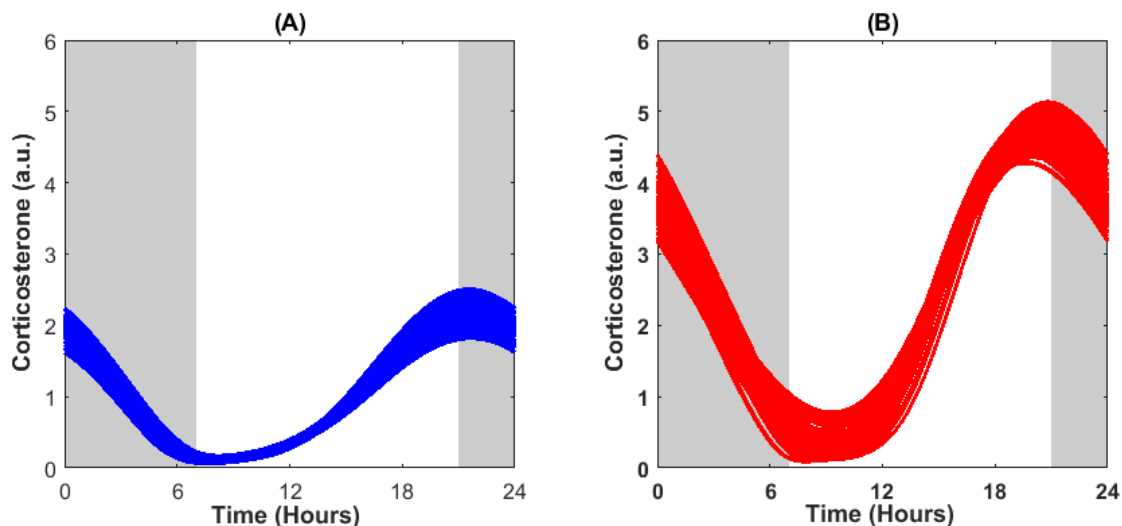


Figure 29: Differences in basal HPA activity between male and female rat populations. The corticosterone profiles for the subpopulations of the male and female rats used in the dosing experiments are given in (A) and (B), respectively. The grey shaded areas represent the time at which the system is not exposed to light. Corticosterone concentration is given in arbitrary units (a.u.).

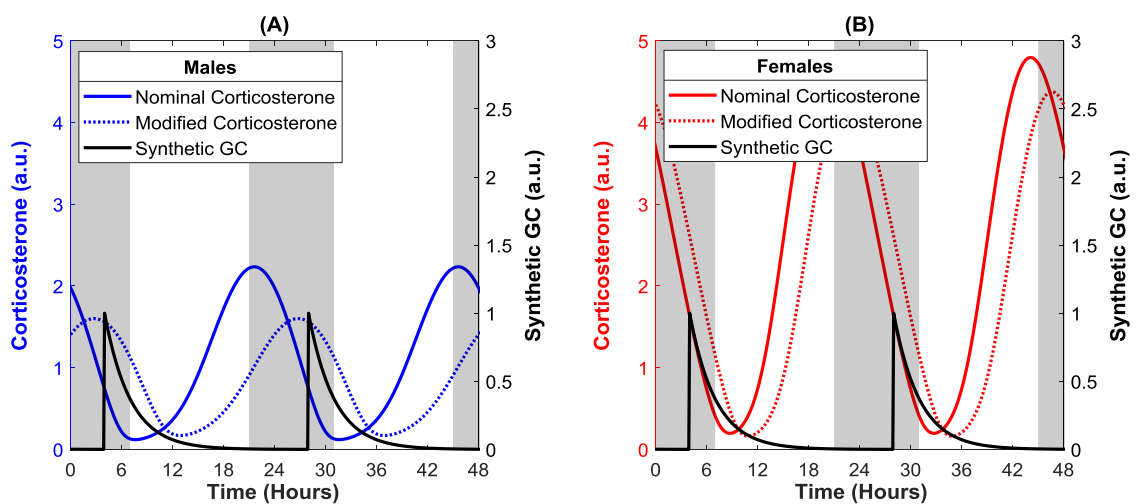


Figure 30: Modified corticosterone profiles after dosing of synthetic glucocorticoids (GC) by bolus injection at the nominal amount (1x). The corticosterone rhythms with and without dosing are given in (A) for male rats and (B) for female rats. The solid line corresponds to the nominal corticosterone profile based on endogenous HPA axis activity. The modified corticosterone rhythm is indicated by the dotted line. The pharmacokinetic profiles for the bolus injection are indicated by the black line. The grey shaded areas represent the time at which the system is not exposed to light. Corticosterone concentration is given in arbitrary units (a.u.).

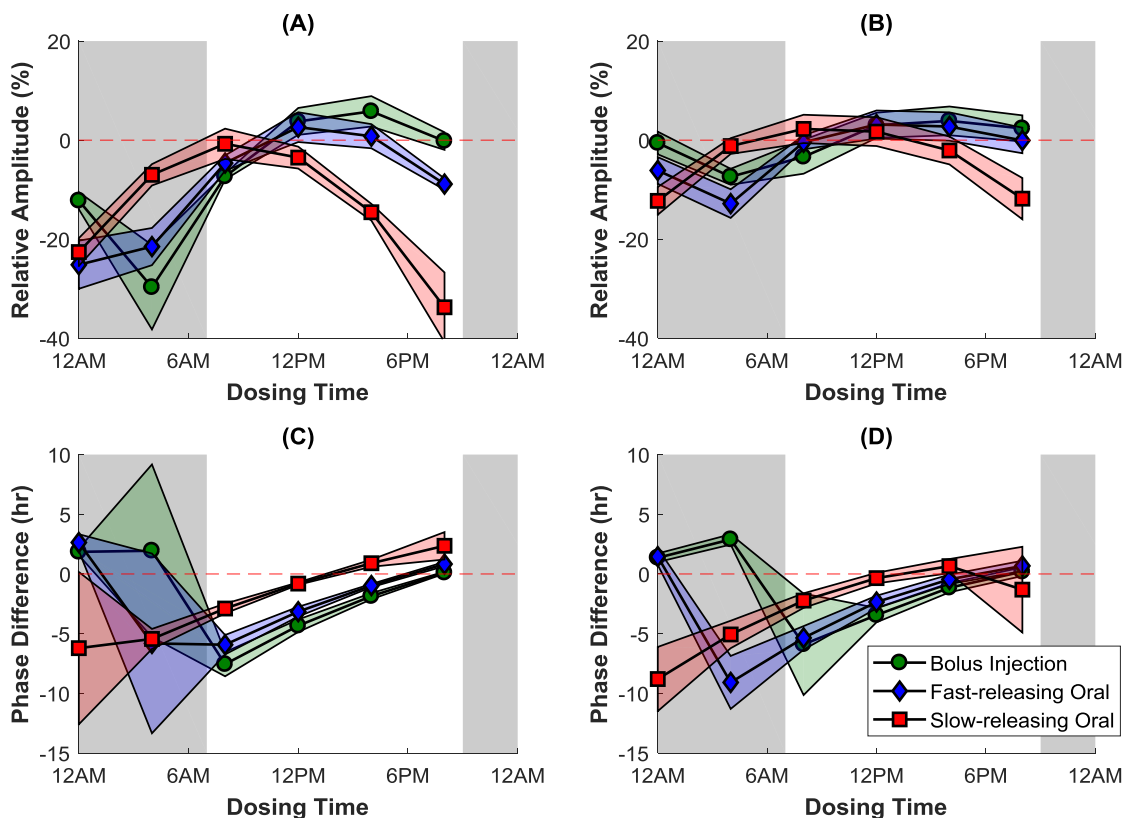


Figure 31: Population mean amplitude and phase of the modified corticosterone rhythm after once-daily chronopharmacological dosing of synthetic glucocorticoids in male rats and female rats. The relative amplitude and difference in the acrophase of the modified corticosterone rhythms after a repeated once-a-day administration of a bolus injection, fast-releasing oral dose, or slow-releasing oral dose are shown in (A) and (C) for male rats and in (B) and (D) for female rats, respectively. The colored shaded areas represent ± 1 standard deviation of the population mean for amplitude and phase changes. The gray shaded areas represent the simulated night. A negative value for phase difference indicates an advance in the acrophase (i.e. peaks earlier in the simulated day) while a positive value indicates a delay in the acrophase (i.e. peaks later in the simulated day).

Once-daily dosing near the normal daily minima of corticosterone levels (~8:00 AM) produced similar modifications to endogenous activity across sexes whereas greater sex differences in response to treatment were observed when dosing near the normal daily maxima (~9:00 PM). In the male rat population, maximal suppression occurred when drug was administered daily at 4:00 AM by bolus injection, 12:00 AM for the fast-releasing oral dose, and 8:00 PM for the slow-releasing oral dose. In the female rat population, maximal suppression occurred at administration times of 4:00 AM for the bolus injection and fast-

release oral dose, and 12:00 AM for the slow-releasing oral dose. Conversely, induction of the endogenous corticosterone secretion was observed at select dosing times, which largely occurred when drug was administered during the simulated day, or the inactive phase of the rats. Furthermore, endogenous corticosterone activity would likely be preserved when synthetic glucocorticoids were administered sometime near the end of the simulated night or near the start of the simulated daytime in both male and female rats, although additional dosing times would be needed to confirm the exact timing. While the time-of-day dependence was qualitatively similar across sexes for the mean phase of the modified rhythms, the male rat population showed greater inter-individual variability when dosing during the simulated night for all three dosage forms. The female rat population revealed the inter-individual variability to be more dependent on the dosage form. The pharmacokinetic profiles for the three dosage forms evaluated in the nocturnal model were given in **Figure 21**.

The circadian characteristics of the modified corticosterone rhythm relative to the individual's sex-dependent regulatory parameters are shown in **Figure 32** following a once-daily injection at 4:00 AM, the dosing time associated with maximal suppression, and 4:00 PM, the dosing time associated with maximal induction. While stronger receptor-mediated feedback to the pituitary gland (K_{p2}) and increased adrenal sensitivity (k_{p3}) in male rats tended to result in greater disruption of the HPA axis following a 4:00 AM injection, stronger negative feedback to the pituitary gland and increased adrenal sensitivity in female rats had the opposite effect. Furthermore, female rats showed an inverse relationship between the strength of receptor-mediated feedback to the hypothalamus and the extent of HPA axis disruption. Despite noticeable sex differences in HPA axis

disruption with 4:00 AM injections, similar behavior was observed in both populations following 4:00 PM injections, where stronger negative feedback to the pituitary gland and greater adrenal sensitivity led to higher amplitudes for the modified corticosterone rhythms. The variability in the regulatory mechanisms underlying HPA axis activity produced opposing trends for 4:00 AM injections, but qualitatively behavior after 4:00 PM injections, although larger modifications were observed for the male rat population at both administration times.

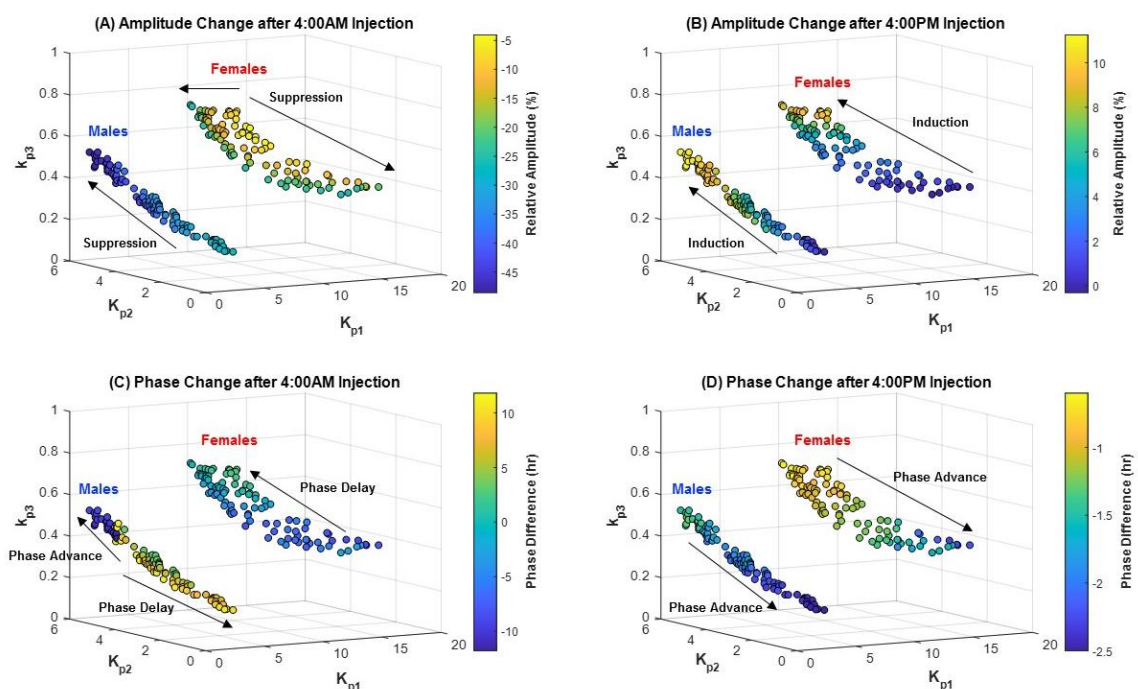


Figure 32: Amplitude and phase of the modified corticosterone rhythm after once-daily injection at 4:00 AM and 4:00 PM in male and female rats. The relative amplitude and phase difference for the modified corticosterone rhythms are given for each individual defined by three sex-dependent parameters.

5.4.3 Influence of dosing strength on the corticosterone activity in male and female rats

The amplitude of the modified corticosterone rhythm associated with the once-daily bolus injection that resulted in the greatest suppressive and inductive effects on the HPA

axis are given in **Figure 33** for dosing strengths of 0.1x, 1x, and 10x. The dose-response relationship showed significant differences between the male and female populations, suggesting that female rats were tolerant of higher doses of synthetic glucocorticoids and male rats were more sensitive to HPA axis disruption when differences in pharmacokinetics were not considered.

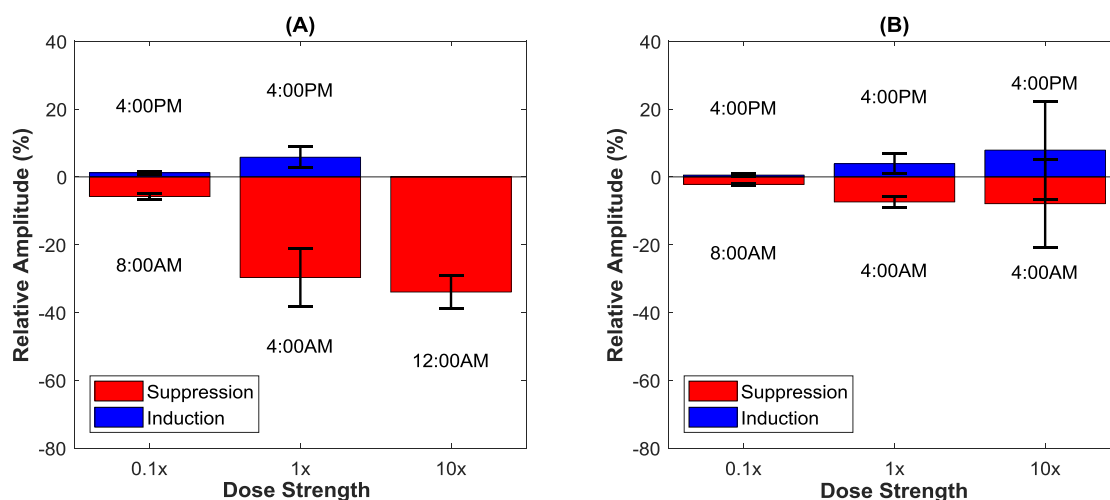


Figure 33: Influence of dosing strength on the amplitude of the modified corticosterone rhythm following chronic once-daily dosing of a bolus injection in male and female rats. The amplitude is given for the dosing times which resulted in the greatest inductive and suppressive effects at each strength in male rats (A) and female rats (B). The error bars represent ± 1 standard deviation of the population mean for amplitude and phase changes.

5.5 Discussion

Given a semi-mechanistic representation of the stimulatory and negative feedback processes of the HPA axis, the responsiveness and adaptability of individuals to chronic chronopharmacological glucocorticoid treatment was studied in a population of male and female rats. This approach enabled an understanding of population differences that explained in part, the susceptibility of some individuals to adverse effects which arise from disruption of endogenous glucocorticoid activity. While the circadian characteristics of the modified rhythms after dosing showed similar time-dependent trends across the rat

population, the magnitude of the observed changes were dependent on the regulatory traits that collectively defined an individual's basal HPA axis activity. Interestingly, the greatest inter-individual variability was observed when the HPA axis was most susceptible to disruption with fewer differences across the population when the HPA axis was more robust to disruption. Furthermore, the range of administration times in which the endogenous activity would be conserved was consistent across the male and female rat populations in these simulations, suggesting that the optimal time of dosing may not require adjustment for sex.

Owing to differences in the regulatory mechanisms underlying the HPA axis, female rats tolerated a higher dose than male rats. That is, a higher dose would be needed in female rats to produce the same suppressive or inductive effects as male rats when only sex differences in pharmacodynamics were considered. An extension of this study would also consider variability in pharmacokinetic parameters driving differences in drug exposure, a scenario that better reflects clinical behavior. Body weight and body surface area, which differ between sexes, have already been recognized as important determinants of clearance and are routinely accounted for in glucocorticoid replacement therapy [233]. By accounting for inter-individual and inter-sex differences in both pharmacokinetics and pharmacodynamics, the putative mechanisms contributing to variability in the dose-response relationship would enable the separation of individuals based on sensitivity or resistance to glucocorticoid treatment, and further support the design of dosing regimens that result in minimal disruption of endogenous corticosterone activity based on individuals or patient subgroups. As emphasized in Chapter 4, the goal of glucocorticoid treatment is often to leverage the anti-inflammatory and immunosuppressive properties of synthetic

glucocorticoids without interrupting HPA axis activity. Conversely, glucocorticoid treatment may be used to correct abnormal glucocorticoid activity. The population simulations provided insight into how administration time and dose can be selected to induce or suppress the HPA axis as needed for successful hormone replacement or other disease states which result in HPA axis dysfunction. Future studies utilizing the *in silico* approach outlined herein has great potential for further minimizing patient risks within the context of the ‘right dose-right time’ paradigm.

Glucocorticoid activity in peripheral tissues can also contribute to inter-individual differences due to variability in the negative feedback, 11β -HSD activity, CBG levels, and active transporters, such as P-glycoprotein, which regulate local glucocorticoid concentrations [234]. Genetic variation in glucocorticoid pathway regulation and activity is a significant factor in inter-individual differences in glucocorticoid treatment [235,236]. For example, polymorphisms in genes involved in glucocorticoid transport and metabolism contribute significantly to inter-individual variability in the efficacy and toxicity of patients suffering from Crohn’s disease and ulcerative colitis [237]. Some patients with inflammatory bowel disease (IBD) require chronic therapy to stay in remission whereas others require intermittent treatment during flare-ups [238]. While intrinsic glucocorticoid resistance leads to drug resistance at pharmacological doses [239], glucocorticoids hypersensitivity can actually aid treatment. For example, lower disease activity of IBD, marked by less gut inflammation and improved mucosal healing, was observed in patients with higher glucocorticoid sensitivity and drug-induced adrenal insufficiency, although other side effects, such as osteoporosis and infections, persisted [240]. Successful treatment is likely due to the favorable increase in glucocorticoid activity in the gut, with epithelium

integrity, cell-cell adhesion, and mucus hypersecretion modulated by local receptor activity [241]. Likewise, polymorphisms in the glucocorticoid receptor gene are sometimes accompanied by cardiovascular risks such as irregular blood pressure, low glucose, or low total cholesterol, which may partially explain why some patients are at a greater risk for such adverse effects while receiving treatment [242]. Inter-individual differences in clock phase may also be clinically relevant and the success of chronopharmacological dosing relies on proper timing of drug exposure with specific physiological functions [243]. Interestingly, the same individual can show significant variability in the magnitude and specificity of action across tissues and even across phases of the cell cycle, requiring a deeper understanding of the signal transduction pathways involved in both therapeutic and adverse effects [244].

Furthermore, cortisol levels tend to reflect long-term individual traits, whereas the responsiveness of the HPA axis to synthetic glucocorticoids appears to be more closely tied to clinical state [227]. For example, patients suffering from post-traumatic stress disorder (PTSD) at the time of the study exhibited greater cortisol suppression following administration of dexamethasone compared to patients without PTSD regardless of whether these patients were previously exposed to trauma [227]. As such, the influence of dosing may also be evaluated under chronically stressed conditions, supporting a more thorough evaluation of the therapeutic and adverse effects of glucocorticoids in yet another patient subgroup.

CHAPTER 6: Conclusions

Physiologically based pharmacokinetic modeling is a key tool in the advancement of personalized medicine to evaluate complex clinical scenarios, making use of physiological information as well as physicochemical data to simulate various physiological states, to predict the distribution of pharmacokinetic responses and to explore the underlying physiological mechanisms contributing to differences across special populations. In Chapter 2, the benefits of global sensitivity analysis for understanding model behavior were demonstrated for four compartment models using GastroPlus™. Global sensitivity analysis, facilitated by the automated framework, revealed insight into the complex relationships that exist between physiological input and pharmacokinetic output that would otherwise be missed by a local method. Global sensitivity analysis provided insight into the model structure, showed how model parameterization strongly influences sensitivity analysis, and demonstrated how relationships between model input and output inform the underlying physiology contributing to the distribution of pharmacokinetic responses. Furthermore, the 2-stage approach significantly reduced computational cost, overcoming the major challenge for implementing global sensitivity analysis for physiologically based pharmacokinetic models.

In Chapter 3, Monte Carlo simulations for a published pharmacokinetic compartment model were used to demonstrate how model input associated with desired clinical phenotypes can be isolated from a generic multivariate parameter space. Such an approach enabled the generation of parameter values by stochastic sampling that were subsequently restricted to the combinations that describe biologically plausible or target model output. Despite limiting the model output to relatively narrow ranges, male and

female phenotypes were associated with wide variability in both individual parameter values and combinations of parameters. Through an integrated approach using a support vector machine, principal component analysis and global sensitivity analysis, our approach revealed that specific combinations of parameters gave rise to a certain clinical phenotype, while individual parameters influenced the shape of plasma concentration profile. Augmenting analysis of the model input with global sensitivity analysis enabled an understanding of both sexual dimorphism and inter-individual variability in pharmacokinetics. While the current study revealed how model input could be separated by sex for a simple compartment model, the approach could be extended to other patient factors, such as age or disease, and to a more complex physiologically based model that describes absorption and drug disposition in detail.

In Chapter 4, an integrated PKPD model was used to demonstrate how chronopharmacological dosing can improve patient safety and maintain pharmacological benefits of long-term synthetic glucocorticoid therapy. These simulations revealed how the circadian features of the endogenous cortisol rhythm, which is critical to host survival and normal physiological function, can be preserved by careful timing of administration and how the pharmacological exposure profile can be manipulated to induce the optimal therapeutic effect. Furthermore, the study highlighted how modeling can be used to study differences in drug response following a single dose or after chronic treatment, and to demonstrate the benefits of using a dynamic semi-mechanistic model to study the dependence of the dose-exposure-response relationship on administration time. Finally, in Chapter 5, the model was re-parameterized to reflect basal differences in endogenous glucocorticoid activity in male and female populations, promoting any understanding of

how chronic synthetic glucocorticoid treatment must be adapted for patient subgroups and inter-individual variability. Extending the model to consider any of the aforementioned population differences continues the transformation towards a more physiologically meaningful and mechanistic representation of the underlying regulatory mechanisms of the HPA axis affecting endogenous glucocorticoid secretion and patient response to chronic treatment. Future work would successfully incorporate such differences for further optimization of chronopharmacological dosing regimens to comprehensively assess patient risk under the ‘right drug-right dose-right time’ paradigm within an integrated *in silico* framework.

Acknowledgement of Publications

This dissertation contains significant portions of the following publications:

1. Hartmanshenn C, Scherholz M, and Androulakis IP. Physiologically-based pharmacokinetic models: approaches for enabling personalized medicine. *J Pharmacokinet Pharmacodyn* (2016): 481-504.
 2. Rao RT, Scherholz ML, Hartmanshenn C, Bae, S, and Androulakis IP. On the analysis of complex biological supply chains: From Process Systems Engineering to Quantitative Systems Pharmacology. *Computers & Chemical Engineering* (2017): 100-110.
 3. Scherholz ML, Forder J, and Androulakis IP. A framework for 2-stage global sensitivity analysis of GastroPlus™ compartmental models. *J Pharmacokinet Pharmacodyn* (2018): 309-327.
 4. Rao RT*, Scherholz ML*, and Androulakis IP. Modeling the influence of chronopharmacological administration of synthetic glucocorticoids on the hypothalamic-pituitary-adrenal axis. *Chronobiology International* (2018): 1-18.
 5. Scherholz ML and Androulakis IP. Exploration of sexual dimorphism and inter-individual variability in multivariate parameter spaces for a pharmacokinetic compartment model. *Mathematical Biosciences* (Submitted 2018).
 6. Scherholz ML, Schelsinger N, and Androulakis IP. Chronopharmacology of glucocorticoids. *Adv Drug Delivery Reviews* (Submitted 2018).
- * Authors contributed equally to the preparation of the manuscript. MLS was responsible for development of the IV and fast-releasing compartment models, integration of the PK models with the HPA axis model, evaluation of the dose-response relationship, comparison of short-term and chronic treatment, including conception of ideas, design of dosing experiments, and execution/analysis of data.

References

1. Noetzli M, Eap CB (2013) Pharmacodynamic, pharmacokinetic and pharmacogenetic aspects of drugs used in the treatment of Alzheimer's disease. *Clin Pharmacokinet* 52 (4):225-241. doi:10.1007/s40262-013-0038-9
2. Schork NJ (2015) Personalized medicine: Time for one-person trials. *Nature* 520 (7549):609-611. doi:10.1038/520609a
3. Lesko LJ, Schmidt S (2012) Individualization of drug therapy: history, present state, and opportunities for the future. *Clin Pharmacol Ther* 92 (4):458-466. doi:10.1038/clpt.2012.113
4. Waldman SA, Terzic A (2011) Patient-centric clinical pharmacology advances the path to personalized medicine. *Biomark Med* 5 (6):697-700. doi:10.2217/bmm.11.78
5. Redekop WK, Mladsi D (2013) The faces of personalized medicine: a framework for understanding its meaning and scope. *Value Health* 16 (6 Suppl):S4-9. doi:10.1016/j.jval.2013.06.005
6. Zhao P, Zhang L, Grillo JA, Liu Q, Bullock JM, Moon YJ, Song P, Brar SS, Madabushi R, Wu TC, Booth BP, Rahman NA, Reynolds KS, Gil Berglund E, Lesko LJ, Huang SM (2011) Applications of physiologically based pharmacokinetic (PBPK) modeling and simulation during regulatory review. *Clin Pharmacol Ther* 89 (2):259-267. doi:10.1038/clpt.2010.298
7. Kiang TK, Sherwin CM, Spigarelli MG, Ensom MH (2012) Fundamentals of population pharmacokinetic modelling: modelling and software. *Clin Pharmacokinet* 51 (8):515-525. doi:10.2165/11634080-000000000-00000
8. Hamburg MA, Collins FS (2010) The path to personalized medicine. *The New England Journal of Medicine*:301-304
9. Teorell T (1937) Kinetics of distribution of substances administered to the body. *Archives Internationales de Pharmacodynamie et de Therapie* 57:205-240
10. Rowland M, Peck C, Tucker G (2011) Physiologically-based pharmacokinetics in drug development and regulatory science. *Annu Rev Pharmacol Toxicol* 51:45-73. doi:10.1146/annurev-pharmtox-010510-100540
11. Huang SM, Abernethy DR, Wang Y, Zhao P, Zineh I (2013) The utility of modeling and simulation in drug development and regulatory review. *J Pharm Sci* 102 (9):2912-2923. doi:10.1002/jps.23570
12. Jiang W, Kim S, Zhang X, Lionberger RA, Davit BM, Conner DP, Yu LX (2011) The role of predictive biopharmaceutical modeling and simulation in drug development and regulatory evaluation. *Int J Pharm* 418 (2):151-160. doi:10.1016/j.ijpharm.2011.07.024
13. Peck CC (2010) Quantitative clinical pharmacology is transforming drug regulation. *J Pharmacokinet Pharmacodyn* 37 (6):617-628. doi:10.1007/s10928-010-9171-3

14. Bonate PL (2011) *Pharmacokinetic-Pharmacodynamic Modeling and Simulation*, 2nd edition. Springer, New York
15. Rosenbaum SE (2011) *Basic Pharmacokinetics and Pharmacodynamics: An Integrated Textbook and Computer Simulations*. John Wiley & Sons, Inc., Hoboken, NJ
16. Tylutki Z, Polak S, Wisniowska B (2016) Top-down, Bottom-up and Middle-out Strategies for Drug Cardiac Safety Assessment via Modeling and Simulations. *Curr Pharmacol Rep* 2:171-177. doi:10.1007/s40495-016-0060-3
17. Kostewicz ES, Aarons L, Bergstrand M, Bolger MB, Galetin A, Hatley O, Jamei M, Lloyd R, Pepin X, Rostami-Hodjegan A, Sjogren E, Tannergren C, Turner DB, Wagner C, Weitschies W, Dressman J (2014) PBPK models for the prediction of in vivo performance of oral dosage forms. *Eur J Pharm Sci* 57:300-321. doi:10.1016/j.ejps.2013.09.008
18. Cao Y, Jusko WJ (2012) Applications of minimal physiologically-based pharmacokinetic models. *J Pharmacokinet Pharmacodyn* 39 (6):711-723. doi:10.1007/s10928-012-9280-2
19. Suenderhauf C, Parrott N (2013) A physiologically based pharmacokinetic model of the minipig: data compilation and model implementation. *Pharm Res* 30 (1):1-15. doi:10.1007/s11095-012-0911-5
20. Loccisano AE, Campbell JL, Jr., Butenhoff JL, Andersen ME, Clewell HJ, 3rd (2012) Comparison and evaluation of pharmacokinetics of PFOA and PFOS in the adult rat using a physiologically based pharmacokinetic model. *Reprod Toxicol* 33 (4):452-467. doi:10.1016/j.reprotox.2011.04.006
21. Worley RR, Fisher J (2015) Application of physiologically-based pharmacokinetic modeling to explore the role of kidney transporters in renal reabsorption of perfluorooctanoic acid in the rat. *Toxicol Appl Pharmacol* 289 (3):428-441. doi:10.1016/j.taap.2015.10.017
22. DiStefano J (2014) *Dynamic Systems Biology Modeling and Simulation*. Academic Press, London
23. Barton HA, Chiu WA, Setzer RW, Andersen ME, Bailer AJ, Bois FY, Dewoskin RS, Hays S, Johanson G, Jones N, Loizou G, Macphail RC, Portier CJ, Spendiff M, Tan YM (2007) Characterizing uncertainty and variability in physiologically based pharmacokinetic models: state of the science and needs for research and implementation. *Toxicol Sci* 99 (2):395-402. doi:10.1093/toxsci/kfm100
24. Nestorov I (2003) Whole body pharmacokinetic models. *Clin Pharmacokinet* 42 (10):883-908. doi:10.2165/00003088-200342100-00002
25. Johansson F., Paterson R Physiologically Based in Silico Models for Prediction of Oral Drug Absorption. 21:486-509
26. Khalil F, Laer S (2011) Physiologically based pharmacokinetic modeling: methodology, applications, and limitations with a focus on its role in pediatric drug development. *J Biomed Biotechnol* 2011:907461. doi:10.1155/2011/907461

27. Bois FY (2000) Statistical analysis of Clewell et al. PBPK model of trichloroethylene kinetics. *Environ Health Perspect* 108 Suppl 2:307-316
28. Thompson CM, Johns DO, Sonawane B, Barton HA, Hattis D, Tardif R, Krishnan K (2009) Database for physiologically based pharmacokinetic (PBPK) modeling: physiological data for healthy and health-impaired elderly. *J Toxicol Environ Health B Crit Rev* 12 (1):1-24. doi:10.1080/10937400802545060
29. Sinha V, Zhao P, Huang SM, Zineh I (2014) Physiologically based pharmacokinetic modeling: from regulatory science to regulatory policy. *Clin Pharmacol Ther* 95 (5):478-480. doi:10.1038/clpt.2014.46
30. Almukainzi M, Jamali F, Aghazadeh-Habashi A, Löbenberg R (2016) Disease specific modeling: Simulation of the pharmacokinetics of meloxicam and ibuprofen in disease state vs. healthy conditions. *European Journal of Pharmaceutics and Biopharmaceutics* 100:77-84. doi:<http://dx.doi.org/10.1016/j.ejpb.2015.12.004>
31. Chetty M, Rose RH, Abduljalil K, Patel N, Lu G, Cain T, Jamei M, Rostami-Hodjegan A (2014) Applications of linking PBPK and PD models to predict the impact of genotypic variability, formulation differences, differences in target binding capacity and target site drug concentrations on drug responses and variability. *Front Pharmacol* 5:258. doi:10.3389/fphar.2014.00258
32. Jamei M, Turner D, Yang J, Neuhoff S, Polak S, Rostami-Hodjegan A, Tucker G (2009) Population-based mechanistic prediction of oral drug absorption. *AAPS J* 11 (2):225-237. doi:10.1208/s12248-009-9099-y
33. Dickschen K, Willmann S, Thelen K, Lippert J, Hempel G, Eissing T (2012) Physiologically-based pharmacokinetic modeling of tamoxifen and its metabolites in women of different CYP2D6 phenotypes provides new insight into the tamoxifen mass balance. *Front Pharmacol* 2012 May 21 3
34. Carrasco-Portugal MdC, Flores-Murrieta FJ (2011) Gender Differences in the Pharmacokinetics of Oral Drugs. *Pharmacology & Pharmacy* 02 (01):31-41. doi:10.4236/pp.2011.21004
35. Khalil F, Laer S (2014) Physiologically based pharmacokinetic models in the prediction of oral drug exposure over the entire pediatric age range-sotalol as a model drug. *AAPS J* 16 (2):226-239. doi:10.1208/s12248-013-9555-6
36. Wening K, Breitzkreutz J (2011) Oral drug delivery in personalized medicine: unmet needs and novel approaches. *Int J Pharm* 404 (1-2):1-9. doi:10.1016/j.ijpharm.2010.11.001
37. Wagner C, Zhao P, Pan Y, Hsu V, Grillo J, Huang SM, Sinha V (2015) Application of Physiologically Based Pharmacokinetic (PBPK) Modeling to Support Dose Selection: Report of an FDA Public Workshop on PBPK. *CPT Pharmacometrics Syst Pharmacol* 4 (4):226-230. doi:10.1002/psp4.33
38. Tucker G, DeSilva B, Dressman J, Ito M, Kumamoto T, Mager D, Mahler HC, Maitland-van der Zee AH, Pauletti GM, Sasaki H, Shah V, Tang D, Ward M (2016) Current Challenges and Potential Opportunities for the Pharmaceutical Sciences to

- Make Global Impact: An FIP Perspective. *J Pharm Sci.*
doi:10.1016/j.xphs.2015.12.001
39. Larson RA, Yin OQ, Hochhaus A, Saglio G, Clark RE, Nakamae H, Gallagher NJ, Demirhan E, Hughes TP, Kantarjian HM, le Coutre PD (2012) Population pharmacokinetic and exposure-response analysis of nilotinib in patients with newly diagnosed Ph+ chronic myeloid leukemia in chronic phase. *Eur J Clin Pharmacol* 68 (5):723-733. doi:10.1007/s00228-011-1200-7
 40. Woodruff TJ, Bois FY, Auslander D, Spear RC (1992) Structure and parameterization of pharmacokinetic models: their impact on model predictions. *Risk Anal* 12 (2):189-201
 41. Harmonization project document No. 9: Characterization and application of physiologically based pharmacokinetic models in risk assessment (2010). World Health Organization International Programme on Chemical Safety Harmonization Project, Ottawa, ON
 42. Strategies, approaches, and challenges in model-informed drug development (MIDD) (2017). FDA Briefing Document - Pharmaceutical Science and Clinical Pharmacology Advisory Committee Meeting, Rockville, MD
 43. McNally K, Cotton R, Loizou GD (2011) A Workflow for Global Sensitivity Analysis of PBPK Models. *Front Pharmacol* 2:31. doi:10.3389/fphar.2011.00031
 44. Gueorguieva, II, Nestorov IA, Rowland M (2004) Fuzzy simulation of pharmacokinetic models: case study of whole body physiologically based model of diazepam. *J Pharmacokinet Pharmacodyn* 31 (3):185-213. doi:1567-567X/04/0600-0185/0
 45. Gueorguieva I, Nestorov I, Rowland M Reducing PBPK models using global sensitivity approach and benefit/cost criterion. In: Population Approach Group Europe, Paris, France, 2002.
 46. Gueorguieva I, Nestorov IA, Rowland M (2006) Reducing whole body physiologically based pharmacokinetic models using global sensitivity analysis: diazepam case study. *J Pharmacokinet Pharmacodyn* 33 (1):1-27. doi:10.1007/s10928-005-0004-8
 47. Makler-Pick V, Gal G, Gorfine M, Hipsey MR, Carmel Y (2011) Sensitivity analysis for complex ecological models - A new approach. *Environmental Modelling & Software* 26:124-134. doi:10.1016/j.envsoft.2010.06.010
 48. Price PS, Conolly RB, Chaisson CF, Gross EA, Young JS, Mathis ET, Tedder DR (2010) Modeling Interindividual Variation in Physiological Factors Used in PBPK Models of Humans. *Critical Reviews in Toxicology* 33 (5):469-503. doi:10.1080/10408440390242324
 49. Jamei M (2016) Recent advances in development and application of physiologically-based pharmacokinetic (PBPK) models: a transition from academic curiosity to regulatory acceptance. *Current Pharmacology Reports* 1 (3):161-169

50. Abbiati RA, Manca D (2016) A modeling tool for the personalization of pharmacokinetic predictions. *Computers & Chemical Engineering* 91:28-37. doi:10.1016/j.compchemeng.2016.03.008
51. Franconi F, Brunelleschi S, Steardo L, Cuomo V (2007) Gender differences in drug responses. *Pharmacol Res* 55 (2):81-95. doi:10.1016/j.phrs.2006.11.001
52. Fletcher CV, Acosta EP, Strykowski JM (1994) Gender differences in human pharmacokinetics and pharmacodynamics. *Journal of Adolescent Health* 15:619-629
53. Whitley H, Lindsey W (2009) Sex-based differences in drug activity. *Am Fam Physician* 80 (11):1254-1258
54. Damoiseaux VA, Proost JH, Jiawan VC, Melgert BN (2014) Sex differences in the pharmacokinetics of antidepressants: influence of female sex hormones and oral contraceptives. *Clin Pharmacokinet* 53 (6):509-519. doi:10.1007/s40262-014-0145-2
55. Regitz-Zagrosek V Sex and Gender Differences in Pharmacology. *Handbook of Experimental Pharmacology*. Springer, Heidelberg
56. Chen ML, Lee SC, Ng MJ, Schuirmann DJ, Lesko LJ, Williams RL (2000) Pharmacokinetic analysis of bioequivalence trials: implications for sex-related issues in clinical pharmacology and biopharmaceutics. *Clin Pharmacol Ther* 68 (5):510-521. doi:10.1067/mcp.2000.111184
57. Greenblatt DJ, Harmatz JS, Roth T, Singh NN, Moline ML, Harris SC, Kapil RP (2013) Comparison of pharmacokinetic profiles of zolpidem buffered sublingual tablet and zolpidem oral immediate-release tablet: results from a single-center, single-dose, randomized, open-label crossover study in healthy adults. *Clin Ther* 35 (5):604-611. doi:10.1016/j.clinthera.2013.03.007
58. Xu H, Gan J, Liu X, Wu R, Jin Y, Li M, Yuan B (2013) Gender-dependent pharmacokinetics of lignans in rats after single and multiple oral administration of *Schisandra chinensis* extract. *J Ethnopharmacol* 147 (1):224-231. doi:10.1016/j.jep.2013.03.008
59. Hu L, Jin Y, Li YG, Borel A (2015) Population pharmacokinetic/pharmacodynamic assessment of pharmacological effect of a selective estrogen receptor β agonist on total testosterone in healthy men. *Clinical Pharmacology in Drug Development* 4 (4):305-314. doi:10.1002/cpdd.184
60. Freire AC, Basit AW, Choudhary R, Piong CW, Merchant HA (2011) Does sex matter? The influence of gender on gastrointestinal physiology and drug delivery. *Int J Pharm* 415 (1-2):15-28. doi:10.1016/j.ijpharm.2011.04.069
61. Marazziti D, Baroni S, Picchetti M, Piccinni A, Carlini M, Vatteroni E, Falaschi V, Lombardi A, Dell'Osso L (2013) Pharmacokinetics and pharmacodynamics of psychotropic drugs: effect of sex. *CNS Spectr* 18 (3):118-127. doi:10.1017/S1092852912001010
62. Soldin OP, Chung SH, Mattison DR (2011) Sex differences in drug disposition. *J Biomed Biotechnol* 2011:187103. doi:10.1155/2011/187103

63. Kashuba AD, Nafziger AN (1998) Physiological changes during the menstrual cycle and their effect on the pharmacokinetics and pharmacodynamics of drugs. *Clin Pharmacokinet* 34 (3):203-218
64. Sheth AN, Lahiri CD, Ofotokun I (2015) Sex Differences in Metabolism and Pharmacokinetics.75-102. doi:10.1007/978-3-319-16438-0_4
65. Anderson GD (2008) Chapter 1 Gender Differences in Pharmacological Response. 83:1-10. doi:10.1016/s0074-7742(08)00001-9
66. Cummins CL, Wu CY, Benet LZ (2002) Sex-related differences in the clearance of cytochrome P450 3A4 substrates may be caused by P-glycoprotein. *Clin Pharmacol Ther* 72 (5):474-489. doi:10.1067/mcp.2002.128388
67. Benet LZ, Cummins CL, Wu CY (2004) Unmasking the dynamic interplay between efflux transporters and metabolic enzymes. *Int J Pharm* 277 (1-2):3-9. doi:10.1016/j.ijpharm.2002.12.002
68. Ibarra M, Vazquez M, Fagiolino P, Derendorf H (2013) Sex related differences on valproic acid pharmacokinetics after oral single dose. *J Pharmacokinet Pharmacodyn* 40 (4):479-486. doi:10.1007/s10928-013-9323-3
69. Waxman DJ, Holloway MG (2009) Sex differences in the expression of hepatic drug metabolizing enzymes. *Mol Pharmacol* 76 (2):215-228. doi:10.1124/mol.109.056705
70. Anderson GD (2005) Sex and racial differences in pharmacological response: where is the evidence? pharmacogenetics, pharmacokinetics, and pharmacodynamics. *Journal of Women's Health*:19-29
71. Mangoni AA, Jackson SH (2004) Age-related changes in pharmacokinetics and pharmacodynamics: basic principles and practical applications. *Br J Clin Pharmacol* 57 (1):6-14
72. Ingrande J, Lemmens HJ (2010) Dose adjustment of anaesthetics in the morbidly obese. *Br J Anaesth* 105 Suppl 1:i16-23. doi:10.1093/bja/aeq312
73. Feng B, LaPerle JL, Chang G, Varma MV (2010) Renal clearance in drug discovery and development: molecular descriptors, drug transporters and disease state. *Expert Opin Drug Metab Toxicol* 6 (8):939-952. doi:10.1517/17425255.2010.482930
74. Baraldo M (2008) The influence of circadian rhythms on the kinetics of drugs in humans. *Expert Opin Drug Metab Toxicol* 4 (2):175-192. doi:10.1517/17425255.4.2.175
75. Binkhorst L, Kloth JS, de Wit AS, de Bruijn P, Lam MH, Chaves I, Burger H, van Alphen RJ, Hamberg P, van Schaik RH, Jager A, Koch BC, Wiemer EA, van Gelder T, van der Horst GT, Mathijssen RH (2015) Circadian variation in tamoxifen pharmacokinetics in mice and breast cancer patients. *Breast Cancer Res Treat* 152 (1):119-128. doi:10.1007/s10549-015-3452-x
76. Dallmann R, Okyar A, Levi F (2016) Dosing-Time Makes the Poison: Circadian Regulation and Pharmacotherapy. *Trends Mol Med* 22 (5):430-445. doi:10.1016/j.molmed.2016.03.004

77. Rao RT, DuBois DC, Almon RR, Jusko WJ, Androulakis IP (2016) Mathematical Modeling of the Circadian Dynamics of the Neuroendocrine-Immune Network in Experimentally Induced Arthritis. *Am J Physiol Endocrinol Metab*:ajpendo 00006 02016. doi:10.1152/ajpendo.00006.2016
78. Ovacik MA, Sukumaran S, Almon RR, DuBois DC, Jusko WJ, Androulakis IP (2010) Circadian signatures in rat liver: from gene expression to pathways. *BMC Bioinformatics* 11:540. doi:10.1186/1471-2105-11-540
79. Almon RR, Yang E, Lai W, Androulakis IP, Ghimbovschi S, Hoffman EP, Jusko WJ, Dubois DC (2008) Relationships between circadian rhythms and modulation of gene expression by glucocorticoids in skeletal muscle. *Am J Physiol Regul Integr Comp Physiol* 295 (4):R1031-1047. doi:10.1152/ajpregu.90399.2008
80. Almon RR, Yang E, Lai W, Androulakis IP, DuBois DC, Jusko WJ (2008) Circadian variations in rat liver gene expression: relationships to drug actions. *J Pharmacol Exp Ther* 326 (3):700-716. doi:10.1124/jpet.108.140186
81. Pierre K, Schlesinger N, Androulakis IP (2016) The role of the hypothalamic-pituitary-adrenal axis in modulating seasonal changes in immunity. *Physiol Genomics:physiolgenomics* 00006 02016. doi:10.1152/physiolgenomics.00006.2016
82. Mavroudis PD, Corbett SA, Calvano SE, Androulakis IP (2015) Circadian characteristics of permissive and suppressive effects of cortisol and their role in homeostasis and the acute inflammatory response. *Math Biosci* 260:54-64. doi:10.1016/j.mbs.2014.10.006
83. Mavroudis PD, Corbett SA, Calvano SE, Androulakis IP (2014) Mathematical modeling of light-mediated HPA axis activity and downstream implications on the entrainment of peripheral clock genes. *Physiol Genomics* 46 (20):766-778. doi:10.1152/physiolgenomics.00026.2014
84. Mavroudis PD, Scheff JD, Calvano SE, Androulakis IP (2013) Systems biology of circadian-immune interactions. *J Innate Immun* 5 (2):153-162. doi:10.1159/000342427
85. Mavroudis PD, Scheff JD, Calvano SE, Lowry SF, Androulakis IP (2012) Entrainment of peripheral clock genes by cortisol. *Physiol Genomics* 44 (11):607-621. doi:10.1152/physiolgenomics.00001.2012
86. Sajan J, Cinu T, Chacko A, LItty J, Jaseeda T (2009) Chronotherapeutics and chronotherapeutic drug delivery systems. *Tropical Journal of Pharmaceutical Research* 8 (5):467-475
87. Haus E, Sackett-Lundeen L, Smolensky MH (2012) Rheumatoid arthritis: circadian rhythms in disease activity, signs and symptoms, and rationale for chronotherapy with corticosteroids and other medications. *Bull NYU Hosp Jt Dis* 70 Suppl 1:3-10
88. Cutolo M, Straub RH (2008) Circadian rhythms in arthritis: hormonal effects on the immune/inflammatory reaction. *Autoimmun Rev* 7 (3):223-228. doi:10.1016/j.autrev.2007.11.019

89. Lemmer B (1999) Chronopharmacokinetics: Implications for Drug Treatment. *Journal of Pharmacy and Pharmacology* 51 (8):887-890. doi:10.1211/0022357991773294
90. Lemmer B (2012) The importance of biological rhythms in drug treatment of hypertension and sex-dependent modifications. *ChronoPhysiology and Therapy*:9. doi:10.2147/cpt.s21861
91. Erkekoglu P, Baydar T (2012) Chronopharmacokinetics of drugs in toxicological aspects: A short review for pharmacy practitioners. *J Res Pharm Pract* 1 (1):3-9. doi:10.4103/2279-042X.99670
92. Okyar A, Dressler C, Hanafy A, Baktir G, Lemmer B, Spahn-Langguth H (2012) Circadian variations in exsorbitive transport: in situ intestinal perfusion data and in vivo relevance. *Chronobiol Int* 29 (4):443-453. doi:10.3109/07420528.2012.668996
93. Iwasaki M, Koyanagi S, Suzuki N, Katamune C, Matsunaga N, Watanabe N, Takahashi M, Izumi T, Ohdo S (2015) Circadian modulation in the intestinal absorption of P-glycoprotein substrates in monkeys. *Mol Pharmacol* 88 (1):29-37. doi:10.1124/mol.114.096735
94. Adil MS, HM A, M I, K MA, Haadi A, K MA, Nematullah M (2014) Chronoterapeutics: targeting the disease at its ideal time. *The Pharma Innovation Journal* 2 (12)
95. Smolensky MH, Peppas NA (2007) Chronobiology, drug delivery, and chronotherapeutics. *Adv Drug Deliv Rev* 59 (9-10):828-851. doi:10.1016/j.addr.2007.07.001
96. Liu Q, Gong Y, Shi Y, Jiang L, Zheng C, Ge L, Liu J, Zhu J (2013) A novel multi-unit tablet for treating circadian rhythm diseases. *AAPS PharmSciTech* 14 (2):861-869. doi:10.1208/s12249-013-9975-8
97. Peng HT, Bouak F, Vartanian O, Cheung B (2013) A physiologically based pharmacokinetics model for melatonin--effects of light and routes of administration. *Int J Pharm* 458 (1):156-168. doi:10.1016/j.ijpharm.2013.09.033
98. Physiologically based pharmacokinetic analyses - Format and content: guidance for industry, draft (2016). U.S. Food and Drug Administration Center for Drug Evaluation and Research (CDER), Rockville, MD
99. Chen GC, Enayati P, Tran T, Lee-Henderson M, Quan C, Dulai G, Arnott I, Sul J, Jutabha R (2006) Sensitivity and inter-observer variability for capsule endoscopy image analysis in a cohort of novice readers. *World J Gastroenterol* 12 (8):1249-1254. doi:10.3748/wjg.v12.i8.1249
100. Zhao P (2017) Report from the EMA workshop on qualification and reporting of physiologically based pharmacokinetic (PBPK) modeling and simulation. *CPT Pharmacometrics Syst Pharmacol* 6 (2):71-72. doi:10.1002/psp4.12166
101. Zhao P, Rowland M, Huang SM (2012) Best practice in the use of physiologically based pharmacokinetic modeling and simulation to address clinical pharmacology regulatory questions. *Clin Pharmacol Ther* 92 (1):17-20. doi:10.1038/clpt.2012.68

102. Watanabe T, Kusuhara H, Sugiyama Y (2010) Application of physiologically based pharmacokinetic modeling and clearance concept to drugs showing transporter-mediated distribution and clearance in humans. *J Pharmacokinet Pharmacodyn* 37 (6):575-590. doi:10.1007/s10928-010-9176-y
103. Li M, Panagi Z, Avgoustakis K, Reineke J (2012) Physiologically based pharmacokinetic modeling of PLGA nanoparticles with varied mPEG content. *Int J Nanomedicine* 7:1345-1356. doi:10.2147/IJN.S23758
104. Zhuang X, Lu C (2016) PBPK modeling and simulation in drug research and development. *Acta Pharm Sin B* 6 (5):430-440. doi:10.1016/j.apsb.2016.04.004
105. Loizou G, Spendiff M, Barton HA, Bessems J, Bois FY, d'Yvoire MB, Buist H, Clewell HJ, 3rd, Meek B, Gundert-Remy U, Goerlitz G, Schmitt W (2008) Development of good modelling practice for physiologically based pharmacokinetic models for use in risk assessment: the first steps. *Regul Toxicol Pharmacol* 50 (3):400-411. doi:10.1016/j.yrtph.2008.01.011
106. Hartmanshenn C, Scherholz M, Androulakis IP (2016) Physiologically-based pharmacokinetic models: approaches for enabling personalized medicine. *J Pharmacokinet Pharmacodyn* 43 (5):481-504. doi:10.1007/s10928-016-9492-y
107. Zi Z (2011) Sensitivity analysis approaches applied to systems biology models. *IET Syst Biol* 5 (6):336-336. doi:10.1049/iet-syb.2011.0015
108. Rodriguez-Fernandez M, Banga JR, Francis J, Doyle I (2011) Novel global sensitivity analysis methodology accounting for the crucial role of the distribution of input parameters: application to systems biology models. *International Journal of Robust and Nonlinear Control* 00:1-18. doi:10.1002/rnc.2797
109. Brochot C, Smith TJ, Bois FY (2007) Development of a physiologically based toxicokinetic model for butadiene and four major metabolites in humans: global sensitivity analysis for experimental design issues. *Chem Biol Interact* 167 (3):168-183. doi:10.1016/j.cbi.2007.02.010
110. Tsamandouras N, Rostami-Hodjegan A, Aarons L (2015) Combining the 'bottom up' and 'top down' approaches in pharmacokinetic modelling: fitting PBPK models to observed clinical data. *Br J Clin Pharmacol* 79 (1):48-55. doi:10.1111/bcp.12234
111. Cariboni J, Gatelli D, Liska R, Saltelli A (2007) The role of sensitivity analysis in ecological modelling. *Ecological Modeling* 203:167-182. doi:10.1016/j.ecolmodel.2005.10.045
112. Rodriguez-Fernandez M, Banga JR (2010) SensSB: a software toolbox for the development and sensitivity analysis of systems biology models. *Bioinformatics* 26 (13):1675-1676. doi:10.1093/bioinformatics/btq242
113. Yu J, Cilfone NA, Large EM, Sarkar U, Wishnok JS, Tannenbaum SR, Hughes DJ, Lauffenburger DA, Griffith LG, Stokes CL, Cirit M (2015) Quantitative systems pharmacology approaches applied to microphysiological systems (MPS): Data interpretation and multi-MPS integration. *CPT Pharmacometrics Syst Pharmacol* 4 (10):585-594. doi:10.1002/psp4.12010

114. Cilfone NA, Pienaar E, Thurber GM, Kirschner DE, Linderman JJ (2015) Systems pharmacology approach toward the design of inhaled formulations of rifampicin and isoniazid for treatment of tuberculosis. *CPT Pharmacometrics Syst Pharmacol* 4 (3):193-203. doi:10.1002/psp4.22
115. Malik PR, Hamadeh A, Phipps C, Edginton AN (2017) Population PBPK modelling of trastuzumab: a framework for quantifying and predicting inter-individual variability. *J Pharmacokinet Pharmacodyn* 44 (4):277-290. doi:10.1007/s10928-017-9515-3
116. Das D, Dhurjati P, Wangikar PP (2008) Prediction of pharmacokinetic behaviour by combining in vivo and in vitro data in physiologically based pharmacokinetic (PBPK) model Parameter estimation and sensitivity analysis. *Journal of the Indian Institute of Science* 88 (1):57-71
117. Chen K, Teo S, Seng KY (2009) Sensitivity analysis on a physiologically-based pharmacokinetic and pharmacodynamic model for diisopropylfluorophosphate-induced toxicity in mice and rats. *Toxicol Mech Methods* 19 (8):486-497. doi:10.1080/15376510903300335
118. Ferretti F, Saltelli A, Tarantola S (2016) Trends in sensitivity analysis practice in the last decade. *Science of the Total Environment* 568:666-670. doi:10.1016/j.scitotenv.2016.02.133
119. Saltelli A, Ratto M, Andres T, Campolongo F, Cariboni J, Gatelli D, Saisana M, Tarantola S (2008) *Global sensitivity analysis: The primer*. John Wiley & Sons, Ltd, England
120. Nossent J, Elsen P, Bauwens W (2011) Sobol' sensitivity analysis of a complex environmental model. *Environmental Modelling & Software* 26 (12):1515-1525. doi:10.1016/j.envsoft.2011.08.010
121. Lumen A, McNally K, George N, Fisher JW, Loizou GD (2015) Quantitative global sensitivity analysis of a biologically based dose-response pregnancy model for the thyroid endocrine system. *Front Pharmacol* 6:107. doi:10.3389/fphar.2015.00107
122. Iooss B, Lemaitre P (2015) A review on global sensitivity analysis methods. In: Dellino G, Meloni C (eds) *Uncertainty Management in Simulation-Optimization of Complex Systems*. Operations Research/Computer Science Interfaces Series, vol 59. Springer, Boston, MA, pp 101-122
123. Morris MD (1991) Factorial sampling plans for preliminary computational experiments. *Technometrics* 33 (2):161-174. doi:10.2307/1269043
124. Campolongo F, Saltelli A, Cariboni J (2011) From screening to quantitative sensitivity analysis. A unified approach. *Computer Physics Communications* 182:978-988. doi:10.1016/j.cpc.2010.12.039
125. Garcia-Sanchez D, Lacarriere B, Musy M, Bourges B (2014) Application of sensitivity analysis in building every simulations: combining first- and second-order elementary effects methods. *Energy Build* 68:741-750. doi:10.1016/j.enbuild.2012.08.048

126. GastroPlus(TM) Verision 9.0 Simulation Software for Drug Discovery and Development - Manual (2015). Simulations Plus, Inc., Lancaster, CA
127. Campolongo F, Cariboni J, Saltelli A (2007) An effective screening design for sensitivity analysis of large models. *Environmental Modelling & Software* 22:1509-1518. doi:10.1016/j.envsoft.2006.10.004
128. Zhang XY, Trame MN, Lesko LJ, Schmidt S (2015) Sobol sensitivity analysis: a tool to guide the development and evaluation of systems pharmacology models. *CPT Pharmacometrics Syst Pharmacol* 4 (2):69-79. doi:10.1002/psp4.6
129. Saltelli A, Annoni P, Azzini I, Campolongo F, Ratto M, Tarantola S (2010) Variance based sensitivity analysis of model output. Design and estimator for the total sensitivity index. *Computer Physics Communications* 181:259-270. doi:10.1016/j.cpc.2009.09.018
130. Guidance for Industry: Statistical approaches to establishing bioequivalence. (2001) U.S. Department of Health and Human Services, Food and Drug Administration, Center for Drug Evaluation and Research. <https://www.fda.gov/downloads/drugs/guidances/ucm070244.pdf>.
131. Singla NK, Parulan C, Samson R, Hutchinson J, Bushnell R, Beja EG, Ang R, Royal MA (2012) Plasma and cerebrospinal fluid pharmacokinetic parameters after single-dose administration of intravenous, oral, or rectal acetaminophen. *Pain Pract* 12 (7):523-532. doi:10.1111/j.1533-2500.2012.00556.x
132. Liu Y, Zhang MQ, Jia JY, Liu YM, Liu GY, Li SJ, Wang W, Weng LP, Yu C (2013) Bioequivalence and pharmacokinetic evaluation of two formulations of risperidone 2 mg : an open-label, single-dose, fasting, randomized-sequence, two-way crossover study in healthy male Chinese volunteers. *Drugs R D* 13 (1):29-36. doi:10.1007/s40268-012-0002-4
133. Sowinski KM, Forrest A, Wilton JH, Taylor AM, 2nd, Wilson MF, Kazierad DJ (1995) Effect of aging on atenolol pharmacokinetics and pharmacodynamics. *J Clin Pharmacol* 35 (8):807-814. doi:10.1002/j.1552-4604.1995.tb04124.x
134. Mason WD, Winer N, Krochak G, Cohen I, Bell R (1979) Kinetics and absolute bioavailability of atenolol. *Clinical Pharmacology & Therapeutics* 25 (4):408-415. doi:10.1002/cpt1979254408
135. Van Wart SA, Shoaf SE, Mallikaarjun S, Mager DE (2014) Population-based meta-analysis of furosemide pharmacokinetics. *Biopharm Drug Dispos* 35 (2):119-133. doi:10.1002/bdd.1874
136. Press WH, Teukolsky SA, Vetterling WT, Flannery BP (1996) Numerical recipes in C. In: *The Art of Scientific Computing*, vol 2. Cambridge University Press, Cambridge, UK, pp 309-315
137. Bratley P, Fox BL (1988) Algorithm 659: Implementing Sobol's quasirandom sequence generator. *ACM Transactions on Mathematical Software (TOMS)* 14 (1):88-100

138. Joe S, Kuo FY (2003) Remark on algorithm 659: Implementing Sobol's quasirandom sequence generator. *ACM Transactions on Mathematical Software (TOMS)* 29 (1):49-57. doi:10.1145/641876.641879
139. Hong HS, Hickernell FJ (2003) Algorithm 823: Implementing scrambled digital sequences. *ACM Transactions on Mathematical Software (TOMS)* 29 (2):95-109. doi:10.1145/779359.779360
140. Matousek J (1998) On the L2-discrepancy for anchored boxes. *J Complex* 14 (4):527-556. doi:10.1006/jcom.1998.0489
141. Blower S, Dowlatabadi H (1994) Sensitivity and uncertainty analysis of complex models of disease transmission: an HIV model, as an example. *International Statistical Review* 2:229-243. doi:10.2307/1403510
142. Sinha VK, Snoeys J, Osselaer NV, Peer AV, Mackie C, Heald D (2012) From preclinical to human--prediction of oral absorption and drug-drug interaction potential using physiologically based pharmacokinetic (PBPK) modeling approach in an industrial setting: a workflow by using case example. *Biopharm Drug Dispos* 33 (2):111-121. doi:10.1002/bdd.1782
143. Watanabe T, Kusuhara H, Maeda K, Shitara Y, Sugiyama Y (2009) Physiologically based pharmacokinetic modeling to predict transporter-mediated clearance and distribution of pravastatin in humans. *J Pharmacol Exp Ther* 328 (2):652-662. doi:10.1124/jpet.108.146647
144. Gobeau N, Stringer R, De Buck S, Tuntland T, Faller B (2016) Evaluation of the GastroPlus Advanced Compartmental and Transit (ACAT) Model in Early Discovery. *Pharm Res* 33 (9). doi:10.1007/s11095-016-1951-z
145. Herman JD, Kollat JB, Reed PM, Wagener T (2013) Technical Note: Method of Morris effectively reduces the computational demands of global sensitivity analysis for distributed watershed models. *Hydrol Earth Syst Sc* 17 (7):2893-2903. doi:10.5194/hess-17-2893-2013
146. Archer GEB, Saltelli A, Sobol IM (1997) Sensitivity measures, ANOVA-like techniques and the use of bootstrap. *J Stat Comput Sim* 58 (2):99-120. doi:10.1080/00949659708811825
147. Menberg K, Heo Y, Choudhary R (2016) Sensitivity analysis methods for building energy models: Comparing computational costs and extractable information. *Energy and Buildings* 133:433-445. doi:10.1016/j.enbuild.2016.10.005
148. Jones HM, Chen Y, Gibson C, Heimbach T, Parrott N, Peters SA, Snoeys J, Upreti VV, Zheng M, Hall SD (2015) Physiologically based pharmacokinetic modeling in drug discovery and development: a pharmaceutical industry perspective. *Clin Pharmacol Ther* 97 (3):247-262. doi:10.1002/cpt.37
149. Wu CY, Benet LZ (2005) Predicting drug disposition via application of BCS: transport/absorption/ elimination interplay and development of a biopharmaceutics drug disposition classification system. *Pharm Res* 22 (1):11-23. doi:10.1007/s11095-004-9004-4

150. Pouton CW (2006) Formulation of poorly water-soluble drugs for oral administration: physicochemical and physiological issues and the lipid formulation classification system. *Eur J Pharm Sci* 29 (3-4):278-287. doi:10.1016/j.ejps.2006.04.016
151. Yu LX (2008) Pharmaceutical quality by design: product and process development, understanding, and control. *Pharm Res* 25 (4):781-791. doi:10.1007/s11095-007-9511-1
152. Wang B, Liu Z, Li D, Yang S, Hu J, Chen H, Sheng L, Li Y (2015) Application of physiologically based pharmacokinetic modeling in the prediction of pharmacokinetics of bicyclol controlled-release formulation in human. *Eur J Pharm Sci* 77:265-272. doi:10.1016/j.ejps.2015.06.020
153. Kesisoglou F, Xia B, Agrawal NG (2015) Comparison of deconvolution-based and absorption modeling IVIVC for extended release formulations of a BCS III drug development candidate. *AAPS J* 17 (6):1492-1500. doi:10.1208/s12248-015-9816-7
154. Wainwright HM, Finsterle S, Jung YJ, Zhou QL, Birkholzer JT (2014) Making sense of global sensitivity analyses. *Comput Geosci* 65:84-94. doi:10.1016/j.cageo.2013.06.006
155. Marino S, Hogue IB, Ray CJ, Kirschner DE (2008) A methodology for performing global uncertainty and sensitivity analysis in systems biology. *Journal of Theoretical Biology* 254 (1):178-196. doi:10.1016/j.jtbi.2008.04.011
156. Xia J, Zheng XG, Adili GZ, Wei YR, Ma WG, Xue XM, Mi XY, Yi Z, Chen SJ, Du W, Muhan M, Duhaxi C, Han T, Gudai B, Huang J (2016) Sequence analysis of peste des petits ruminants virus from ibexes in Xinjiang, China. *Genet Mol Res* 15 (2):1-7. doi:10.4238/gmr.15027783
157. Alqahtani S, Kaddoumi A (2015) Development of Physiologically Based Pharmacokinetic/Pharmacodynamic Model for Indomethacin Disposition in Pregnancy. *PLOS ONE* 10 (10):1-18. doi:10.1371/journal.pone.0139762
158. Zamora-Sillero E, Hafner M, Ibig A, Stelling J, Wagner A (2011) Efficient characterization of high-dimensional parameter spaces for systems biology. *BMC Syst Biol* 5 (1):142-164. doi:10.1186/1752-0509-5-142
159. Bois FY (2000) Statistical analysis of Fisher et al. PBPK model of trichloroethylene kinetics. *Environ Health Perspect* 108 Suppl 2:275-282
160. Timchalk C, Kousba A, Poet TS (2002) Monte Carlo analysis of the human chlorpyrifos-oxonase (PON1) polymorphism using a physiologically based pharmacokinetic and pharmacodynamic (PBPK/PD) model. *Toxicol Lett* 135 (1-2):51-59
161. Scherholz ML, Forder J, Androulakis IP (2018) A framework for 2-stage global sensitivity analysis of GastroPlus compartmental models. *J Pharmacokinetic Pharmacodyn* 45 (2):309-327. doi:10.1007/s10928-018-9573-1
162. Hu L, Agbokponto JE, Li X, Ding L, Liu B, Zhong S, Zhang X, Du Y (2015) In vivo and in vitro evidence of the sex-dependent pharmacokinetics and disposition of

- G004, a potential hypoglycemic agent, in rats. *Eur J Drug Metab Pharmacokinet* 40 (2):187-202. doi:10.1007/s13318-014-0196-7
163. Bernillon P, Bois FY (2000) Statistical issues in toxicokinetic modeling: a bayesian perspective. *Environ Health Perspect* 108 Suppl 5:883-893
 164. Woodruff TJ, Bois FY (1993) Optimization issues in physiological toxicokinetic modeling: a case study with benzene. *Toxicol Lett* 69 (2):181-196
 165. Bois FY, Jamei M, Clewell HJ (2010) PBPK modelling of inter-individual variability in the pharmacokinetics of environmental chemicals. *Toxicology* 278 (3):256-267. doi:10.1016/j.tox.2010.06.007
 166. Sweeney LM, Tyler TR, Kirman CR, Corley RA, Reitz RH, Paustenbach DJ, Holson JF, Whorton MD, Thompson KM, Gargas ML (2001) Proposed occupational exposure limits for select ethylene glycol ethers using PBPK models and Monte Carlo simulations. *Toxicol Sci* 62 (1):124-139
 167. Allen RJ, Rieger TR, Musante CJ (2016) Efficient Generation and Selection of Virtual Populations in Quantitative Systems Pharmacology Models. *CPT Pharmacometrics Syst Pharmacol* 5 (3):140-146. doi:10.1002/psp4.12063
 168. Schmidt BJ, Casey FP, Paterson T, Chan JR (2013) Alternate virtual populations elucidate the type I interferon signature predictive of the response to rituximab in rheumatoid arthritis. *BMC Bioinformatics* 14:221. doi:10.1186/1471-2105-14-221
 169. Klink DJ, 2nd (2008) Integrating epidemiological data into a mechanistic model of type 2 diabetes: validating the prevalence of virtual patients. *Ann Biomed Eng* 36 (2):321-334. doi:10.1007/s10439-007-9410-y
 170. Arlt W, Stewart PM (2005) Adrenal corticosteroid biosynthesis, metabolism, and action. *Endocrinol Metab Clin North Am* 34 (2):293-313, viii. doi:10.1016/j.ecl.2005.01.002
 171. Fietta P, Delsante G (2009) Central nervous system effects of natural and synthetic glucocorticoids. *Psychiatry Clin Neurosci* 63 (5):613-622. doi:10.1111/j.1440-1819.2009.02005.x
 172. Spiga F, Walker JJ, Terry JR, Lightman SL (2014) HPA Axis-Rhythms. In: Terjung R (ed) *Comprehensive Physiology*. John Wiley & Sons, Inc., Hoboken, NJ, USA, pp 1273-1298
 173. McMaster A, Ray DW (2007) Modelling the glucocorticoid receptor and producing therapeutic agents with anti-inflammatory effects but reduced side-effects. *Exp Physiol* 92 (2):299-309. doi:10.1113/expphysiol.2006.036194
 174. Nicolaidis NC, Charmandari E, Kino T, Chrousos GP (2017) Stress-Related and Circadian Secretion and Target Tissue Actions of Glucocorticoids: Impact on Health. *Front Endocrinol (Lausanne)* 8:70. doi:10.3389/fendo.2017.00070
 175. Smith SM, Vale WW (2006) The role of the hypothalamic-pituitary-adrenal axis in neuroendocrine responses to stress. *Dialogues Clin Neurosci* 8 (4):383-395

176. Hench PS, Kendall EC, Slocumb CH, Polley HF (1949) The effect of a hormone of the adrenal cortex (17-hydroxy-11-dehydrocorticosterone: compound E) and of pituitary adrenocortical hormone in arthritis: preliminary report. *Ann Rheum Dis* 8 (2):97-104
177. Edwards C (2012) Sixty years after Hench--corticosteroids and chronic inflammatory disease. *J Clin Endocrinol Metab* 97 (5):1443-1451. doi:10.1210/jc.2011-2879
178. Kirwan JR, Clarke L, Hunt LP, Perry MG, Straub RH, Jessop DS (2010) Effect of novel therapeutic glucocorticoids on circadian rhythms of hormones and cytokines in rheumatoid arthritis. *Ann N Y Acad Sci* 1193:127-133. doi:10.1111/j.1749-6632.2009.05289.x
179. Fisher LE, Ludwig EA, Wald JA, Sloan RR, Middleton E, Jr., Jusko WJ (1992) Pharmacokinetics and pharmacodynamics of methylprednisolone when administered at 8 am versus 4 pm. *Clin Pharmacol Ther* 51 (6):677-688
180. Buttgerit F, Burmester GR, Lipworth BJ (2005) Optimised glucocorticoid therapy: the sharpening of an old spear. *Lancet* 365 (9461):801-803. doi:10.1016/S0140-6736(05)17989-6
181. Alangari AA (2010) Genomic and non-genomic actions of glucocorticoids in asthma. *Ann Thorac Med* 5 (3):133-139. doi:10.4103/1817-1737.65040
182. Czock D, Keller F, Rasche FM, Haussler U (2005) Pharmacokinetics and pharmacodynamics of systemically administered glucocorticoids. *Clin Pharmacokinet* 44 (1):61-98. doi:10.2165/00003088-200544010-00003
183. Beltrametti SP, Ianniello A, Ricci C (2016) Chronotherapy with low-dose modified-release prednisone for the management of rheumatoid arthritis: a review. *Ther Clin Risk Manag* 12:1763-1776. doi:10.2147/TCRM.S112685
184. Xu J, Winkler J, Sabarinath SN, Derendorf H (2008) Assessment of the impact of dosing time on the pharmacokinetics/pharmacodynamics of prednisolone. *AAPS J* 10 (2):331-341. doi:10.1208/s12248-008-9038-3
185. Curtis JR, Westfall AO, Allison J, Bijlsma JW, Freeman A, George V, Kovac SH, Spettell CM, Saag KG (2006) Population-based assessment of adverse events associated with long-term glucocorticoid use. *Arthritis Rheum* 55 (3):420-426. doi:10.1002/art.21984
186. Rhen T, Cidlowski JA (2005) Antiinflammatory action of glucocorticoids--new mechanisms for old drugs. *N Engl J Med* 353 (16):1711-1723. doi:10.1056/NEJMra050541
187. Liu D, Ahmet A, Ward L, Krishnamoorthy P, Mandelcorn ED, Leigh R, Brown JP, Cohen A, Kim H (2013) A practical guide to the monitoring and management of the complications of systemic corticosteroid therapy. *Allergy Asthma Clin Immunol* 9 (1):30. doi:10.1186/1710-1492-9-30
188. Oster H, Challet E, Ott V, Arvat E, Ronald de Kloet E, Dijk DJ, Lightman S, Vgontzas A, Van Cauter E (2017) The Functional and Clinical Significance of the

- 24-Hour Rhythm of Circulating Glucocorticoids. *Endocr Rev* 38 (1):3-45. doi:10.1210/er.2015-1080
189. Fardet L, Petersen I, Nazareth I (2012) Suicidal behavior and severe neuropsychiatric disorders following glucocorticoid therapy in primary care. *Am J Psychiatry* 169 (5):491-497. doi:10.1176/appi.ajp.2011.11071009
 190. Hwang JL, Weiss RE (2014) Steroid-induced diabetes: a clinical and molecular approach to understanding and treatment. *Diabetes Metab Res Rev* 30 (2):96-102. doi:10.1002/dmrr.2486
 191. Moghadam-Kia S, Werth VP (2010) Prevention and treatment of systemic glucocorticoid side effects. *International journal of dermatology* 49 (3):239-248
 192. Ohdo S, Koyanagi S, Matsunaga N (2010) Chronopharmacological strategies: Intra- and inter-individual variability of molecular clock. *Adv Drug Deliv Rev* 62 (9-10):885-897. doi:10.1016/j.addr.2010.04.005
 193. Dibner C, Schibler U, Albrecht U (2010) The mammalian circadian timing system: organization and coordination of central and peripheral clocks. *Annu Rev Physiol* 72:517-549. doi:10.1146/annurev-physiol-021909-135821
 194. Cutolo M (2016) Glucocorticoids and chronotherapy in rheumatoid arthritis. *RMD Open* 2 (1):e000203. doi:10.1136/rmdopen-2015-000203
 195. Kirwan JR (2011) Targeting the time of day for glucocorticoid delivery in rheumatoid arthritis. *Int J Clin Rheumatol* 6 (3):273-279. doi:doi: 10.2217/IJR.11.23
 196. Newell-Price J, Whiteman M, Rostami-Hodjegan A, Darzy K, Shalet S, Tucker GT, Ross RJ (2008) Modified-release hydrocortisone for circadian therapy: a proof-of-principle study in dexamethasone-suppressed normal volunteers. *Clin Endocrinol (Oxf)* 68 (1):130-135. doi:10.1111/j.1365-2265.2007.03011.x
 197. Bae S-A, Androulakis IP (2017) The Synergistic Role of Light-Feeding Phase Relations on Entraining Robust Circadian Rhythms in the Periphery. *Gene Regul Syst Bio* 11:1177625017702393
 198. Goodwin BC (1965) Oscillatory behavior in enzymatic control processes. *Adv Enzyme Regul* 3:425-438
 199. Sriram K, Rodriguez-Fernandez M, Doyle FJ (2012) Modeling Cortisol Dynamics in the Neuro-endocrine Axis Distinguishes Normal, Depression, and Post-traumatic Stress Disorder (PTSD) in Humans. *PLoS Computational Biology* 8 (2). doi:10.1371/journal.pcbi.1002379
 200. Rao RT, Androulakis IP (2017) Modeling the Sex Differences and Inter-individual Variability in the Activity of the Hypothalamic-Pituitary-Adrenal Axis. *Endocrinology*. doi:10.1210/en.2017-00544
 201. Kalsbeek A, Fliers E, Hofman MA, Swaab DF, Buijs RM (2010) Vasopressin and the output of the hypothalamic biological clock. *J Neuroendocrinol* 22 (5):362-372. doi:10.1111/j.1365-2826.2010.01956.x

202. Bordyugov G, Abraham U, Granada A, Rose P, Imkeller K, Kramer A, Herzel H (2015) Tuning the phase of circadian entrainment. *J R Soc Interface* 12 (108):20150282. doi:10.1098/rsif.2015.0282
203. Schmal C, Myung J, Herzel H, Bordyugov G (2015) A theoretical study on seasonality. *Front Neurol* 6:94. doi:10.3389/fneur.2015.00094
204. Jung CM, Khalsa SB, Scheer FA, Cajochen C, Lockley SW, Czeisler CA, Wright KP, Jr. (2010) Acute effects of bright light exposure on cortisol levels. *J Biol Rhythms* 25 (3):208-216. doi:10.1177/0748730410368413
205. Xu J, Winkler J, Derendorf H (2007) A pharmacokinetic/pharmacodynamic approach to predict total prednisolone concentrations in human plasma. *J Pharmacokinet Pharmacodyn* 34 (3):355-372. doi:10.1007/s10928-007-9050-8
206. Mould DR, Upton RN (2013) Basic concepts in population modeling, simulation, and model-based drug development-part 2: introduction to pharmacokinetic modeling methods. *CPT Pharmacometrics Syst Pharmacol* 2:e38. doi:10.1038/psp.2013.14
207. Cirincione B, Edwards J, Mager DE (2017) Population Pharmacokinetics of an Extended-Release Formulation of Exenatide Following Single- and Multiple-Dose Administration. *AAPS J* 19 (2):487-496. doi:10.1208/s12248-016-9975-1
208. Buttgerit F, Mehta D, Kirwan J, Szechinski J, Boers M, Alten RE, Supronik J, Szombati I, Romer U, Witte S, Saag KG (2013) Low-dose prednisone chronotherapy for rheumatoid arthritis: a randomised clinical trial (CAPRA-2). *Annals of the Rheumatic Diseases* 72 (2):204-210. doi:10.1136/annrheumdis-2011-201067
209. Johnson CH (1992) Phase response curves: what can they tell us about circadian clocks. *Circadian Clocks from Cell to Human*:209-249
210. Ballesta A, Innominato PF, Dallmann R, Rand DA, Levi FA (2017) Systems Chronotherapeutics. *Pharmacol Rev* 69 (2):161-199. doi:10.1124/pr.116.013441
211. Levi F, Schibler U (2007) Circadian Rhythms: Mechanisms and Therapeutic Implications. *Annual Review of Pharmacology and Toxicology* 47 (1):593-628. doi:10.1146/annurev.pharmtox.47.120505.105208
212. Bodick N, Lufkin J, Willwerth C, Kumar A, Bolognese J, Schoonmaker C, Ballal R, Hunter D, Clayman M (2015) An intra-articular, extended-release formulation of triamcinolone acetonide prolongs and amplifies analgesic effect in patients with osteoarthritis of the knee: a randomized clinical trial. *J Bone Joint Surg Am* 97 (11):877-888. doi:10.2106/JBJS.N.00918
213. Johannsson G, Bergthorsdottir R, Nilsson AG, Lennernas H, Hedner T, Skrtic S (2009) Improving glucocorticoid replacement therapy using a novel modified-release hydrocortisone tablet: a pharmacokinetic study. *Eur J Endocrinol* 161 (1):119-130. doi:10.1530/EJE-09-0170
214. Forss M, Batcheller G, Skrtic S, Johannsson G (2012) Current practice of glucocorticoid replacement therapy and patient-perceived health outcomes in adrenal

- insufficiency - a worldwide patient survey. *BMC Endocr Disord* 12:8. doi:10.1186/1472-6823-12-8
215. Sukumaran S, Almon RR, DuBois DC, Jusko WJ (2010) Circadian rhythms in gene expression: Relationship to physiology, disease, drug disposition and drug action. *Adv Drug Deliv Rev* 62 (9-10):904-917. doi:10.1016/j.addr.2010.05.009
 216. Buijs RM, van Eden CG, Goncharuk VD, Kalsbeek A (2003) The biological clock tunes the organs of the body: timing by hormones and the autonomic nervous system. *J Endocrinol* 177 (1):17-26
 217. Potter GD, Skene DJ, Arendt J, Cade JE, Grant PJ, Hardie LJ (2016) Circadian Rhythm and Sleep Disruption: Causes, Metabolic Consequences, and Countermeasures. *Endocr Rev* 37 (6):584-608. doi:10.1210/er.2016-1083
 218. Pulivarthy SR, Tanaka N, Welsh DK, De Haro L, Verma IM, Panda S (2007) Reciprocity between phase shifts and amplitude changes in the mammalian circadian clock. *Proc Natl Acad Sci U S A* 104 (51):20356-20361. doi:10.1073/pnas.0708877104
 219. Spoelstra K, Albrecht U, van der Horst GT, Brauer V, Daan S (2004) Phase responses to light pulses in mice lacking functional *per* or *cry* genes. *J Biol Rhythms* 19 (6):518-529. doi:10.1177/0748730404268122
 220. Malisch JL, Breuner CW, Gomes FR, Chappell MA, Garland T, Jr. (2008) Circadian pattern of total and free corticosterone concentrations, corticosteroid-binding globulin, and physical activity in mice selectively bred for high voluntary wheel-running behavior. *Gen Comp Endocrinol* 156 (2):210-217. doi:10.1016/j.ygcen.2008.01.020
 221. Angeli A, Frajria R, Bisbocci D, Ceresa F (1977) Temporal changes in plasma transcortin (CBG) binding capacity during the menstrual cycle. *Biol Rhythm Res* 8 (3-4):237-242
 222. Harris AP, Holmes MC, de Kloet ER, Chapman KE, Seckl JR (2013) Mineralocorticoid and glucocorticoid receptor balance in control of HPA axis and behaviour. *Psychoneuroendocrinology* 38 (5):648-658. doi:10.1016/j.psyneuen.2012.08.007
 223. Ebner K, Singewald N (2017) Individual differences in stress susceptibility and stress inhibitory mechanisms. *Current Opinion in Behavioral Sciences* 14:54-64
 224. Cutolo M, Villaggio B, Otsa K, Aakre O, Sulli A, Serio B (2005) Altered circadian rhythms in rheumatoid arthritis patients play a role in the disease's symptoms. *Autoimmunity Reviews* 4 (8):497-502. doi:10.1016/j.autrev.2005.04.019
 225. Kouri V-P, Olkkonen J, Kaivosoja E, Ainola M, Juhila J, Hovatta I, Kontinen YT, Mandelin J (2013) Circadian Timekeeping Is Disturbed in Rheumatoid Arthritis at Molecular Level. *PLoS ONE* 8 (1). doi:10.1371/journal.pone.0054049
 226. Chrousos GP (2010) Stress and sex versus immunity and inflammation. *Sci Signal* 3 (143):pe36. doi:10.1126/scisignal.3143pe36

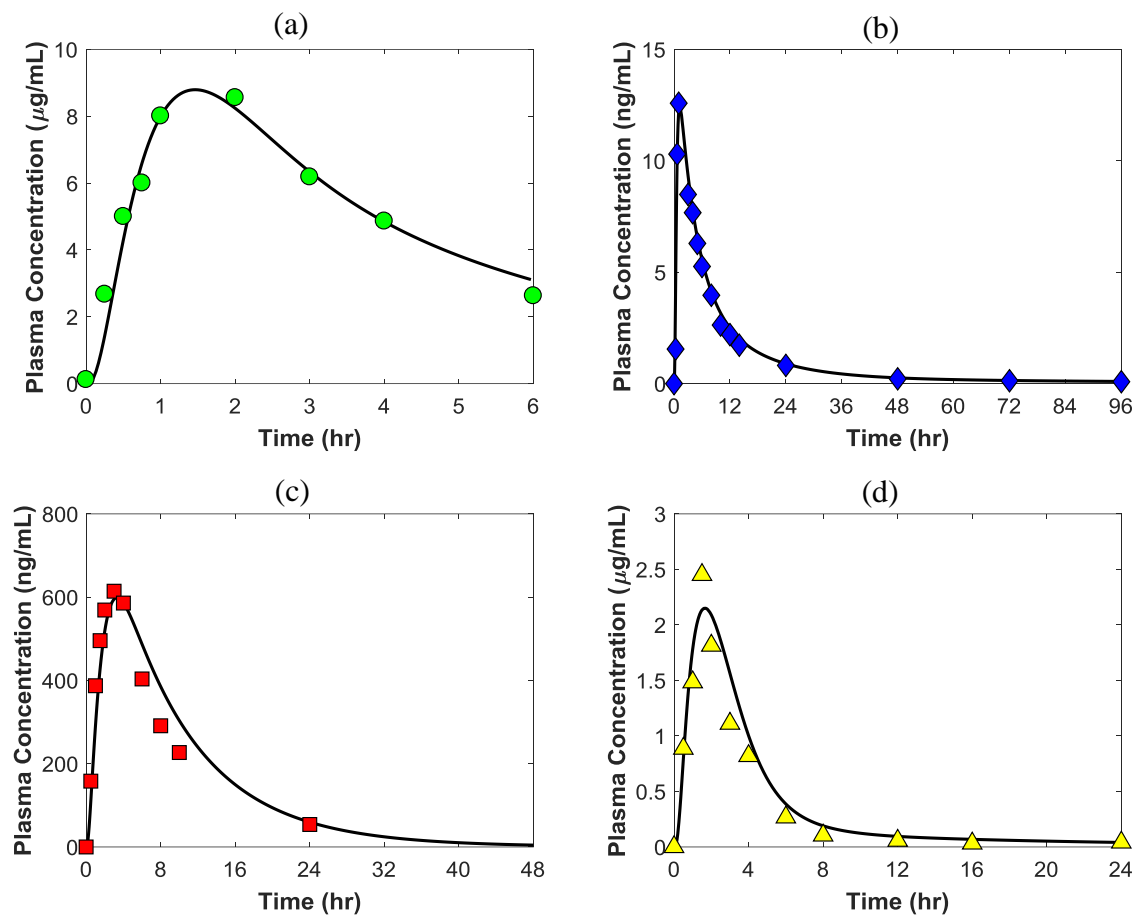
227. Yehuda R, Halligan SL, Grossman R, Golier JA, Wong C (2002) The cortisol and glucocorticoid receptor response to low dose dexamethasone administration in aging combat veterans and holocaust survivors with and without posttraumatic stress disorder. *Biol Psychiatry* 52 (5):393-403
228. Lew KH, Ludwig EA, Milad MA, Donovan K, Middleton E, Jr., Ferry JJ, Jusko WJ (1993) Gender-based effects on methylprednisolone pharmacokinetics and pharmacodynamics. *Clin Pharmacol Ther* 54 (4):402-414
229. Magee MH, Blum RA, Lates CD, Jusko WJ (2001) Prednisolone pharmacokinetics and pharmacodynamics in relation to sex and race. *J Clin Pharmacol* 41 (11):1180-1194
230. Crown A, Lightman S (2005) Why is the management of glucocorticoid deficiency still controversial: a review of the literature. *Clin Endocrinol (Oxf)* 63 (5):483-492. doi:10.1111/j.1365-2265.2005.02320.x
231. Alten R, Wiebe E (2015) Hypothalamic-pituitary-adrenal axis function in patients with rheumatoid arthritis treated with different glucocorticoid approaches. *Neuroimmunomodulation* 22 (1-2):83-88. doi:10.1159/000362731
232. Kalsbeek A, Verhagen LA, Schaliij I, Foppen E, Saboureau M, Bothorel B, Buijs RM, Pevet P (2008) Opposite actions of hypothalamic vasopressin on circadian corticosterone rhythm in nocturnal versus diurnal species. *Eur J Neurosci* 27 (4):818-827. doi:10.1111/j.1460-9568.2008.06057.x
233. Debono M, Price JN, Ross RJ (2009) Novel strategies for hydrocortisone replacement. *Best Pract Res Clin Endocrinol Metab* 23 (2):221-232. doi:10.1016/j.beem.2008.09.010
234. Quax RA, Manenschijn L, Koper JW, Hazes JM, Lamberts SW, van Rossum EF, Feelders RA (2013) Glucocorticoid sensitivity in health and disease. *Nat Rev Endocrinol* 9 (11):670-686. doi:10.1038/nrendo.2013.183
235. Debono M, Ross RJ, Newell-Price J (2009) Inadequacies of glucocorticoid replacement and improvements by physiological circadian therapy. *Eur J Endocrinol* 160 (5):719-729. doi:10.1530/EJE-08-0874
236. Song QQ, Xie WY, Tang YJ, Zhang J, Liu J (2017) Genetic variation in the glucocorticoid pathway involved in interindividual differences in the glucocorticoid treatment. *Pharmacogenomics* 18 (3):293-316. doi:10.2217/pgs-2016-0151
237. De Iudicibus S, Franca R, Martellosi S, Ventura A, Decorti G (2011) Molecular mechanism of glucocorticoid resistance in inflammatory bowel disease. *World J Gastroenterol* 17 (9):1095-1108. doi:10.3748/wjg.v17.i9.1095
238. Franchimont D, Kino T, Galon J, Meduri GU, Chrousos G (2002) Glucocorticoids and inflammation revisited: the state of the art. NIH clinical staff conference. *Neuroimmunomodulation* 10 (5):247-260. doi:10.1159/000069969
239. Kino T, Charmandari E, Chrousos GP (2011) Glucocorticoid receptor: implications for rheumatic diseases. *Clin Exp Rheumatol* 29 (5 Suppl 68):S32-41

240. Ibrahim A, Dahlqvist P, Olsson T, Lundgren D, Werner M, Suhr OB, Karling P (2017) The clinical course after glucocorticoid treatment in patients with inflammatory bowel disease is linked to suppression of the hypothalamic-pituitary-adrenal axis: a retrospective observational study. *Therap Adv Gastroenterol* 10 (11):829-836. doi:10.1177/1756283X17730748
241. Pujolsa L, Mullol J, Picado C (2009) Glucocorticoid receptor in human respiratory epithelial cells. *Neuroimmunomodulation* 16 (5):290-299. doi:10.1159/000216187
242. Yan YX, Dong J, Wu LJ, Shao S, Zhang J, Zhang L, Wang W, He Y, Liu YQ (2013) Associations between polymorphisms in the glucocorticoid-receptor gene and cardiovascular risk factors in a Chinese population. *J Epidemiol* 23 (5):389-395
243. Dallmann R, Brown SA, Gachon F (2014) Chronopharmacology: new insights and therapeutic implications. *Annu Rev Pharmacol Toxicol* 54:339-361. doi:10.1146/annurev-pharmtox-011613-135923
244. Oakley RH, Cidlowski JA (2011) Cellular processing of the glucocorticoid receptor gene and protein: new mechanisms for generating tissue-specific actions of glucocorticoids. *J Biol Chem* 286 (5):3177-3184. doi:10.1074/jbc.R110.179325
245. EMBL-EBI Acetaminophen (Compound Report Card). <https://www.ebi.ac.uk/chembl/db/compound/inspect/CHEMBL112>. Accessed 2017
246. DrugBank Risperidone. Canadian Institutes of Health Research. <https://www.drugbank.ca/drugs/DB00734>.
247. Granero GE, Longhi MR, Mora MJ, Junginger HE, Midha KK, Shah VP, Stavchansky S, Dressman JB, Barends DM (2010) Biowaiver monographs for immediate release solid oral dosage forms: furosemide. *J Pharm Sci* 99 (6):2544-2556. doi:10.1002/jps.22030
248. Kalantzi L, Reppas C, Dressman JB, Amidon GL, Junginger HE, Midha KK, Shah VP, Stavchansky SA, Barends DM (2006) Biowaiver monographs for immediate release solid oral dosage forms: acetaminophen (paracetamol). *J Pharm Sci* 95 (1):4-14. doi:10.1002/jps.20477
249. Jug M, Kos I, Becirevic-Lacan M (2009) The pH-dependent complexation between risperidone and hydroxypropyl-beta-cyclodextrin. *J Incl Phenom Macrocycl Chem* 64:163-171
250. Chow ECY, Talattof A, Tsakalozou E, Fan J, Zhao L, Zhang X (2016) Using physiologically based pharmacokinetic (PBPK) modeling to evaluate the impact of pharmaceutical excipients on oral drug absorption: sensitivity analyses. *The AAPS Journal*
251. Mermelstein NH (2010) Simulating Digestion. *Food Technology: Food Safety & Quality*:71-76
252. Zakeri-Milani P, Valizadeh H, Tajerzadeh H, Azarmi Y, Islambolchilar Z, Barzegar S, Barzegar-Jalali M (2007) Predicting human intestinal permeability using single-pass intestinal perfusion in rat. *J Pharm Pharm Sci* 10 (3):368-379

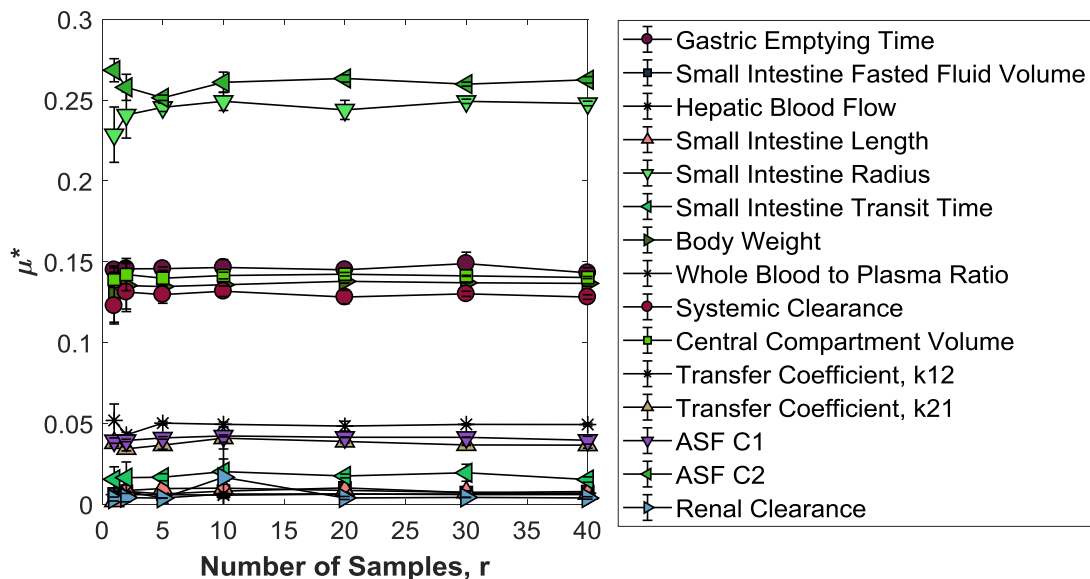
253. Shaw LR, Irwin WJ, Grattan TJ, Conway BR (2005) The effect of selected water-soluble excipients on the dissolution of paracetamol and Ibuprofen. *Drug Dev Ind Pharm* 31 (6):515-525. doi:10.1080/03639040500215784
254. Jiang X-L, Zhao P, Lesko LJ, Schmidt S (2013) Mechanistic prediction of acetaminophen metabolism and pharmacokinetics in children using a physiologically-based pharmacokinetic (PBPK) modeling approach. Paper presented at the Annual Meeting of the Population Approach Group in Europe, Scotland,
255. Taylor EA, Turner P (1981) The distribution of propranolol, pindolol and atenolol between human erythrocytes and plasma. *Br J Clin Pharmacol* 12 (4):543-548
256. Barber HE, Hawksworth GM, Kitteringham NR, Petersen J, Petrie JC, Swann JM (1978) Protein binding of atenolol and propranolol to human serum albumin and in human plasma [proceedings]. *Br J Clin Pharmacol* 6 (5):446P-447P
257. Najib N, Idkaidek N, Beshtawi M, Bader M, Admour I, Alam SM, Zaman Q, Dham R (2003) Bioequivalence evaluation of two brands of furosemide 40 mg tablets (Salurin and Lasix) in healthy human volunteers. *Biopharm Drug Dispos* 24 (6):245-249. doi:10.1002/bdd.361
258. Ramakrishnan R, DuBois DC, Almon RR, Pyszczynski NA, Jusko WJ (2002) Fifth-generation model for corticosteroid pharmacodynamics: application to steady-state receptor down-regulation and enzyme induction patterns during seven-day continuous infusion of methylprednisolone in rats. *Journal of Pharmacokinetics and Pharmacodynamics* 29 (1):1-24

Appendix

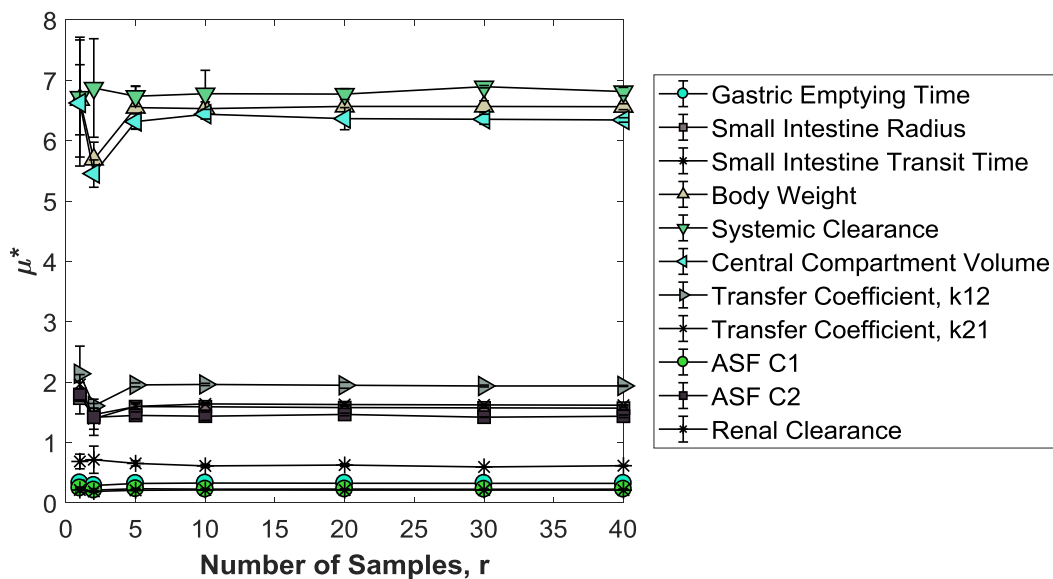
6.1 Supplementary Figures



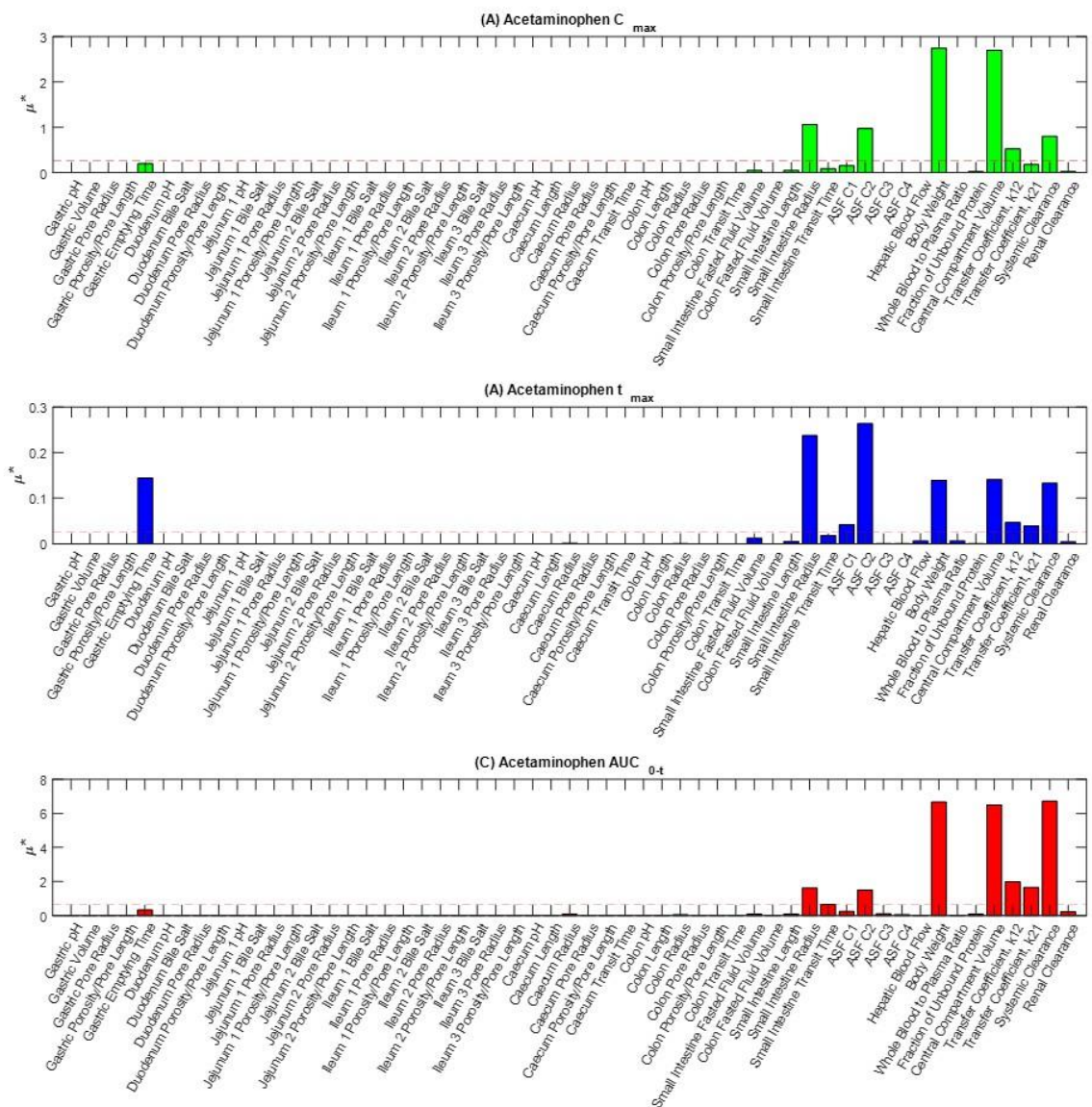
Supplementary Figure 1: Baseline plasma concentration profiles for (a) acetaminophen, (b) risperidone, (c) atenolol, and (d) furosemide predicted by the calibrated GastroPlus models



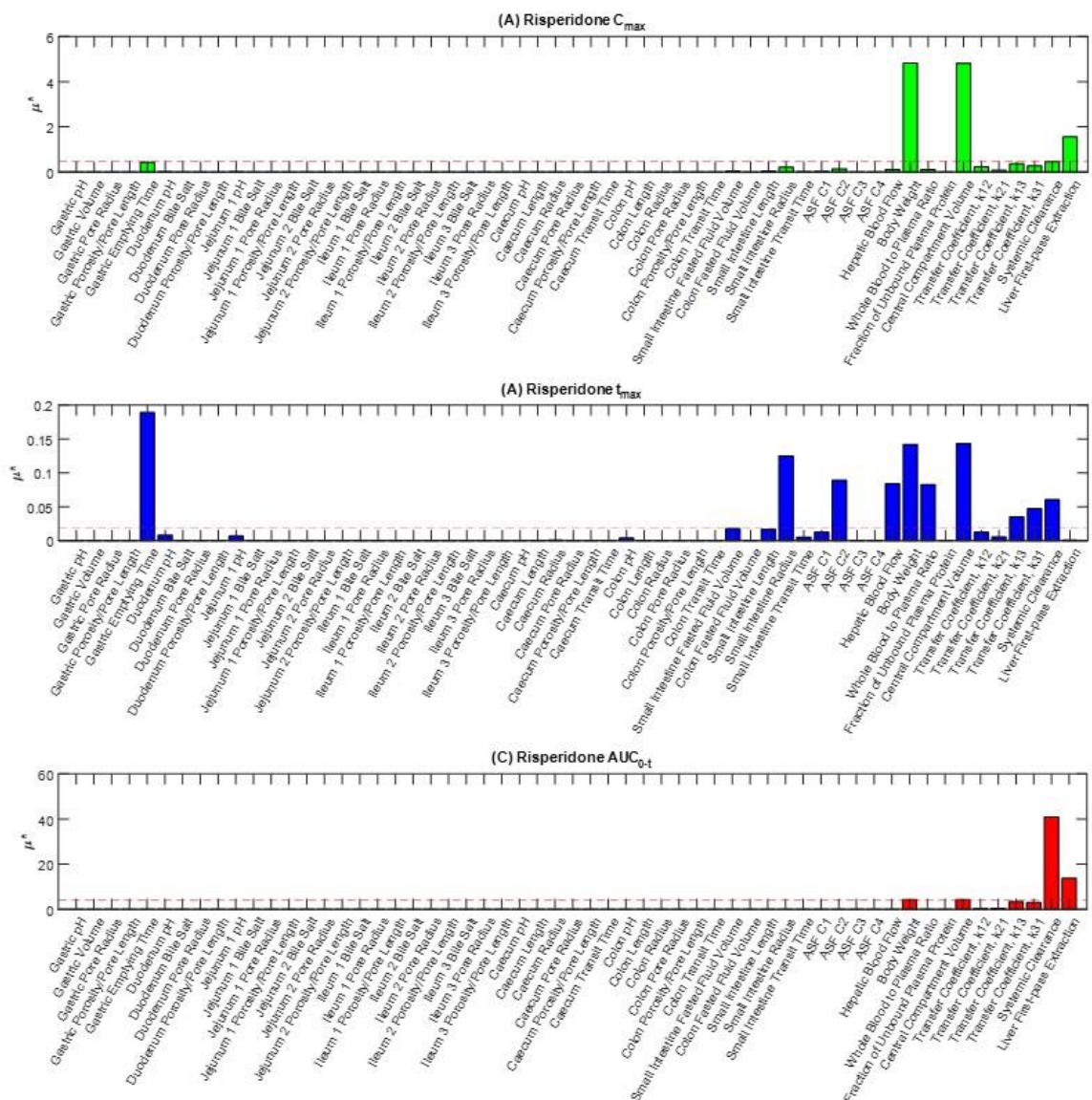
Supplementary Figure 2: Morris Method results for acetaminophen t_{max} using $r = 1$ to 40 and sampling bounds of $\pm 20\%$. The error bars represent the standard deviation in μ^* from 3 independent analyses at each r .



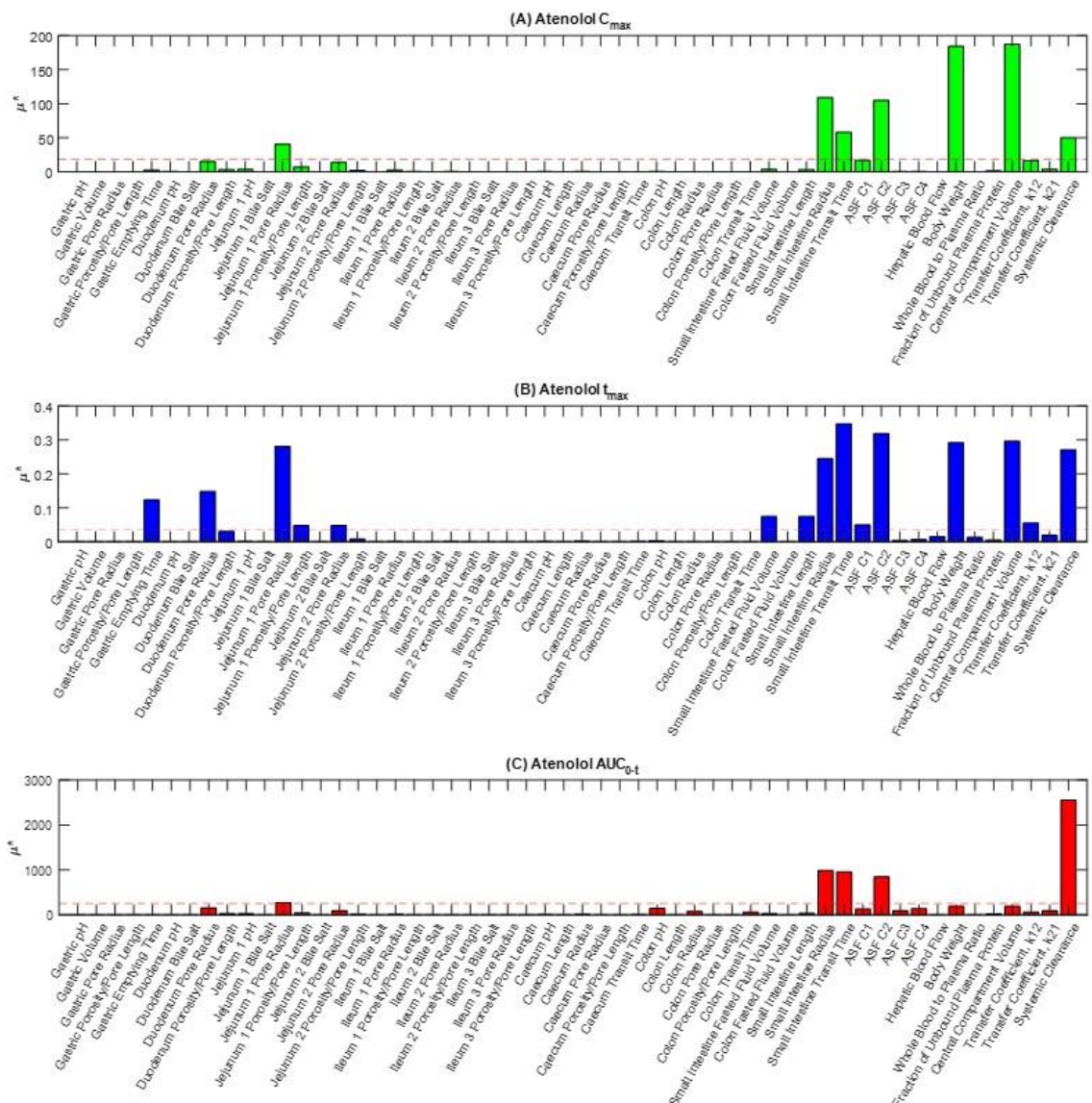
Supplementary Figure 3: Morris Method results for acetaminophen AUC_{0-t} using $r = 1$ to 40 and sampling bounds of $\pm 20\%$. The error bars represent the standard deviation in μ^* from 3 independent analyses at each r .



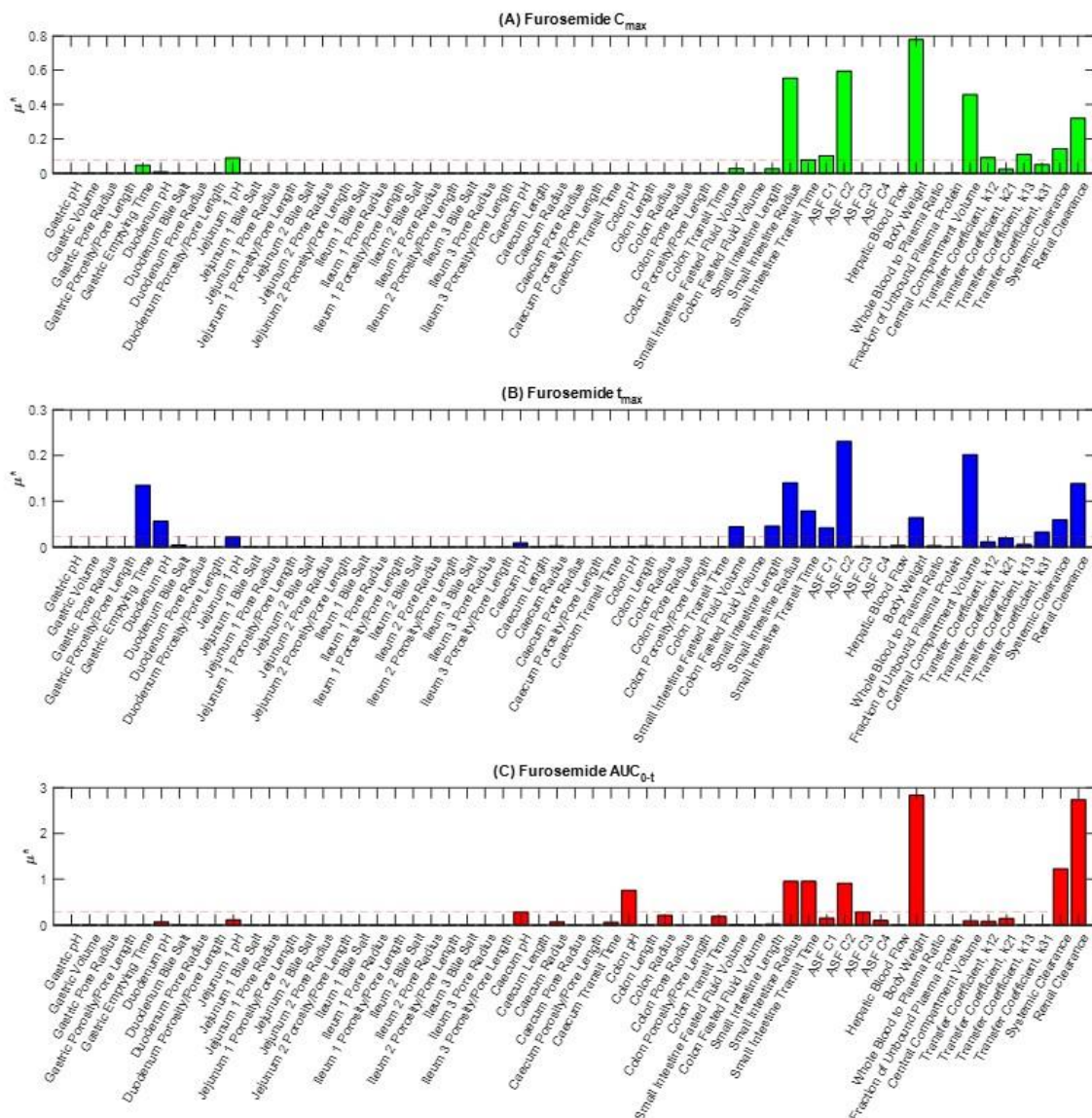
Supplementary Figure 4: Representative Morris Method results for acetaminophen C_{max} , t_{max} , and AUC_{0-t} . The values of μ^* were determined using $r = 20$ and sampling bounds of $\pm 20\%$. The cutoff for significance (indicated by dotted red line), corresponded to 10% of the maximum μ^* associated with each output.



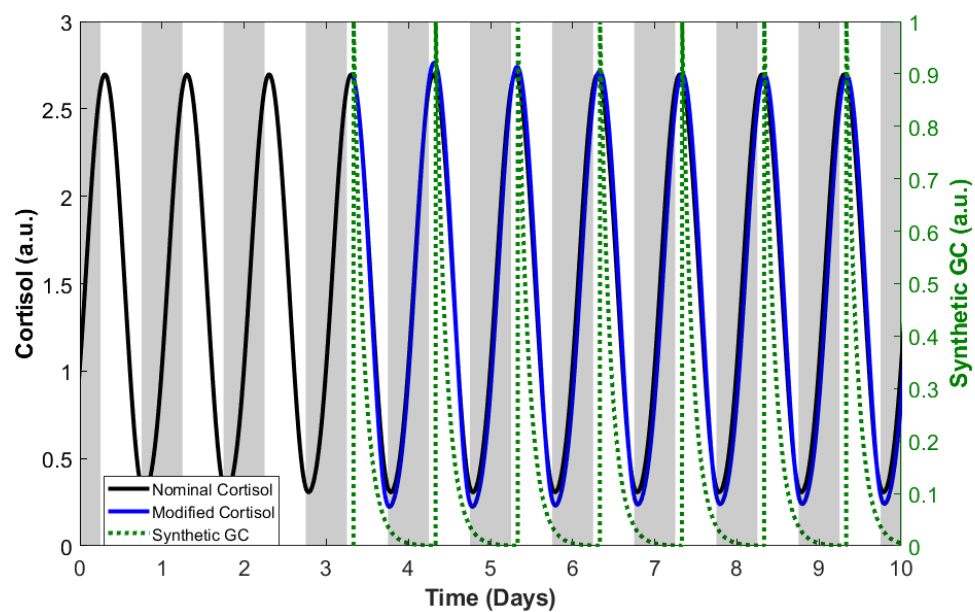
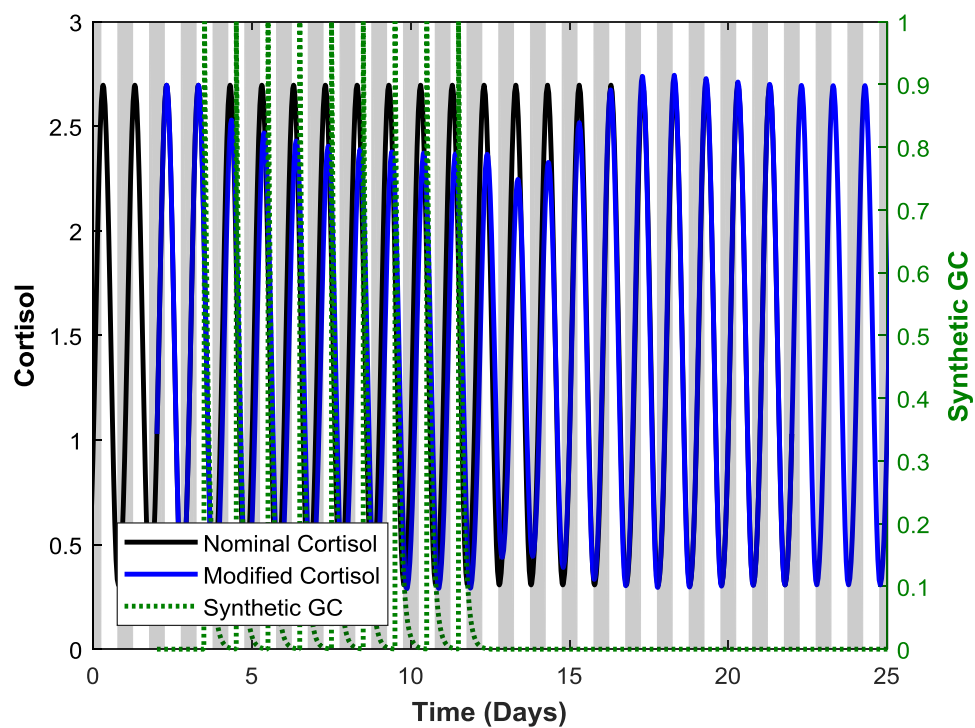
Supplementary Figure 5: Representative Morris Method results for risperidone C_{max} , t_{max} , and AUC_{0-t} . The values of μ^* were determined using $r = 20$ and sampling bounds of $\pm 20\%$. The cutoff for significance (indicated by dotted red line), corresponded to 10% of the maximum μ^* associated with each output.



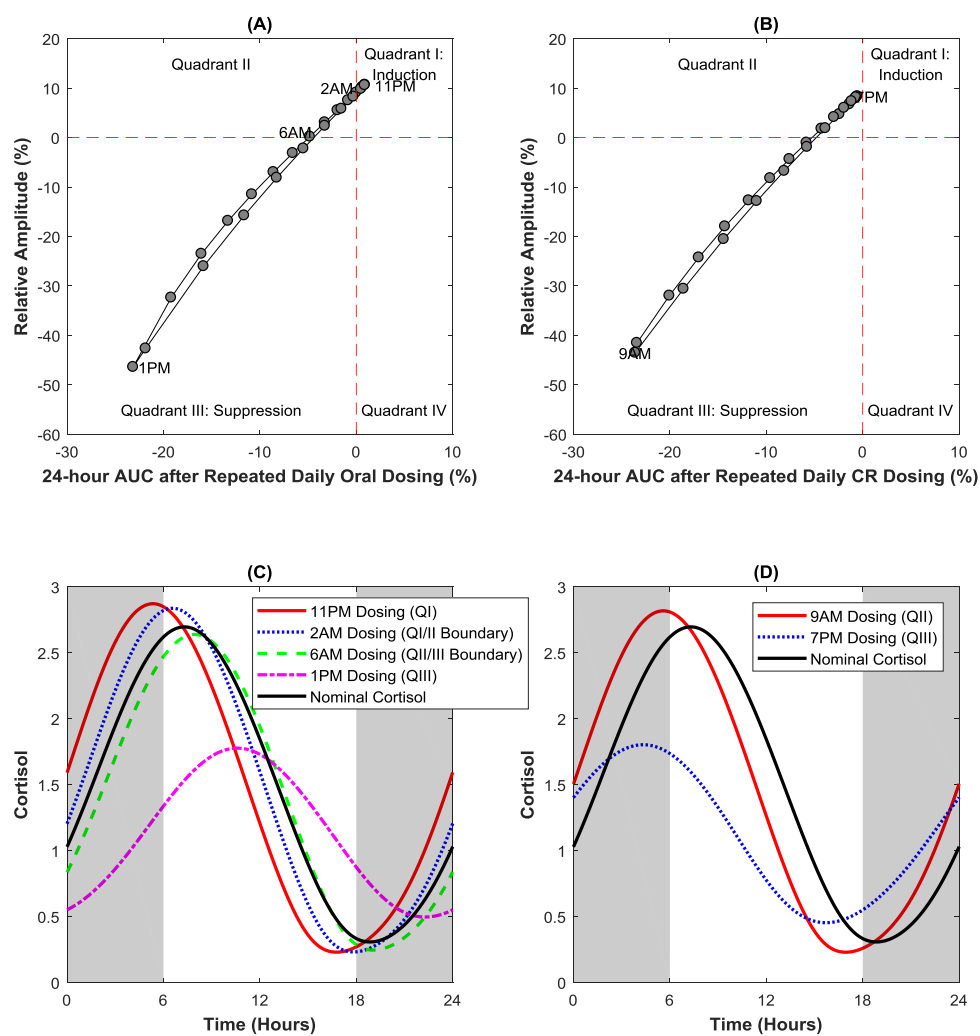
Supplementary Figure 6: Representative Morris Method results for atenolol C_{max} , t_{max} , and AUC_{0-t} . The values of μ^* were determined using $r = 20$ and sampling bounds of $\pm 20\%$. The cutoff for significance (indicated by dotted red line), corresponded to 10% of the maximum μ^* associated with each output.



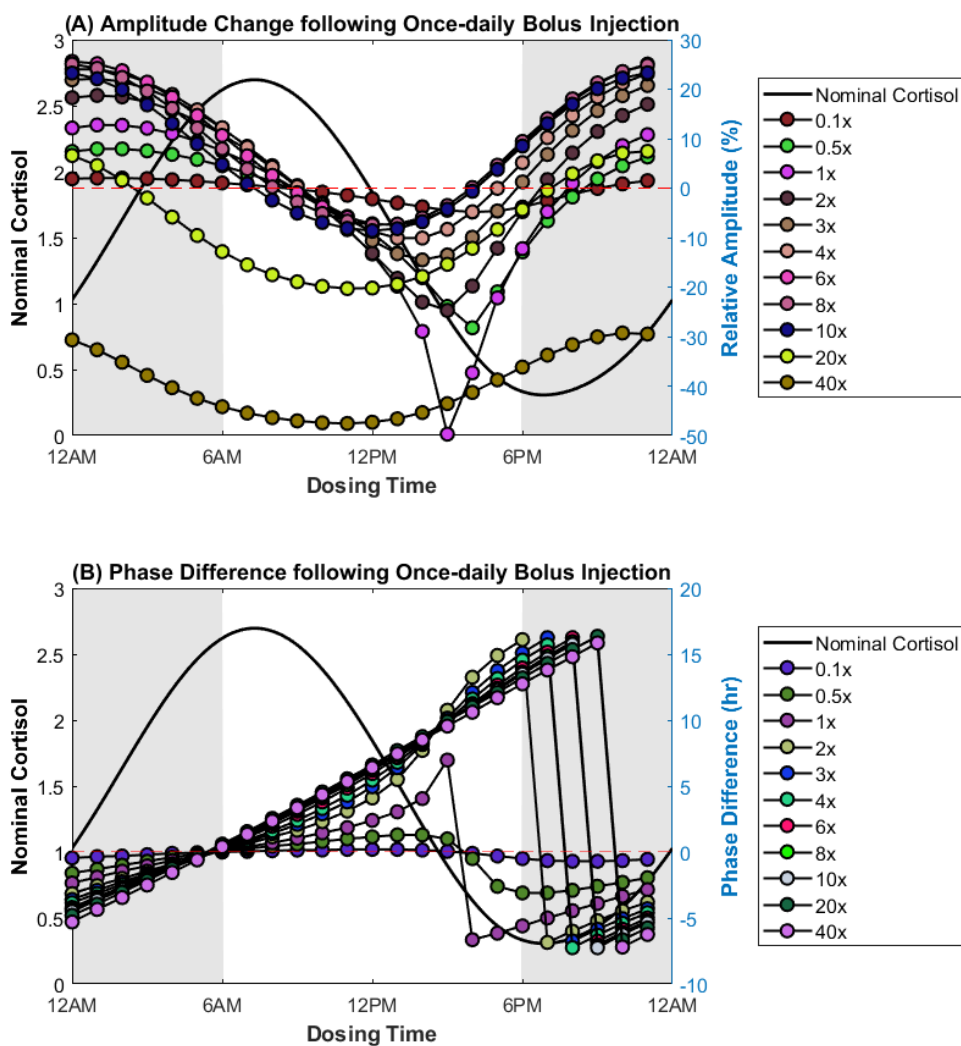
Supplementary Figure 7: Representative Morris Method results for furosemide C_{max} , t_{max} , and AUC_{0-t} . The values of μ^* were determined using $r = 20$ and sampling bounds of $\pm 20\%$. The cutoff for significance (indicated by dotted red line), corresponded to 10% of the maximum μ^* associated with each output.



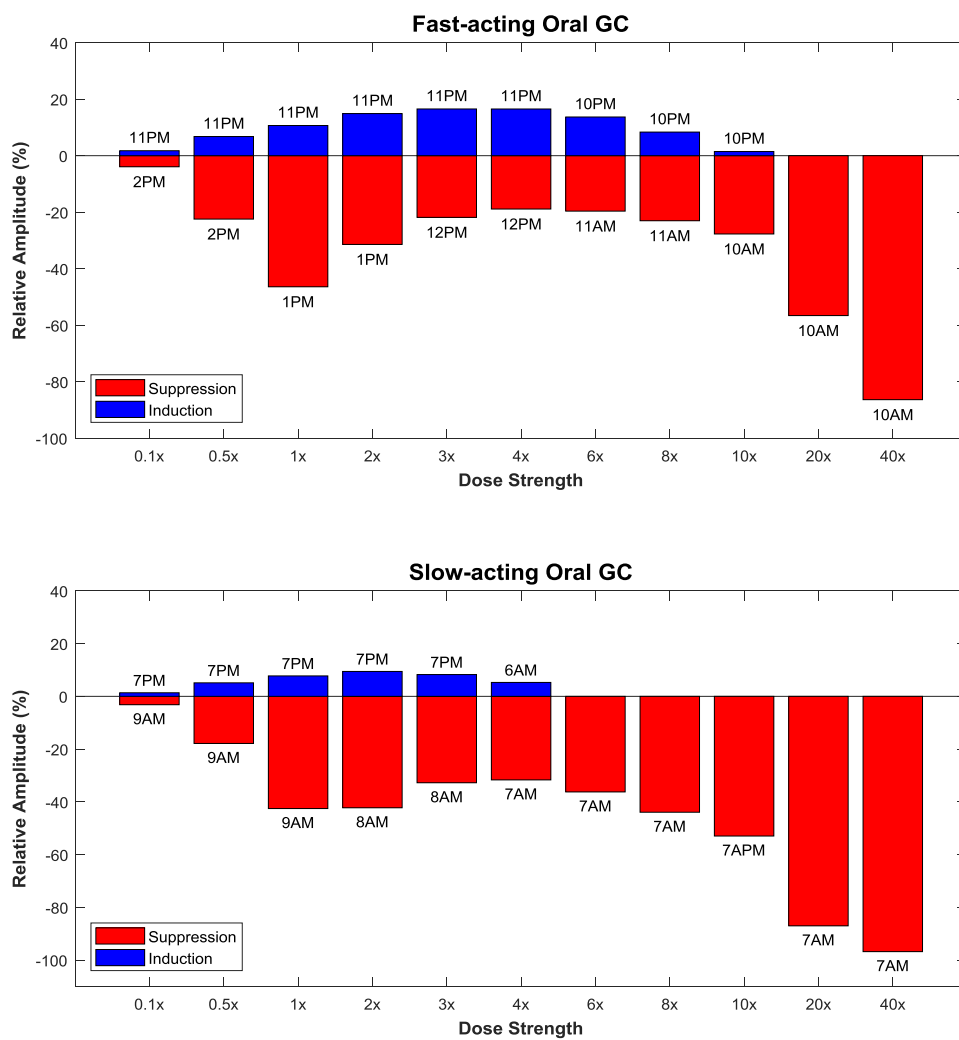
Supplementary Figure 8: Top - Modified cortisol profile after dosing of synthetic glucocorticoids by bolus injection at the nominal amount (1x) returns to baseline when dosing ceases. Bottom - Modified cortisol profile with minimal disruption of the circadian rhythm after once-daily administration of synthetic GCs.



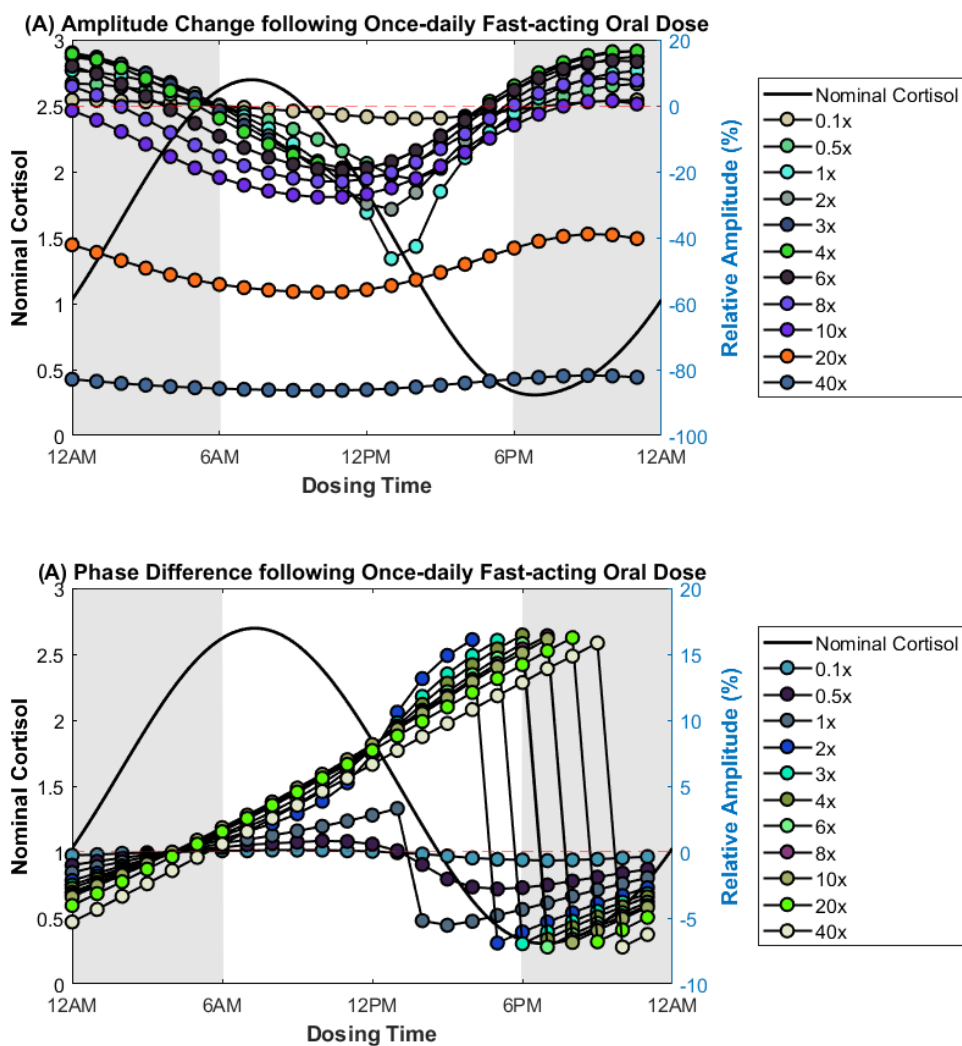
Supplementary Figure 10: Influence of chronic once-daily chronopharmacological dosing on the total cortisol exposure for fast-acting (A,C), and slow-acting (B,D) oral synthetic glucocorticoids



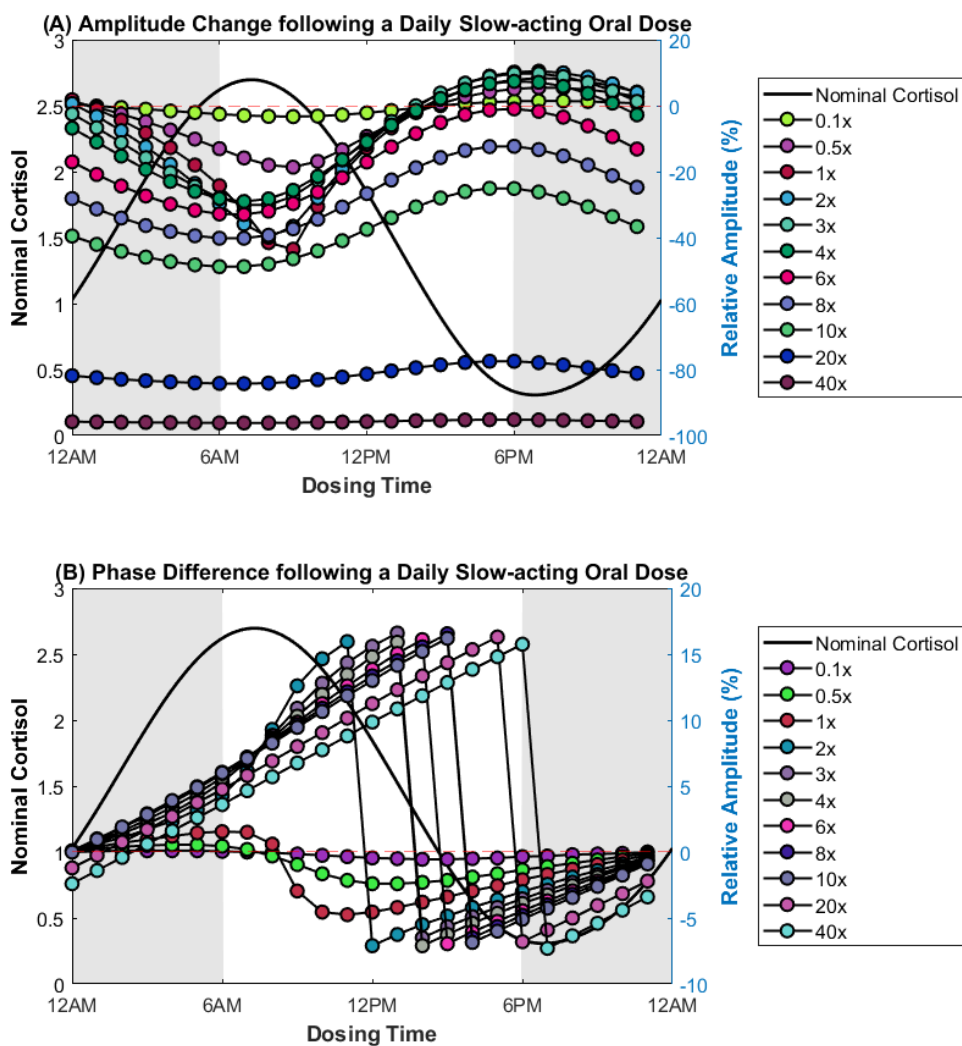
Supplementary Figure 11: Amplitude and phase of the modified cortisol rhythm after once-daily chronopharmacological dosing of synthetic glucocorticoids by bolus injection for several dosing strengths



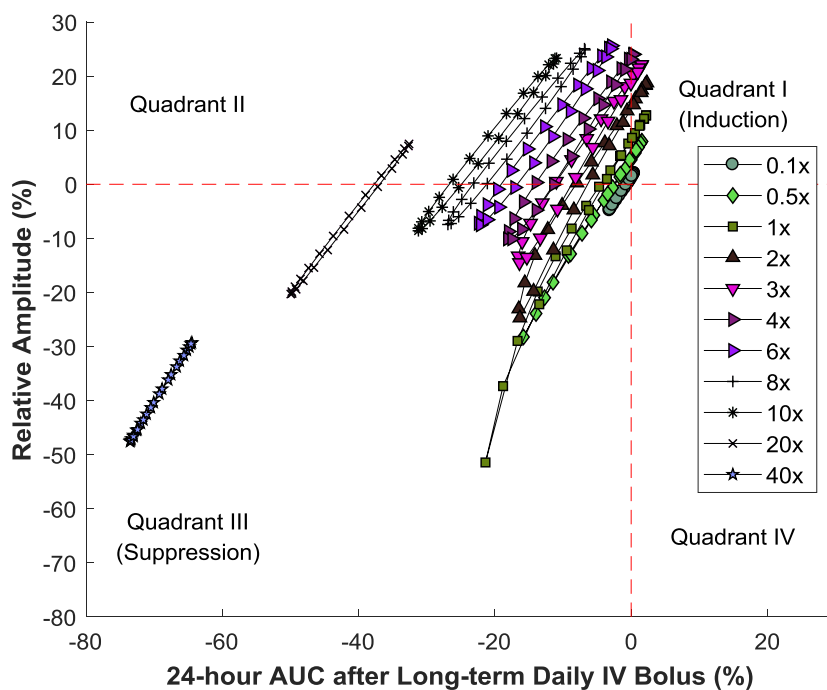
Supplementary Figure 12: Influence of dosing strength on the relative amplitude after chronic once-daily chronopharmacological dosing of fast-acting and slow-acting oral synthetic GCs



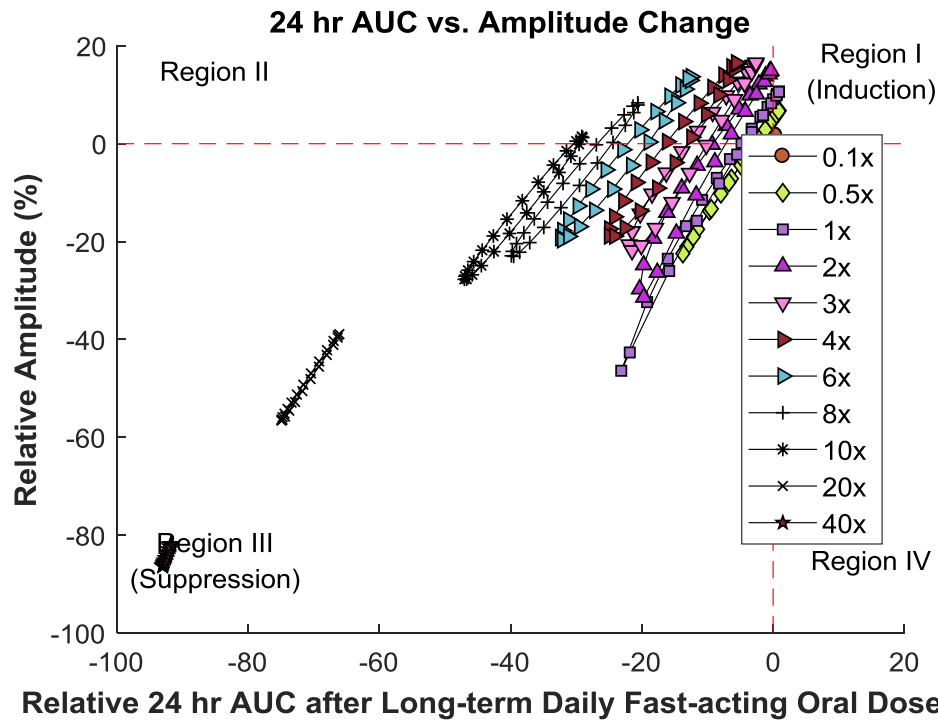
Supplementary Figure 13: Amplitude and phase of the modified cortisol rhythm after once-daily chronopharmacological dosing of a fast-acting synthetic glucocorticoids for several dosing strengths



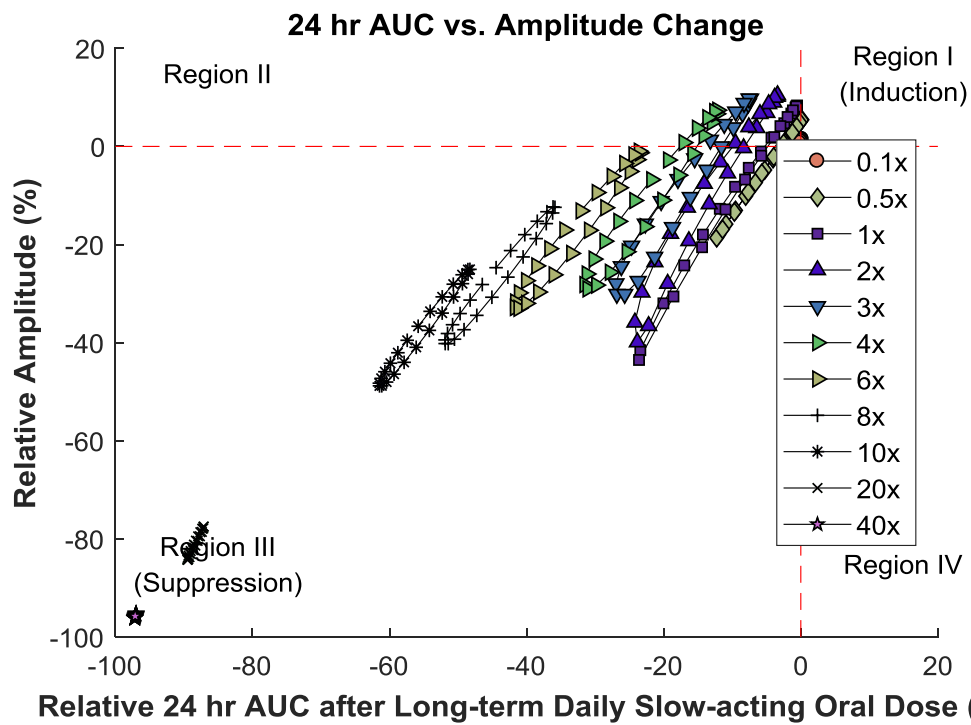
Supplementary Figure 14: Amplitude and phase of the modified cortisol rhythm after once-daily chronopharmacological dosing of a slow-acting synthetic glucocorticoids for several dosing strengths



Supplementary Figure 15: Influence of chronic once-daily chronopharmacological dosing on the total cortisol exposure following bolus injection of synthetic GCs at several dosing strengths



Supplementary Figure 16: Influence of chronic once-daily chronopharmacological dosing on the total cortisol exposure for fast-acting synthetic GCs at several dosing strengths



Supplementary Figure 17: Influence of chronic once-daily chronopharmacological dosing on the total cortisol exposure for slow-acting synthetic GCs at several dosing strengths.

6.2 Supplementary Tables

Supplementary Table 1: GastroPlus input for acetaminophen, risperidone, atenolol, and furosemide

Parameter	Acetaminophen	Risperidone	Atenolol	Furosemide
Biopharmaceutical Classification	I	II	III	IV
Dosage Form	IR: Tablet	IR: Tablet	IR: Tablet	IR: Tablet
Single Dose (mg)	1000 [131]	2 [132]	100 [133]	80 [135]
Dose Volume (mL)	250	240 [132]	250	240 [135]
Reference $\log D$	0.47 at pH 7.4 [245]	2.5 @ pH -1 [246]	0.45 @ pH -1	-0.69 at pH 7.4 [247]
Reference Solubility (mg/mL)	23.7 at pH 7 [248]	3.375 at pH 6; 0.458 at pH 7.4; 0.131 at pH 8; 0.043 at pH 9; 0.028 at pH 10.4 [249]	17.07 at pH 11.22	21.9 at pH 8 [247]
Precipitation Time (s)	900	900 [250]	900	900
Diffusion Coefficient (cm ² /s)	1.143 x 10 ⁻⁵ [248]	0.64 x 10 ⁻⁵ [250]	0.76 x 10 ⁻⁵	0.878 x 10 ⁻⁵
Drug Particle Density (g/mL)	1.29 [251]	1.2 [250]	1.2	1.2
Human Effective Permeability (cm/s)	0.86 x 10 ⁻⁴ (Rat) [248]	1.95 x 10 ⁻⁴ [250]	0.78 x 10 ⁻⁴	0.643 x 10 ⁻⁴ [252]
pKa	9.5 (Acid) [248]	8.547 (Base)	9.64 (Base)	-0.59 (Base); 3.88 (Acid); 9.37 (Acid)
Solubility Factor	13 [253]	126.1	11.66	367
Body Weight (kg)	60 [131]	63.2 [132]	88.4 [133]	73.3 [135]
Systemic Clearance, CL (L/h)	19.7 [131]	12.919	10.944	2.02 [135]
Renal Clearance, CL_R (L/h/kg)	0.010 [131]	0	0	0.0637 [135]
Central Compartment Volume, V_C (L/kg)	0.990 [131]	1.470	0.967	0.0814 [135]
Transfer Coefficient, k_{12} (h ⁻¹)	0.291 [131]	0.0577	0.0469	0.184 [135]
Transfer Coefficient, k_{21} (h ⁻¹)	0.641 [131]	0.1429	0.1436	0.061 [135]
Transfer Coefficient, k_{13} (h ⁻¹)	0	0.0289	0	0.427 [135]
Transfer Coefficient, k_{31} (h ⁻¹)	0	0.0150	0	0.847 [135]
Reference for Clinical Data	Singh et al. [131]	Liu et al. [132]	Sowinski et al. [133]	Van Wart et al. [135]
Blood to Plasma Concentration Ratio, R_{bp}	1.59 [254]	0.67 [250]	1.07 [255]	1
Unbound Plasma Protein, F_{up} (%)	82 [254]	10 [132]	97 [256]	2.3 [257]
Liver First-pass Extraction (%)	0	23.61	0	0
Gut First-pass Extraction (%)	0	0	0	0

Supplementary Table 2: Computational time for GastroPlus global sensitivity analysis

Analysis	Drug	Number of Samples	Number of Parameters, k	Computational Cost, Nt	Simulation Time
Morris	Acetaminophen	r=1	55	56	28 min
		r=2	55	112	56 min
		r=5	55	280	2.3 hr
		r=10	55	560	4.7 hr
		r=20	55	1120	9.3 hr
		r=30	55	1680	14.0 hr
		r=40	55	2240	18.7 hr
	Risperidone	r=20	57	1160	9.7 hr
	Atenolol	r=20	54	1100	9.2 hr
	Furosemide	r=20	57	1160	9.7 hr
Sobol	Acetaminophen	N=4000	6	32,000	11.1 days
	Risperidone	N=3000	3	15,000	5.2 days
	Atenolol	N=4000	7	36,000	12.5 days
	Furosemide	N=5000	11	65,000	22.6 days

Supplementary Table 3: GastroPlus Physiological Parameters evaluated by Global Sensitivity Analysis

Category	Parameter
Absorption	Gastric pH; Gastric Volume; Gastric Pore Radius; Gastric Porosity/Pore Length; Gastric Transit Time
	Fasted Fluid Volume (FFV) in Small Intestine; Small Intestine Length; Small Intestine Radius; Small Intestine Transit Time
	Duodenum pH; Duodenum Bile Salt Concentration; Duodenum Pore Radius; Duodenum Porosity/Pore Length
	Jejunum 1 pH; Jejunum 1 Bile Salt Concentration; Jejunum 1 Pore Radius; Jejunum 1 Porosity/Pore Length
	Jejunum 2 Bile Salt Concentration; Jejunum 2 Pore Radius; Jejunum 2 Porosity/Pore Length
	Ileum 1 Bile Salt Concentration; Ileum 1 Pore Radius; Ileum 1 Porosity/Pore Length
	Ileum 2 Bile Salt Concentration; Ileum 2 Pore Radius; Ileum 2 Porosity/Pore Length
	Ileum 3 Bile Salt Concentration; Ileum 3 Pore Radius; Ileum 3 Porosity/Pore Length
	Caecum pH; Caecum Length; Caecum Radius; Caecum Pore Radius; Caecum Porosity/Pore Length; Caecum Transit Time
	Colon pH; Colon Length; Colon Radius; Colon Pore Radius; Colon Porosity/Pore Length; Colon Transit Time; Fasted Fluid Volume (FFV) in Colon
Absorption Scaling Factor Model Coefficient 1 (ASF C1); Absorption Scaling Factor Model Coefficient 2 (ASF C2); Absorption Scaling Factor Model Coefficient 3 (ASF C3); Absorption Scaling Factor Model Coefficient 4 (ASF C4)	
Distribution	Hepatic Blood Flow (Q_H)
	Body Weight (BW)
	Whole Blood to Plasma Concentration Ratio (R_{bp})
	Fraction of Unbound Plasma Protein (F_{up})
	Central Compartment Volume (V_C)
	Transfer Coefficient from Central to Peripheral Compartment (k_{12})
	Transfer Coefficient from Peripheral to Central Compartment (k_{21})
	Transfer Coefficient from Central to Peripheral Compartment (k_{13})
Transfer Coefficient from Peripheral to Central Compartment (k_{31})	
Excretion	Systemic Clearance (CL)
	Renal Clearance (CL_R)
	Liver First-pass Extraction (FPE)

Supplementary Table 4: Model Parameters for the Mixed Population

Model Parameters	Mean (μ)	Std. Dev. (σ)	Lower Bound	Upper Bound
Absorption rate constant, k_a	1.62	0.40	0.435	2.81
Central compartment volume, V_C	9.47	2.01	3.45	15.5
Peripheral compartment volume, V_P	4.95	1.18	1.40	8.50
Distribution Clearance, CL_D	0.559	0.089	0.291	0.827
Onset of enterohepatic recirculation, T_{EHC}	8.27	1.56	3.58	13.0
Rate constant for enterohepatic recirculation, k_{EHC}	1.2	0.46	0	2.59
Elimination clearance, CL	0.741	0.157	0.2695	1.2115
Fraction reabsorbed, F_E	0.340	0.140	0	0.7592
Initial lag time, t_{lag}	2.11	0.794	0	4.4858

Note: For parameters that were dependent on body weight (k_a and V_C), the mean body weight of the mixed population (70 kg) was used to determine the mean values of these parameters using the point estimates for θ_i . For parameters common to both sexes (V_P , CL_D , T_{EHC} , k_{EHC}), the point estimates for θ_i were used as the mean parameter values. For sexual dimorphic parameters (CL , F_E , and t_{lag}), the average of the male and female parameter values was used. Sampling bounds were set to $\pm 3\sigma$. The minimum sampling bounds for k_{EHC} and t_{lag} were set to zero since these parameters cannot have a negative value. The minimum and maximum feasible sampling bounds for F_E were 0 and 1, respectively.

Supplementary Table 5: Comparison of model parameters for the simulated male and female populations

Parameters	Comparison of Distributions Kolmogorov-Smirnov p-value	Comparison of Medians Wilcoxon Rank Sum p-value
Absorption, Rate Constant k_a (hr^{-1})	3.3e-96	3.6e-140
Central Compartment Volume, V_C (L)	0	0
Peripheral Compartment Volume, V_P (L)	5.1e-43	1.7e-61
Distribution Clearance, CL_D (L/hr)	2.1e-03	1.6e-03
Elimination Clearance, CL (L/hr)	0	0
Reabsorption Fraction, F_E	1.1e-176	2.5e-248
Initial Lag Time, t_{lag} (hr)	0	0
Onset of Reabsorption Event, T_{EHC} (hr)	5.4e-54	2.6e-63
Reabsorption Rate Constant, k_{EHC} (hr^{-1})	0.8988	0.8309

NS = Not significant (Parameter values for males and females were not statistically different.)

Supplementary Table 6: Parameter estimates for clinical and simulated female populations

Parameters	Clinical Females		Simulated Females		WRS p-value
	Mean	Sigma	Mean	Sigma	
Absorption, Rate Constant k_a (hr^{-1})	1.82	0.45	1.66	0.37	0.91
Central Compartment Vol., V_C (L)	9.49	2.01	7.55	0.87	0.14
Peripheral Compartment Vol., V_P (L)	4.95	1.18	4.87	1.15	0.76
Distribution Clearance, CL_D (L/hr)	0.559	0.09	0.55	0.09	0.97
Elimination Clearance, CL (L/hr)	0.581	0.123	0.65	0.10	0.33
Reabsorption Fraction, F_E	0.462	0.190	0.36	0.13	0.54
Initial Lag Time, t_{lag} (hr)	2.21	0.833	2.32	0.60	0.08
Onset of Reabsorption, T_{EHC} (hr)	8.27	1.56	8.38	1.52	0.74
Reabsorption Rate Constant, k_{EHC} (hr^{-1})	1.2	0.46	1.20	0.45	0.99

NS = Not Significant (Parameters for the simulated and clinical populations were not statistically different.)

Supplementary Table 7: Parameter estimates for the clinical and simulated male populations

Parameters	Clinical Males		Simulated Males		WRS p-value
	Mean	Sigma	Mean	Sigma	
Absorption, Rate Constant k_a (hr^{-1})	1.46	0.36	1.50	0.35	0.54
Central Compartment Vol., V_C (L)	9.45	2.00	11.05	1.20	0.08
Peripheral Compartment Vol., V_P (L)	4.95	1.18	5.21	1.15	0.92
Distribution Clearance, CL_D (L/hr)	0.559	0.09	0.56	0.09	0.93
Elimination Clearance, CL (L/hr)	0.900	0.191	0.97	0.08	0.39
Reabsorption Fraction, F_E	0.218	0.090	0.28	0.13	0.35
Initial Lag Time, t_{lag} (hr)	2.00	0.754	1.66	0.23	0.90
Onset of Reabsorption, T_{EHC} (hr)	8.27	1.56	7.94	1.53	0.92
Reabsorption Rate Constant, k_{EHC} (hr^{-1})	1.2	0.46	1.21	0.45	1.00

NS = Not Significant (Parameters for the simulated and clinical populations were not statistically different.)

Supplementary Table 8: Comparison of model output for the clinical and simulated populations

	C_{max} (mg/L)	T_{max} (hr)	AUC_{0-48} (mg h/L)
Clinical Men	35.6 (5.2)	3.9 (0.7)	496.6 (55.2)
Clinical Women	55.3 (9.4)	4.3 (1.1)	809.4 (148.4)
Sex Differences	p-value<0.05	NS	p-value<0.05
Simulated Men	35.6 (2.9)	3.5 (0.34)	518.5 (25.4)
Simulated Women	52.0 (4.7)	4.0 (0.61)	764.4 (73.3)
Sex Differences	p-value=0	p-value=0	p-value=0

Supplementary Table 9: Dirunal HPA Axis Model Parameters

Parameter	Value	Description
k_{p1}	0.28643 μMh^{-1}	Estimated, zero order synthesis rate constant of CRH
K_{p1}	1.4911 μM	Estimated, Michaelis-Menten constant for glucocorticoid-induced CRH inhibition
V_{d1}	0.3492 μMh^{-1}	Estimated, first order rate constant for CRH degradation
K_{d1}	4.3875 μM	Estimated, Michaelis-Menten constant for CRH degradation
k_{p2}	0.4333 μMh^{-1}	Estimated, first order rate constant for synthesis of ACTH
K_{p2}	4.7662 μM	Estimated, Michaelis-Menten constant for glucocorticoid-induced ACTH inhibition
V_{d2}	1.0015 μMh^{-1}	Estimated, first order rate constant for degradation of ACTH
K_{d2}	0.8488 μM	Estimated, Michaelis-Menten constant for ACTH degradation
k_{p3}	0.557 μMh^{-1}	Estimated, first order rate constant for synthesis of cortisol
V_{d3}	0.7245 μMh^{-1}	Estimated, first order rate constant for CORT degradation
K_{d3}	0.1807 μM	Estimated, Michaelis-Menten constant for CORT degradation
$GR(0)$	540.7 $\text{nmol L}^{-1} \text{mg protein}^{-1}$	Initial GR content, [77]
$GR_{mRNA}(0)$	25.8 fmolg^{-1}	Initial GR mRNA content, [77]
k_{synGRm}	2.9 $\text{fmolg}^{-1} \text{h}^{-1}$	Zero order rate constant for synthesis of GR mRNA, [77]
r_f	0.49	GR recycle fraction from nucleus to cytoplasm, [77]
k_{re}	0.57 h^{-1}	Rate of GR recycling from nucleus to cytoplasm, [77]
k_{on}	0.00329 $\text{L nmol}^{-1} \text{h}^{-1}$	Second-order rate constant for CORT-GR binding, [77]
$k_{deg,GRm}$	$k_{synGRm}/GR_{mRNA}(0)$	First-order rate constant for degradation of GR mRNA, [77]
$k_{deg,GR}$	0.0572 h^{-1}	First order rate constant for degradation of GR, [77]
$k_{syn,GR}$	$GR(0) \cdot k_{deg,GR} / GR_{mRNA}(0)$	First order rate constant for synthesis of GR, [77]
k_T	0.63 h^{-1}	Rate of GR translocation from cytoplasm to nucleus, [77]
k_{imp}	0.5	Strength of ACTH impulse
$k_{stress.out}$	6.79 h^{-1}	Rate constant for clearance of stressor
k_s	40	Strength of induction of CRH production by stressor
k_a	0.42 hr^{-1}	First-order absorption rate constant for PNL [205]
k_e	0.33 hr^{-1}	First-order elimination rate constant for PNL [205]
$k_{t1}, k_{t2}, k_{t3}, k_{t4}, k_{t5}$	1 hr^{-1}	Rate constants for transfer between transit compartments

Abbreviations: a.u. - arbitrary units; mRNA – messenger RNA

Supplementary Table 10: Nocturnal HPA Axis Model Parameters Common to Both Sexes

Parameter	Value	Description
k_{p1}	0.3819 μMh^{-1}	Estimated, zero order synthesis rate constant of CRH
V_{d1}	0.3492 μMh^{-1}	Estimated, first order rate constant for CRH degradation
K_{d1}	4.3875 μM	Estimated, Michaelis-Menten constant for CRH degradation
k_{p2}	0.4561 μMh^{-1}	Estimated, first order rate constant for synthesis of ACTH
V_{d2}	1.0015 μMh^{-1}	Estimated, first order rate constant for degradation of ACTH
K_{d2}	0.8488 μM	Estimated, Michaelis-Menten constant for ACTH degradation
V_{d3}	0.7245 μMh^{-1}	Estimated, first order rate constant for CORT degradation
K_{d3}	0.1807 μM	Estimated, Michaelis-Menten constant for CORT degradation
$GR(0)$	540.7 $\text{nmol L}^{-1} \text{mg protein}^{-1}$	Initial GR content, [258]
$GR_{mRNA}(0)$	25.8 fmol g^{-1}	Initial GR mRNA content, [258]
k_{synGRm}	2.9 $\text{fmol g}^{-1} \text{h}^{-1}$	Zero order rate constant for synthesis of GR mRNA, [258]
r_f	0.49	GR recycle fraction from nucleus to cytoplasm, [258]
k_{re}	0.57 h^{-1}	Rate of GR recycling from nucleus to cytoplasm, [258]
k_{on}	0.00329 $\text{L nmol}^{-1} \text{h}^{-1}$	Second-order rate constant for CORT-GR binding, [258]
$k_{deg,GRm}$	$k_{synGRm}/GR_{mRNA}(0)$	First-order rate constant for degradation of GR mRNA, [258]
$k_{deg,GR}$	0.0572 h^{-1}	First order rate constant for degradation of GR, [258]
$k_{syn,GR}$	$GR(0) \cdot k_{deg,GR} / GR_{mRNA}(0)$	First order rate constant for synthesis of GR, [258]
k_T	0.63 h^{-1}	Rate of GR translocation from cytoplasm to nucleus, [258]
k_{imp}	0.5	Strength of ACTH impulse
$k_{stress.out}$	6.79 h^{-1}	Rate constant for clearance of stressor
k_s	40 a.u.	Strength of induction of CRH production by stressor
k_t	0.92 a.u.	Estimated, rate constant for light transduction
k_{us}	1 a.u.	Estimated, rate constant for production of light effect
n	2 a.u.	Estimated, Hill coefficient for light effect
$k_{deg,us}$	0.92 a.u.	Estimated, rate constant for degradation for light effect
k_{eff}	24 a.u.	Estimated, strength of induction of light-effect degradation
k_a	0.42 hr^{-1}	First-order absorption rate constant for PNL [205]
k_e	0.33 hr^{-1}	First-order elimination rate constant for PNL [205]
$k_{t1}, k_{t2}, k_{t3}, k_{t4}, k_{t5}$	1 hr^{-1}	Rate constants for transfer between transit compartments

Abbreviations: a.u. - arbitrary units; mRNA – messenger RNA